2017

Cellular Determinants of Coronavirus Entry Routes

James Thomas Earnest
Loyola University Chicago

LOYOLA UNIVERSTIY CHICAGO

CELLULAR DETERMINANTS OF CORONAVIRUS ENTRY ROUTES

A DISSERTATION SUBMITTED TO
THE FACULTY OF THE GRADUATE SCHOOL
IN CANDIDACY FOR THE DEGREE OF
DOCTOR OF PHILOSOPHY

PROGRAM IN MICROBIOLOGY AND IMMUNOLOGY

BY
JAMES THOMAS EARNEST
CHICAGO, ILLINOIS
MAY 2017

ACKNOWLEDGEMENTS

I would like to thank my mentor Dr. Tom Gallagher for his invaluable leadership and assistance. TG is a singular person and I hope I can call on him as I make my way out into the world. His guidance has made me a better scientist and person. I would also like to thank Drs. Ed Campbell, Susan Baker, Adam Driks, and Seth Robia for their guidance of my project while on my dissertation committee. Furthermore, the faculty staff and students of the Department of Microbiology and Immunology deserve praise for creating a unique learning environment that produces superlative thinkers and scientists. I would finally like to emphasize my gratitude for my lab mates Dr. Jung-Eun Park, Mike Hantak, Enya Qing, Arlene Barlan, Natalie Nidetz, Dr. Mayukh Sarkar, and Jennifer Novak for both their experimental assistance and discussion of results and potential experiments. I also thank Drs. Stan Perlman, Paul McCray, and Kun Li for their collaboration with my project.

I thank my family and friends for their support throughout my academic career. My parents, David and Margaret, have been unwavering in their assistance and encouragement of my dreams. I especially thank my all of my grandparents who have helped me throughout my academic career. I can only hope they can understand my inability to put my gratitude into words. Finally, I would like to acknowledge my friends in Chicago, Georgia, North Carolina, and throughout the country for keeping me sane throughout this somewhat arduous process.

One must imagine Sisyphus happy.

-Albert Camus

TABLE OF CONTENTS

LIST OF TABLES

LIST OF FIGURES

LIST OF ABREVIATIONS

α	anti-
Ad5	adenovirus 5
ACE2	angiotensin converting enzyme 2
APN	aminopeptidase N
CAS9	CRISPR associated protein 9
catK	cathepsin K
catL	cathepsin L
CD	cluster of differentiation
CEACAM	carcinoembryonic antigen-related cell adhesion molecules
cDNA	complementary DNA
CHAPS	3-((3-cholamidopropyl) dimethlyammonio)-1-propanesulfonate
chol	cholesterol
cm	centimeter
CoV	coronavirus
CRISPR	clustered regularly interspaced short palindromic repeats
^{o}C	degrees Celsius
DBT	delayed brain tumor cells
DMEM	Dulbecco's Modified Eagle's Medium
DNA	deoxyribonucleic acid
DPP4	dipeptidyl peptidase 4
dpi	days post infection
E	envelope protein
EC_{50}	half maximal effective concentration
EDTA	ethlenediaminetertaacetic acid
ER	endoplasmic reticulum
FACS	fluorescence activated cell sorting

FCS	fetal calf serum
FIPV	Feline infectious peritonitis virus
fluc	firefly luciferase
FP	fusion peptide
g	g-force (m/s^2)
GFP	green fluorescent protein
gluc	*gaussia* luciferase
HA	hemagglutinin
HAT	human airway trypsin-like protease
hCoV	human coronavirus
HD	high density fraction
HEK	human embryonic kidney
HIV	human immunodeficiency virus
hpi	hours post infection
hpt	hours post transduction
HR	heptad repeat
HRP	horse radish peroxidase
HPIA	highly pathogenic influenza A virus
IAV	influenza A virus
IFA	immunofluorescence assay
IFN	interferon
Ig	immunoglobulin
IgG	immunoglobulin G
kDa	kilo Dalton
KD	knockdown
KO	knockout
LD	low density fraction
LET1	lung epithelial type 1 cells
luc	luciferase
M	molar
MERS	Middle East Respiratory Syndrome

µg	microgram
µl	microliter
µM	micromolar
ml	milliliter
mM	millimolar
MHV	mouse hepatitis virus
min	minutes
MOI	multiplicity of infection
nM	nanomolar
PAGE	polyacrylamide gel electrophoresis
palm	palmitate
PBS	phosphate buffered saline
PCR	polymerase chain reaction
PFU	plaque forming units
PLA	proximity ligation assay
pp	pseudoparticle
PR8	influenza A/Puerto Rico/8/1934 H1N1
qPCR	quantitative polymerase chain reaction
r	recombinant
RBD	receptor binding domain
RNA	ribonucleic acid
R/S	arginine-serine sequence
S	spike glycoprotein
SARS	Sudden Acute Respiratory Syndrome
SD	standard deviation
SDS	sodium dodecyl sulfate-polyacrylamide gel electrophoresis
shRNA	small hairpin RNA
siRNA	small interfering RNA
TEM	tetraspanin-enriched microdomain
TfR	transferrin receptor
TMPRSS	transmembrane protease, serine

toco	tocopherol
Tspan	tetraspanin
TTSP	transmembrane serine protease
VSV	vesicular stomatitis virus
w/v	weight per unit volume
WT	wild-type

CHAPTER I

INTRODUCTION

Enveloped Virus Entry.

Enveloped viruses are produced coated in a lipid membrane. Thus, enveloped virus-cell entry requires fusion of viral and host cell membranes. Numerous glycoproteins extending from the viral membrane catalyze this fusion reaction. These fusion glycoproteins store energy upon folding in the producer cell [reviewed in [1]] . This energy is held through internal interactions [2] or by associated viral proteins [3]. This stored energy is released upon unfolding and refolding of the glycoprotein and provides the force necessary to overcome the energy barrier for membrane fusion [4]. The structural transformations that the glycoproteins undergo upon triggering are unstable and tend towards a lower energy state, releasing the energy required for membrane fusion [2, 5]. Therefore, once the "trigger" of a fusion glycoprotein is pulled, and its stored energy released, it will rapidly become inactive [6]. It is necessary that these glycoproteins remain catalytically-inactive on extracellular virus particles and only become triggered to unfold in an environment that is ideal for successful membrane fusion and infection. To increase the odds of successful infection, enveloped viruses have developed strategies to undergo the fusion reaction only in response to cellular and environmental factors.

Fusion glycoprotein triggering factors include host cell receptors, endosomal acids, and proteases. Many viruses require a single, soluble trigger, for example, influenza A virus (IAV) fusion proteins are triggered by protons within the target-cell

endosome [7]. Other viruses require two triggering agents, for example, ASLV fusion proteins are partially advanced into fusion-catalyzing forms by host cell receptor binding [8], and then fully execute fusion after being exposed to endosomal protons [9].

Although there is a large variety in the structure and mechanisms of fusion glycoproteins, the membrane fusion process has many common features. When fusion glycoproteins are in their folded, "loaded" conformation they bury hydrophobic domains called fusion peptides [10]. Upon triggering, the fusion glycoprotein will undergo structural transitions that extend this fusion peptide towards the target membrane. Due to its hydrophobicity, the fusion peptide will insert into the hydrophobic region of the cell's lipid bilayer. Further structural transitions bring the viral and cellular membranes into close proximity. After being brought into contact, the outer leaflets will meld. This state, where only one leaflet of each membrane is joined but there is no pore is called hemifusion [4, 11, 12]. Hemifusion is relatively stable [13], but is not sufficient for infection. For successful infection, the virus must form a fusion pore through further structural transitions. It is likely that most if not all enveloped viruses require the simultaneous refolding of multiple fusion glycoproteins to overcome the membrane fusion energy barrier and form the fusion pore [13]. Once the fusion pore forms, it expands due to favorable energetics [9, 12], releasing the genetic and protein contents of the virion into the cytoplasm.

Coronaviruses.

Coronaviruses (CoVs) are enveloped, positive-sense RNA viruses in the order *Nidovirales*. The single-stranded genome is the largest amongst RNA viruses at a length of up to 32 kb. The family *Coronaviridae* is divided into 4 genera based on sequence similarity: Alpha-, Beta-, Gamma-, and Deltacoronaviruses. Coronaviruses were first isolated in chickens in 1931 [14] and subsequently isolated as pathogens of mammals including swine [15] and mice [16]. In 1967, the first human CoVs, human coronavirus 229E (HCoV-229E) and human coronavirus OC43 (HCoV-OC43) were identified from upper respiratory tract samples taken a year earlier [17]. This study was the first to characterize coronaviruses as a viral family based on the morphology of the virions when observed by electron microscopy. Since then, other CoVs from the *alpha-* and *beta-* genera have been isolated from humans. However, until 2002, human CoVs were thought to cause only mild respiratory infections and posed no threat to global health [18, 19]. Recent outbreaks of zoonotic-origin CoVs have led to a greater interest in the threat of CoV pandemics.

Coronaviruses as threats to global health. The two most notable human CoV pathogens are the Severe Acute Respiratory Syndrome (SARS)-CoV and Middle East Respiratory Syndrome (MERS)-CoV which have caused pandemics in recent years. The SARS epidemic started in November 2002 in the Guangdong province of southern China. From there, it spread to the more populated Hong Kong, where it exhibited somewhat efficient human-to-human transmission. The virulence and transmissibility of the SARS-CoV led to fears of a possible global pandemic. Before transmission was stopped using

effective epidemiologic techniques [20], SARS infected 8,096 people and caused 774 deaths [WHO, SARS report].

The MERS epidemic started in Saudi Arabia in 2012 [21] and has since spread to multiple countries throughout the Middle East and the world, most notably causing a large outbreak in South Korea in 2015. As of December 2016, MERS-CoV has infected 1,841 people with 652 reported fatalities [WHO, MERS report]. While MERS-CoV causes a severe respiratory disease like SARS-CoV, many patients succumbed to renal failure [21, 22] and MERS-CoV has been shown to infect kidney cells [23]. As of this writing, MERS is still circulating in populations in the Middle East.

Zoonotic transmission of coronaviruses. Most, if not all, human CoVs likely originated as viruses circulating in animal populations. The alphacoronavirus HCoV-229E likely had a bat coronavirus as an ancestor before spreading into humans around 200 years ago [24]. The betacoronavirus HCoV-OC43, which causes mild respiratory illness in humans, shares sequence similarity with bovine coronavirus (BCoV) and a molecular clock analysis of the HCoV-OC43 S protein suggests the virus spread from cows into human about 120 years ago [25]. Interestingly, both pandemic CoVs likely originated in bats before transmitting to an intermediate host and eventually to humans [26-28]. The ability to move between species likely contributes to the dangers posed by pandemic-potential CoVs. This is in line with many other zoonotic diseases that have recently posed threats to global health including influenza A [29], Ebola virus [30], zika virus [31], and several alphaviruses [32].

The SARS-CoV originated in Chinese horseshoe bats [33] which can likely harbor multiple SARS-like coronaviruses without adverse effects [34]. The virus then moved to small mammals, such as palm civet cats, which were held in close proximity in Chinese markets. Interestingly, the S protein of these viruses were capable of binding to bat, civet, and human ACE2. This diversity of receptor utilization facilitated SARS transmission to humans and the beginning of the SARS epidemic.

MERS-CoV, like SARS, also likely started in bats [27], moved to an intermediate host [35], and then transmitted to humans. The closest, sequenced relative to MERS-CoV are the bat viruses HKU4 and HKU5 [27, 28]. Furthermore, an RNA fragment of the RNA-dependent RNA polymerase identical to MERS-CoV was isolated in both an Egyptian Tomb bat and several dromedary camels in Saudi Arabia [36]. These data, along with the discovery of MERS-neutralizing antibodies in camel populations [37], suggest that a MERS-like virus moved from bat populations into camels and then into humans who were in close contact. MERS S proteins can bind to both human and bat versions of the DPP4 receptor and the DPP4 gene from several bats shows evidence of adaptive evolution [38]. This suggests that MERS-like viruses may have spread in bat populations for some time and are pathogenic enough to exert a selective pressure on bat DPP4 genes. There is no study that determines if camel DPP4 genes have evolved in a similar manner in the presence of MERS-like CoV infections. These studies suggest that pathogenic, MERS-like viruses have been circulating in bats for some time and have only recently transmitted to camels and humans.

It is unclear why long-circulating MERS-like bat CoVs have only recently spread to new hosts. Identifying host factors that facilitate CoV infections may provide an explanation. A partial explanation for the effective transmission of CoVs between host species is the relative flexibility of CoV entry routes, which expands the available entry factors a given zoonotic CoV may utilize. This dissertation focuses on the multiple cellular factors that contribute to CoV entry into host cells. Unlike many enveloped viruses, where membrane fusion occurs at a single, well-defined location, CoVs can participate in entry at multiple locations in the target cell. Recent studies, including our own, have uncovered the subcellular location of these entry events and have characterized both the viral and host-cell factors that determine which route a CoV is likely to take.

Coronavirus Entry.

Coronavirus entry relies on membrane fusion catalyzed by the Spike (S) glycoprotein [39]. The S protein is a class I fusion glycoprotein like the influenza hemagglutinin (HA), human immunodeficiency virus (HIV) gp41, and ebolavirus GP. Trimeric class I fusion glycoproteins are characterized by their helical fusion domains [1, 6, 40]. Upon a triggering event, these helices extend towards the target membrane and embed the fusion peptide. This structure, called the “extended intermediate” [2], was once thought to be unstable but more recent studies of influenza HA [2] and HIV gp41 [41] suggest these structures can exist on the order of minutes, if not indefinitely. In order to complete the fusion process, the fusion intermediate must collapse to bring the

fusion peptide and the viral membrane into close proximity. This process is facilitated by the strong interaction of two helical heptad repeat (HR) regions within the fusion protein [6, 8, 11, 42, 43]. The affinity for these two domains for each other leads to a "zippering" of the extended intermediate onto itself leading to their direct interaction [6, 44]. This process brings together the two membranes and fuses the outer leaflet of each, causing hemifusion. Completion of this rearrangement connects the two HRs of each trimer and forms the final structure called a "six-helix bundle" [44, 45]. The formation of the remarkably thermally stable six-helix bundle coincides with pore formation and it is likely that pore formation requires fusion proteins to form a six-helix bundle. Studies using influenza suggest that 3-6 adjacent glycoproteins must participate in fold-back to provide enough energy for pore formation and six-helix bundle formation [2].

While CoV S proteins share the basic structure and function of other class-I viral fusion proteins, they also have some unique features. CoV S proteins are composed of the S1 domain, which is responsible for receptor binding [46], and the S2 domain, which carries out the fusion reaction [39]. The S1 domain is separated into two further domains, the N-terminal domain (NTD) and the C-terminal domain (CTD), which can participate in binding to target cells using various cellular factors. Generally, the NTD region binds to sugar moieties on target cells [47-50] while the CTD binds proteinaceous receptors [51-53]. Only the NTD of MHV is unique in that it appears to have evolved from binding sugars to binding the protein carcinoembryonic antigen-related adhesion molecule 1 (CEACAM) [54]. The S1 domain also acts as a shield of S2 and keeps the fusion machinery locked in place and free from immune detection (Figure 2) [55].

In order for CoV S proteins to complete fusion, the S1 domain must be shed from the S2 following receptor binding. This process is facilitated by cleavage events that occur at two cleavage sites, the S1/S2 and the S2'. These sites are unstructured regions of the S [56] that generally contain arginine-serine (R/S) sequences that act as targets for cleavage by serine proteases [57-60] and likely contain as-yet unidentified substrates for cysteine proteases [61-63].

A defined cleavage site exists at the interface of the S1 and S2 domains. This S1/S2 cleavage site is exposed in native viruses. Therefore, the site can be cleaved in producer cells [59], in the extracellular space [64], or on target cells following receptor binding. The cleavage at S1/S2 does not remove the S1 domain, as it must remain associated through non-covalent bonds to S2 to facilitate receptor binding, but it allows for more flexibility in the S trimer and primes the virus for the triggering cleavage [65]. While cleavage at S1/S2 does not appear to be strictly required for successful fusion, the extent to which S1/S2 is cleaved drastically affects CoV entry routes (see "Viral Determinants of Entry Routes").

While direct experimental evidence is lacking, cleavage at the S2' site is thought to be the triggering mechanism for CoV fusion [57, 59]. In the native state, the S2' region exists in an alpha-helix on the surface of the S2. Receptor binding causes structural changes to S2 that cause the S2' region to become unstructured and available to cellular proteases [56]. Therefore, proteolytic cleavage of S2'occurs only on receptor-bound viral S (Figure 1) [65, 66]. Cleavage at S2' is presumed to release stored energy, extend the HR regions, and insert the fusion peptide into the target membrane forming

the extended intermediate. Like other class I viral fusion peptides, the extended intermediate zippers to bring the HR1 and HR2 regions together, ultimately leading to the formation of the six-helix bundle [43, 67, 68] and the fusion pore. Likely, as with influenza A virus, fusion occurs only after triggering of multiple adjacent S proteins.

While there are no FDA approved inhibitors of CoV entry, there are several known mechanisms for blocking S-mediated entry. Antibodies can be generated by humoral immune responses and generally bind to S1and prevent CoV binding to cells [69]. While these antibodies are effective in preventing infection, they can drive evolution of escape mutants. Antibodies to the fusion machinery are rare due to burying of these domains in the internal glycoprotein structure. Protease inhibitors can prevent cleavage of S2' by cellular proteases and can be effective in blocking CoV infections in cell culture [70-73]. Furthermore, a recent study using a mouse model of SARS demonstrated that serine protease inhibitors prevent spread of the virus in mice [74]. A broad range of inhibitors may be necessary to prevent infection, due to the flexibility of CoV entry routes (discussed below), which may limit the usefulness of these drugs in clinical settings. Additionally, small peptides corresponding to the HR2 region of the S (Figure 1) can prevent entry by preventing the pore that follows triggering. These peptides take advantage of the strong affinity between HR1 and HR2. HR2 peptides bind to HR1 while the spike is in the extended intermediate conformation. This binding sterically blocks intramolecular HR1 and HR2 interactions and, thus, prevents complete S zippering and six-helix bundle formation [75]. These peptides have limited efficacy because extended S trimers exist for a short time and may only be present in the

endosomal compartment during late entry (Figure 3). Furthermore, as seen with blocking antibodies, HR2 peptide escape mutants have been characterized in MHV [76]. Thus, while there are many potential mechanisms for preventing CoV fusion and infection, none have proven broadly effective.

Entry routes: early vs. late. Generally, enveloped virus fusion occurs at a specific subcellular location in target cells. CoVs, however, show a unique flexibility in the location of the fusion event. CoVs can fuse at the cell surface, in what is called "early entry" [65, 70, 77-79], or in the late endocytic compartment, in what is termed "late entry" [63, 71, 80, 81]. The central principle of CoV entry is that the subcellular location of a sufficient number of S2' cleavages determines which route the virus ultimately uses (Figure 3). Understanding this tenet, we can examine CoV entry based on the cleavage state of CoV S proteins at specific subcellular locations.

Early entry occurs at the cell surface or very soon after endocytosis. Viruses that enter early are cleaved at S2' by cell-surface transmembrane serine proteases (TTSPs) [70, 73, 77, 79, 82, 83] or proprotein convertases [59]. Thus, early entry is susceptible to inhibition by serine protease inhibitors such as camostat and leupeptin. CoV early entry is completely resistant to cysteine protease inhibitors (which inhibit cathepsins) and alteration of the pH in target endosomes. In early entry, fusion can occur at the cell surface [84] in the amount of time it takes for transmembrane proteases to cleave S substrates. This results in a very rapid delivery of the viral genome into the cytoplasm of the cell. Viruses that enter early may bypass innate immune sensors or antiviral effectors that are found in the endosomal compartment [77, 79].

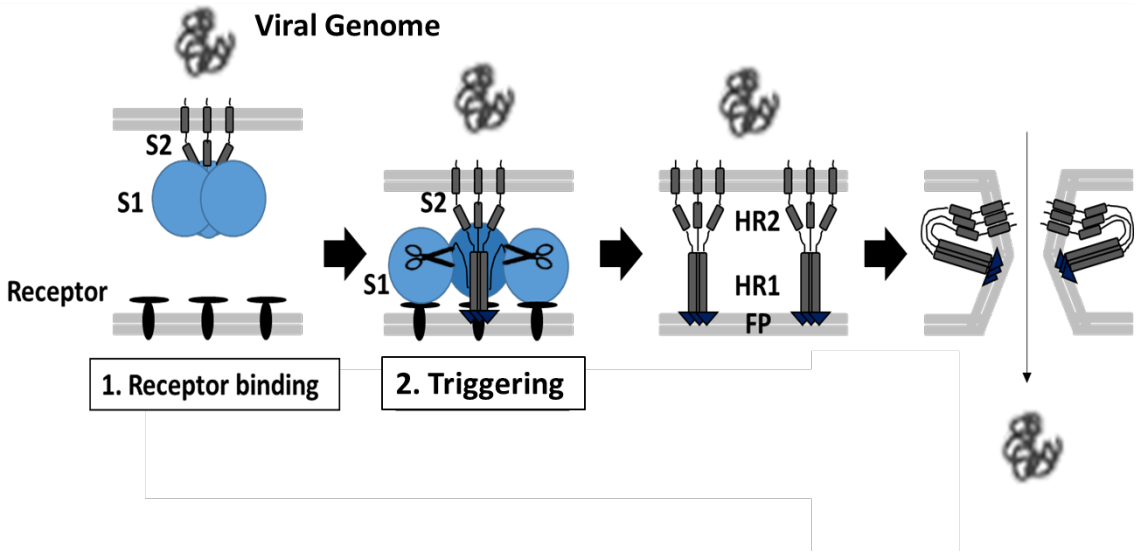

Figure 1. The coronavirus fusion reaction. The structural transitions of CoV S proteins are illustrated proceeding from receptor binding on the left to successful fusion on the right. S1 binds to a receptor on the target cells which induces a conformational in the S, exposing cleavage sites between S1 and S2. Cellular proteases (scissors) then cleave S1 away from the fusion machinery contained in S2. The fusion peptide (FP) inserts into the target membrane anchoring the virus and cell together. The heptad repeat 2 (HR2) then zippers up to interact with the heptad repeat 1 (HR1) bringing the membranes together. The successful refolding of enough adjacent S2s leads to fusion of viral and cell membranes and release of the viral genome into the target cell. Figure adapted from Jung-Eun Park.

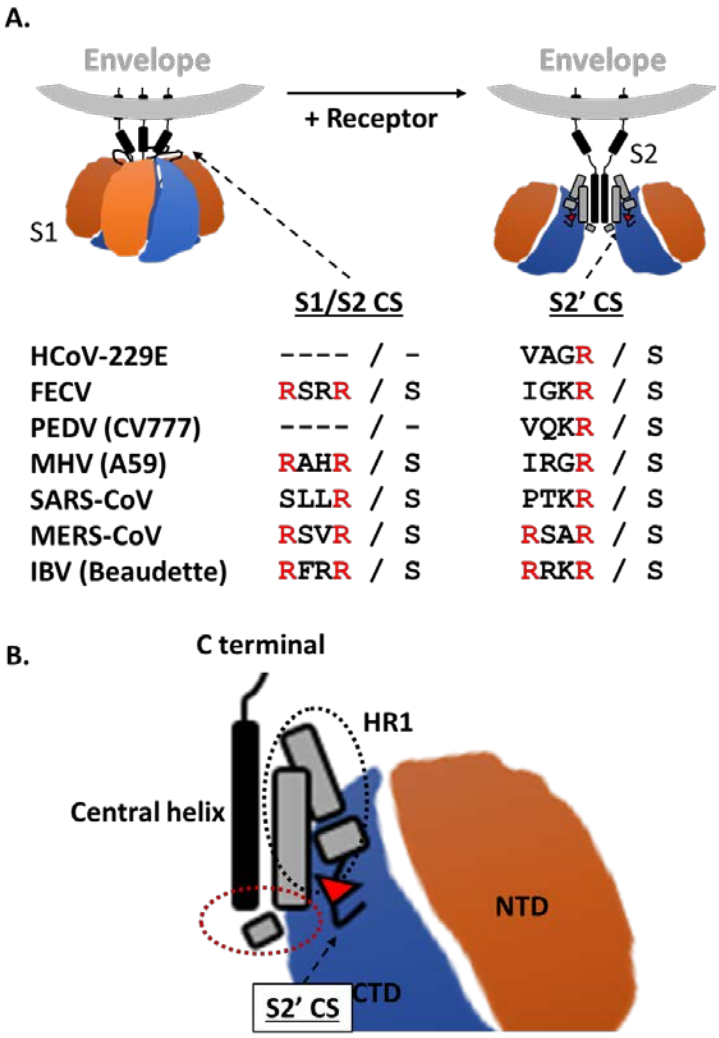

Figure 2. Coronavirus Spike structure and cleavage sites. **(A)** The coronavirus S trimer is depicted in a native (left) and receptor bound conformation with one monomer removed for clarity (right). The S1 domain, represented by the globular head of the S protein, is divided into two regions the N-terminal domain (NTD, orange) and C-terminal domain (CTD, blue). The S1/S2 cleavage site (S1/S2 CS) is shown in its uncleaved, native state and resides in an unstructured region between S1 and S2. The S2' cleavage site (S2' CS) is exposed only after receptor binding and is immediately N-terminal to the fusion peptide (red triangle). The amino acid sequences of S1/S2 and S2' CS of various CoVs are listed below. **(B)** Close-up view of receptor-bound S shows folded conformation of S1 structure before S2' cleavage. The black oval denotes region of the HR1 thought to participate in intramolecular interactions while the red oval indicates the region of the HR1 that interacts with the CTD. Figure adapted from Dr. Jung-Eun Park.

Late entry occurs in the late endosome or lysosomal compartment. Late entry is dependent on cathepsin-mediated cleavage of S2' leading to S2 triggering [57, 61, 63, 71, 73, 80, 81, 85, 86]. Therefore, late entry is indirectly dependent on pH, as a low pH is required for activation of cathepsins [87]. Furthermore, late entry is inhibited by cysteine protease inhibitors such as E64D [65]. Late entry takes a much longer time than entry at the cell surface due to delayed activation of CoV S proteins by endosomal proteases. Indeed, viruses may take more than an hour to successfully fuse when dependent on late entry [85]. While viruses that enter late have a longer time span with which to successfully fuse, they may be exposed to the harsh environment of the lysosomal compartment and encounter a larger amount of innate immune sensors before they complete the entry process. Indeed, over-proteolysis of MERS S proteins leads to non-functional fragments which are incapable of infection [65, 82]. Perhaps because of this, late entry is less efficient than early entry in many *in vitro* [65, 73, 79] and *in vivo* [74] settings.

Viral determinants of entry routes. ***S2' cleavage***. As mentioned above, the S2' cleavage site contains arginine-serine (R/S) sequences that act as targets for serine proteases. Most CoV S proteins contain only a single arginine (R/S) at the S2' site (See Figure 2A), which acts as a somewhat inefficient substrate for PCs and TTSPs at the cell surface. However, some CoV S proteins (e.g., MERS-CoV and infectious bronchitis virus strain [IBV] Beaudette) have multiple arginines arranged in an RxxR/S motif (See Figure 2A). The RxxR/S motif is a classical substrate for proprotein convertases such as furins. Therefore, the S proteins

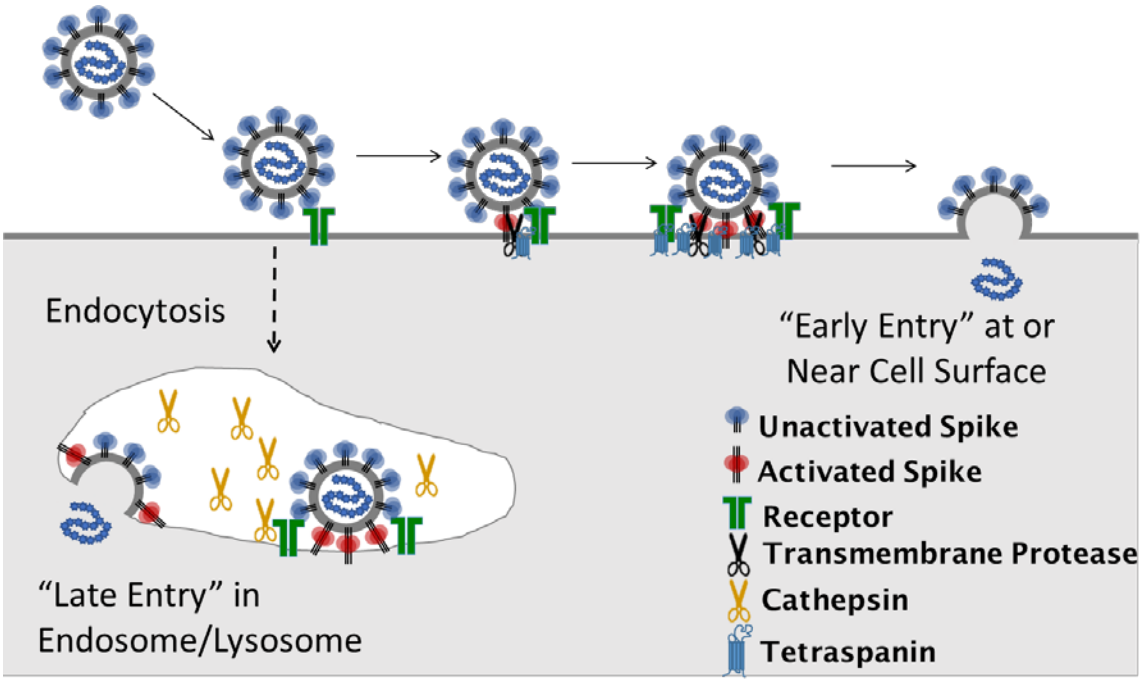

Figure 3. Model of CoV Entry Routes. CoVs enter cells through the cell surface "early" entry route or endosomal "late" entry route depending on which proteases activate the Spike proteins. Early entry depends on complexes of receptors and transmembrane proteases held together by tetraspanin scaffolding proteins. Early entry occurs at or near the cell surface and occurs relatively rapidly. If a CoV S is unable to be cleaved by transmembrane proteases, due to S sequence or target cell protease expression, the virus must undergo endocytosis and be activated by cathepsins in the late endosome/lysosome. This late entry is slower, likely due to the time necessary to cleave a sufficient number of S proteins.

containing RxxR/S motifs have an expanded range of host cell proteases available for S activation [59, 88]. This expanded range is evidenced by the fact that these viruses become significantly resistant to cathepsin inhibitors and bafilomycin A treatment[59, 65, 73].

Reverse genetics experiments have further emphasized the role of the S2' cleavage site in determining entry routes. For example, introducing furin substrate sequences in the S2' site of SARS-CoV, MHV, and PEDV S proteins renders these viruses independent of endosomal cathepsins [58, 80, 84] and more likely to undergo early entry. Furthermore, mutating the RxxR/S motif to SxxG/S renders MERS entry completely dependent on cathepsins and independent of TTSPs (observed by Jung-Eun Park). These results also confirm that there is an as-yet unknown cathepsin cleavage site near the fusion peptide can also act as a triggering target.

S1/S2 cleavage. The S1/S2 cleavage site plays a role in entry route determination in part by determining the stability of the S proteins upon interaction with target cells. Because the S1/S2 site is exposed on native viruses [56], cleavage of S1/S2 can occur in producer cells [59], in the extracellular space [64], or on target cells following receptor binding [70, 89]. The cleavage state of S1/S2 upon encountering a target cell influences the entry route by determining the likelihood of S2' cleavage at the surface or in the endosome. A CoV with a cleaved S1/S2 will be less stable and will more efficiently transition to a state in which the S2' site is exposed [65]. Conversely, a virus with an uncleaved S1/S2 will remain rigid and will either require a higher concentration/specific

activity of target cell proteases to perform the S2' triggering cleavage or would need some other stimulus to destabilize the S and expose the S2' site.

Many CoV S proteins contain a furin substrate sequence at S1/S2 cleavage site (See Figure 2A), thereby S1/S2 cleavage is mostly carried out by furin and related proprotein convertases in the exocytic pathway of virus producer cells [90]. This is the case for most MHV strains, which can participate in both early and late entry events. By contrast, the MHV strain 2 (MHV-2) S lacks this furin substrate site and is secreted from producer cells in an uncleaved state [91]. MHV-2 entry is strikingly more sensitive to inhibitors of endosomal cathepsins [63], which suggests that MHV-2 enters cells late. These data support the conclusions of Park et al. that a change in the S1/S2 sequence can determine the entry route of related viruses.

Like MHV-2, SARS-CoV is produced with an uncleaved S protein. However, studies indicate that SARS-CoV S proteins can be proteolyzed by extracellular proteases such as trypsin and elastase [64]. Cleaving SARS S by these extracellular proteases or reverse genetics inclusion of furin substrate sequences at S1/S2 cleavage site facilitated SARS-CoV entry in target cells, including lung like epithelial cells [57, 65]. These data suggest that the efficiency of serine protease cleavage of S1/S2 can affect CoV cell tropism.

Recent experiments with MERS-CoV have reinforced the importance of S1/S2 on cell tropism and infection. Like MHV, the MERS S protein contains a furin substrate site at S1/S2 and is cleaved in producer cells [65, 92]. S1/S2 cleavage renders MERS viruses

capable of infecting cells through both early and late entry pathways. However, removal of furin-mediated S1/S2 cleavage sites limits virus entry to only those cells that contain sufficient amounts of endosomal proteases and renders the viruses unresponsive to TTSP expression[65]. This is important, because the lung cell types known to be infected by MERS-CoV have relatively low expression of the priming cathepsin L [65, 73, 93]. These data suggest that the relative stability of S proteins upon encountering target cells is an important determinant of CoV entry routes.

S1 domain. The S2' cleavage site can only be exposed following receptor binding by and shedding of the S1 domain [65, 94, 95]. Importantly, many residues in S1 domain form interactions with S2 domain, which stabilize the S proteins and prevent abortive activation of the fusion reaction. A recent structural study of a human coronavirus HKU1 S protein highlighted the interaction between residues in the HR1 and the S1 domain in the pre-fusion structure (Figure 2B) [56]. Mutations of these residues could potentially lead to destabilization of the S protein and increased utilization of early entry routes.

A recent study may provide insights into the possibility of S stabilizing interactions determining viral entry routes. Several amino acid differences were identified in the S1 domain of HCoV-229E clinical isolates compared to a cell-culture adapted lab strain [79]. Two of these mutations (R642M and N714K) correlated with a decreased reliance on cathepsin proteases and an increased utilization of TMPRSS2 *in vitro*. Furthermore, upon passage in TTSP-poor cells the viruses gained a second site mutation (I577S) to reacquire the ability to utilize cathepsins. The nature of this

mutation, from a nonpolar to a polar amino acid, suggests that intramolecular interactions may play a role in determining protease utilization. Interestingly, all of these mutations occurred in the CTD which is thought to participate in many stabilizing intramolecular interactions.

Cellular determinants of entry routes. Recent studies indicate that early entry of CoVs requires coordination of several cellular proteins at the cell surface [96]. CoV S proteins must be cleaved by transmembrane proteases while attached to a receptor in order to successfully complete the fusion reaction [65, 94, 95]. Furthermore, it is likely that many adjacent S proteins must be cleaved for fusion pore formation, as seen with other class I viruses [2]. This means that cellular receptors and activating proteases must reside in close proximity on the cell surface and with a high enough concentration/activity to trigger multiple adjacent S proteins. Thus, early entry is dependent on the close proximity and concentration of receptors and transmembrane proteases. Unlike membrane-anchored TTSPs, cathepsins are soluble proteases. Thus, activating cleavage of S proteins by cathepsins is dependent mainly on their concentration/specific activity instead of their precise localization.

CoV receptors. The first step in CoV entry is virion attachment to target cells. CoVs can attach to a diverse array of transmembrane anchored molecules. While some CoVs, such as the Betacoronavirus HCoV-OC43 and the Gammacoronavirus infectious bronchitis virus (IBV), bind to sugar moieties on membrane proteins [97, 98], the majority of CoVs bind proteinaceous receptors. Indeed, receptors are the primary determinant of target cell susceptibility to a CoV. While there is no evidence that

receptors directly determine CoV entry routes, it is also apparent that CoVs utilize specific proteinaceous receptors for reasons that go beyond simply binding to cells. Indeed, there are interesting findings that suggest that CoVs evolve to use receptors that can facilitate **early** entry.

There appears to be little structural conservation among CoV receptors and even related CoVs can use drastically different receptors. For example, the Betacoronaviruses SARS and MERS use the zinc peptidase angiotensin converting enzyme 2 (ACE2) [99] and the unrelated serine peptidase dipeptidyl peptidase 4 (DPP4) [100] as receptors, respectively. Conversely, distantly related CoVs have convergently evolved to use the same receptor. The Alphacoronavirus HCoV-NL63, which is phylogenetically distant from SARS-CoV, uses ACE2 [101] as a receptor. Furthermore, HCoV-NL63 binds at a different domain of ACE2 than SARS, which suggests convergent evolution of the two viruses as opposed to a shared ancestry [102].

The diversity of CoV receptor usage along with evidence of convergent evolution suggests that the viruses select receptors based on common properties. One common theme is that, with the exception of the MHV receptor CEACAM, all the CoV receptors (ACE2, DPP4 and aminopeptidase N [APN]) are peptidases. Interestingly, the catalytic activity of these peptidases is dispensable for CoV entry in all cases [99, 100, 103]. Thus, there is a property of these receptors that is important for CoV entry that is distinct from their peptidase function.

The subcellular locations of transmembrane peptidases are thought to be tightly regulated [104], as mislocalization can lead to a number of disorders [105]. Thus, it is likely that cell-surface peptidases are held in protease-rich regions of the cell that could facilitate close interaction of the receptor and an activating protease. Indeed, multiple CoV receptors have been shown to interact with tetraspanin partner proteins (discussed below) along with transmembrane serine proteases [96]. Thus, the driving factor for CoV utilization of receptors may be their ability to form complexes with scaffolding proteins and priming proteases.

Cellular Proteases. Producer and target cell proteases are the most important factor in determining the route of CoV entry. As discussed above, host proteases can cleave CoV S proteins in producer cells, in the extracellular space, and/or on the target cell. The abundance and identity of the different proteases present in producer cells and target cells can influence the entry route of an incoming CoV.

Cleavage of the S1/S2 site can occur in the producer cells during transit of nascent virions through the trans-Golgi network [57, 59]. These cleavages are performed largely by proprotein convertases, especially furin. These proteases cleave at the S1/S2 interface of the S protein (Figure 2) and generally destabilize the S. As discussed above, this destabilization is thought to facilitate early entry events [57, 65], likely by more rapidly exposing the S2' cleavage sites to target cell transmembrane proteases. MERS viruses produced in cells that lack furin activity enter target cells less efficiently and with a greater dependence on cathepsins [65]. Thus, furin activity in producer cells correlates

with CoV early entry. Interestingly, proprotein convertases can also cleave incoming CoV S proteins and may be potent facilitators of early entry [59].

The most important classes of proteases for early entry are the members of the type two serine protease (TTSP) family. The TTSPs are a family of at least 17 transmembrane serine proteases that are active at the cell surface [106]. While many TTSPs are theoretically capable of functioning as CoV activating proteases, the best studied is the transmembrane protease serine 2 (TMPRSS2) which is important for the entry of multiple CoVs [70, 73, 77, 82, 83, 107, 108]. TMPRSS2 performs the activating cleavage at S2', but only does so efficiently when encountering viruses already cleaved at S1/S2 [65]. Viruses that are activated by TMPRSS2 bypass the late entry pathway and likely fuse at or near the cell surface. The subcellular location of these proteases is tightly regulated [105, 108, 109] due to potential damaging effects to organisms upon mislocalization of transmembrane proteases [105]. Therefore, TTSPs are sequestered to protease-rich membrane domains, likely enriched with tetraspanins, and may be scarce elsewhere on the membrane [96].

Cathepsins are a class of proteases that are active in the late endosome/lysosomal compartment [87] and are necessary for CoV late entry. The most important cathepsins for CoV entry are the cysteine proteases cathepsin B and cathepsin L [62, 65, 81]. The triggering cleavage performed by cathepsin is presumably in a region nearby the serine protease cleavage sites [57, 61, 65]. MERS-CoV includes three putative cathepsin cleavage sites N-terminal of the S2' and multiple sites in the vicinity of S1/S2 [65].

Because cathepsins are soluble, they may be able to access receptor bound S proteins more efficiently than the serine proteases that are embedded in the membrane.

The relative expression levels of TTSPs and cathepsins in target cells have been experimentally shown to influence the entry of CoVs. For example, MERS entry into the TTSP-rich, but cathepsin poor Calu3 cell line is highly susceptible to serine protease inhibitors but completely resistant to cathepsin inhibitors. Furthermore, a MERS mutant with an S1/S2 mutation that prevents early entry was unable to efficiently enter these cells. Similar results were seen with primary human airway epithelial cells, which supported early entry but not late entry [65]. Many groups have observed disparate expression of TTSPs and cathepsins in different cell lines and animal models. Cell lines used for the isolation and testing of CoVs generally have lower TTSP expression than primary cells and tissues, with the few exceptions being lung-cell derived cell lines like Calu3 [65] and lung epithelial type 1 (LET1) cells [110]. This is likely due to the fact that a high level of TTSP expression is harmful to cells *in vitro* [111]. Consequently, viruses passaged in cell culture tend to favor late entry when compared to clinical isolates. This is the case for HCoV-229E, for which clinical isolates enter cells more rapidly and are more dependent on TTSPs than cell culture adapted viruses [79]. Furthermore, cell culture adaptation may select for CoVs with more stable S proteins as these viruses may be more likely to survive passaging. Without the selective pressures imposed on CoVs by *in vivo* infections, the stability of the S proteins may be the most important evolutionary factor. Thus, cell culture adaptation may drive evolution of CoVs to accumulate mutations associated with late entry.

Tetraspanins. Recent reports have shown that these entry co-factors must be held in close proximity by membrane scaffolding proteins called tetraspanins [96]. Tetraspanins (described below) act as scaffolds and hold CoV receptors and TTSPs in close proximity at the cell surface. Thus, tetraspanin-rich regions on the cell surface act as early entry portals for CoVs. Tetraspanins are known to influence the entry of MHV, SARS, 229E, and MERS, indicating that tetraspanin utilization is a common feature of CoV entry.

Cholesterol. Membrane cholesterol facilitates the entry of multiple CoVs [112-116]. While the specific function of cholesterol in CoV entry is unknown, it is likely that cholesterol is present in the membranes with which CoV fusion occurs. Cholesterol is present in lipid rafts that may facilitate the interactions of tetraspanin scaffolding proteins with their CoV-receptor partners (discussed below). Therefore, cholesterol may promote early rather than late entry.

Tetraspanins.

Tetraspanins (see Figure 4) are a highly evolutionarily conserved family of transmembrane scaffolding proteins that are the focus of this dissertation. There are 34 identified tetraspanins in humans, 35 in mice, and 27 in *Drosophila*. The tetraspanin protein family dates back to the last common ancestor of amoebae, plants, and metazoans [117]. The sequence conservation of tetraspanins suggests an essential role for these proteins in regulating cell membrane processes and facilitating multicellularity. Indeed, tetraspanins form homo- and hetero-interactions with other tetraspanin proteins as well as

specific interactions with transmembrane partner proteins. These interactions lead to a complex "web" of tetraspanin-mediated interactions between transmembrane proteins (Figure 5). The study of tetraspanins encompasses diverse fields such as signal transduction, oncology, reproduction, and of course virology.

Tetraspanin structure. Members of the tetraspanin family are highly conserved structurally. Tetraspanins are small, 200-300 amino acid proteins that protrude 3-5 nm from the membrane. As the name implies, each protein has four helical transmembrane domains that are connected by a short extracellular loop (13-30 amino acids), a very small intracellular loop, a large-extracellular loop (LEL) and short N- and C-terminal cytoplasmic tails (Figure 4) [118]. Most of the variation observed among members of the tetraspanin family is in the LEL. The LEL varies in length, sequence, and structure and is the main antigenic determinant of the different tetraspanins [119].

The transmembrane (TM) domains are left-handed coiled coils that form a "cone" in the membrane that tapers on the cytoplasmic side [118]. These domains are the most highly conserved regions in the protein, which suggests they play an important role in tetraspanin functions. Indeed, it is likely that the majority of tetraspanin-tetraspanin interactions are facilitated by the TM domains. Evidence for this is given by experiments that showed the CD151 with the LEL removed still associated with other tetraspanins [120]. The 4 TM domains are numbered I-IV starting at the N-terminal TM domain. The TM domains interact with each other in a specific manner, with I binding to II and IV at different faces and so on (Figure 3, right). Conserved, polar residues in the TM regions facilitate the homo- and hetero- interactions of tetraspanin proteins (Figure 5, left)[121].

Furthermore, TM I is necessary for tetraspanins to leave the endoplasmic reticulum and can perform this function without being covalently linked to the rest of the tetraspanin molecule [122].

Zimmerman et al.'s 2016 structural study of CD81 discovered that the four TM domains favorably form an interaction with a single cholesterol molecule (Figure 4, right). The presence or absence of a cholesterol molecule between the four TM regions affected not only the structure of the LEL, but also its ability to bind a partner protein. CD81 starved of cholesterol exhibits an "open" conformation in the LEL which was

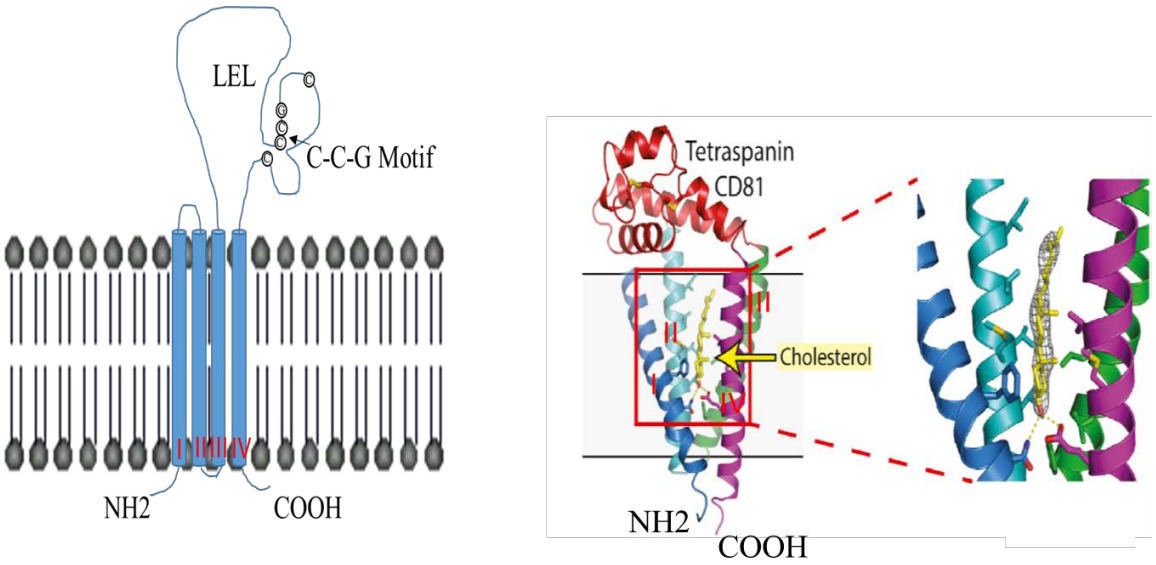

Figure 4. Structure of a tetraspanin protein. A tetraspanin protein consists of 4 helical transmembrane (TM) domains (labeled from N-terminal to C-terminal I-IV in red) connected by short sequences of amino acids. TM domains I and II are connected by the short extracellular loop while TM domains III and IV are connected by the large-extracellular loop (LEL). The LEL is largely characterized by secondary protein structures formed by intraloop interactions which are commonly facilitated by cysteines (C). A common intraloop interaction is the C-C-G motif depicted on this tetraspanin. A ribbon structure for the tetraspanin CD81 shows how the TM domains surround a single cholesterol molecule (yellow). Structure work was done by Zimmerman et al, 2016).

shown to decrease binding to a transmembrane partner protein. Thus, tetraspanin interactions can be regulated by altering the local concentration of cholesterol in the membrane.

Adjacent to the TM domains are several conserved cysteine residues that are palmitoylated under normal conditions [123, 124]. Palmitoylation of tetraspanins facilitates hetero- interactions with other tetraspanins family members. Tetraspanins produced in the presence of 2-bromopalmitate, which prevents palmitoylation, were much more likely to form homodimers in the trans-Golgi network. Interestingly, there are conflicting reports regarding whether palmitoylation affects tetraspanin interactions with non-tetraspanin partner proteins [125, 126]. These disparate results suggest that tetraspanin-partner protein interactions are facilitated by TM domains as well as other domains.

The LEL is the most variable region of the tetraspanin proteins. Structural studies of CD81 reveal the LEL to consist of multiple helices connected by unstructured regions [118]. Three of these helices are conserved among tetraspanins while two are variable. The conserved helices are found at the N- and C-terminal regions of the LEL and the folded loop structure mostly contains the variable helices. All LELs contain 2-4 cysteine pairs that participate in a disulfide bond across the loop and are necessary for proper folding of the LEL (Figure 4, left) [127]. One of these pairs is a 100% conserved CCG motif that is a defining feature of tetraspanin proteins.

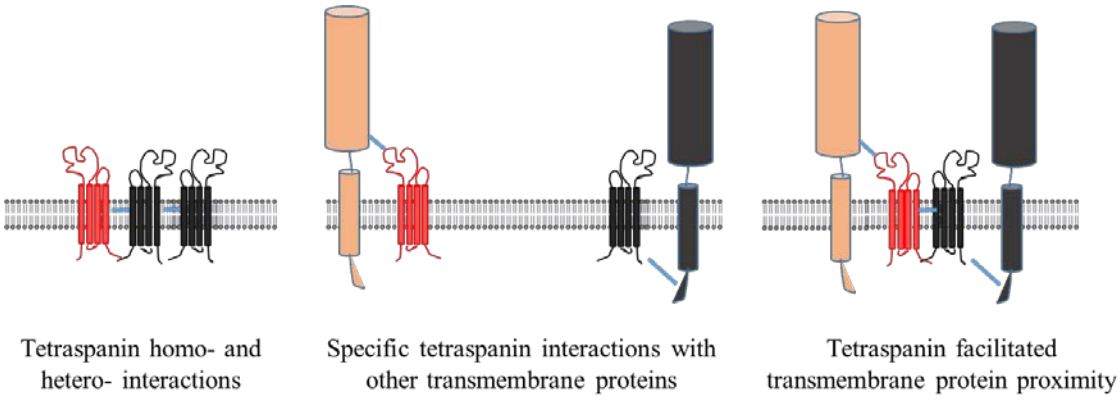

Figure 5. Tetraspanin interactions with transmembrane proteins. Tetraspanins are small 4-pass, integral membrane proteins that act as scaffolds for many transmembrane proteins. A given tetraspanin can form a homodimer with a like tetraspanin or participate in hetero- complex formations (left). Tetraspanins likely form homo- and hetero- interactions with each other via regions in the transmembrane helices. Tetraspanins also form specific interactions with various transmembrane proteins (middle). Tetraspanins generally interact with transmembrane partners through their extracellular loop structures or cytoplasmic tails. Tetraspanins that are interacting simultaneously with specific transmembrane proteins and other tetraspanins can form important protein complexes (right). These complexes may be useful for keeping proteins in the same signaling pathway in close proximity or for concentrating cellular factors.

Several studies have suggested that the LEL is important for tetraspanin interactions with partner transmembrane proteins. For example, the $_{194}$QRD$_{196}$ residues in the LEL of CD151 are necessary for its interaction with integrins at the cell surface [128]. The location of this domain, on an outward face of one of the LEL variable helices, corresponds with a putative CD9-pertner interacting motif that is responsible for sperm-egg fusion [129]. LELs are also important attachment points for pathogens that bind to tetraspanins. For example, the hepatitis C virus directly binds the LEL of CD81 during

its entry process [130]. Similarly, plasmodium parasites bind to the conserved region of the CD81 LEL, but not CD9 [131]. These studies suggest very specific interactions between pathogens and tetraspanin LEL regions.

Tetraspanin microdomains. A common theme of early tetraspanin research has been that tetraspanins interact with multiple other tetraspanins and partner proteins to form complex, semi-stable membrane microdomains at the cell surface. The evidence for these tetraspanin-enriched microdomains (TEMs) has come primarily from co-immunoprecipitation, cross-linking, and isolation of tetraspanin-rich membrane fractions following detergent solubilization of cells. Solubilization in certain zwitterionic detergents like CHAPS and Brij99 can conserve membrane fractions enriched in tetraspanins and associated proteins [132]. However, non-ionic detergents such as Triton X-100, which are commonly used to isolate lipid rafts, ablate tetraspanin interactions. This is one of the defining features of tetraspanin-enriched membranes and separates them from lipid rafts [133]. Zwitterionic detergents likely maintain tetraspanin-partner protein interaction as well as the hydrophobic interaction within the TM domains shown to be important for tetraspanin-tetraspanin clustering [134]. However, isolation of detergent resistant membranes does not allow for the analysis of tetraspanin dynamics in the plasma membrane of a living cell.

Two studies, using single-molecule microscopy, have examined the nature of tetraspanin interactions at the cell surface in intact cells. The first, performed by Espenel and colleagues in 2008, concluded that single tetraspanin proteins cycle between tetraspanin-rich areas and the rest of the membrane. While in the general membrane, the

CD9 molecule exhibits Brownian diffusion, but decreased diffusion rates were observed within the tetraspanin rich area. Building on this work, Zuidscherwoude and colleagues used stimulated emission depletion microscopy to trace the fate of multiple tetraspanins on the surface of living cells. They found clusters of 3-4 tetraspanins forming homo-interactions (e.g. CD9-CD9 interactions) and interactions with partner transmembrane proteins with very little direct interaction with other tetraspanin family members. Together, these results suggest that tetraspanin interactions are less heterotypic than previously thought. Therefore, for the purposes of this dissertation, TEMs will be defined solely as detergent-solubilized membrane fractions and not necessarily reflect intact, native tetraspanin complexes found at the cell surface.

Fluorescence resonance energy transfer (FRET) and proximity ligation assays (PLA) are valuable tools for examining tetraspanin-mediated interactions beyond single molecules *in situ*. FRET analysis can be valuable in identifying homo- and hetero-typic tetraspanin interactions as well as confirming specific tetraspanin partner proteins. However, FRET analysis has been inefficient in identifying partner protein complexes formed by tetraspanins. Because partner proteins held together by tetraspanins do not generally directly interact, the distance between the proteins prevents FRET. PLAs provide a tool to investigate tetraspanin-mediated interactions that are not detected by FRET. In PLAs, antibodies differentially tagged with oligonucleotide probes are applied to cells, and their close spacing (<40 nm) allows for probe hybridization into DNA polymerization templates [135], which provide a locus point for fluorescent DNA synthesis [136]. These assays have been used to detect tetraspanin interactions with

partner proteins [137, 138] and presumably can identify partner proteins that are held in close proximity by tetraspanins.

General tetraspanin functions. Many roles have been described for tetraspanin proteins in both cell culture and animal models. The majority of these roles involve holding two or more cellular proteins in close proximity at the cell surface. Tetraspanins do this by forming a "web" of interactions between transmembrane partner proteins and other tetraspanins (Figure 4). Dysregulation of tetraspanin expression or localization can lead to observable phenotypes (Table 1) and serious health problems in both humans and mice. Through study of these phenotypes, tetraspanin proteins have been shown to be important regulators of cell mobility, adherence, cell to cell signaling, apoptotic events, membrane fusion events, and adaptive immune responses.

The most interesting functions of tetraspanin proteins for our studies is the role that tetraspanins play in regulating the localization and activity of transmembrane proteases. An example is the interaction between CD9 and the transmembrane metalloprotease A disintegrin and metalloprotease 17 (ADAM17). It was observed that CD9 expression negatively regulates the proteolytic activity of ADAM17, leading to decreased shedding of tumor necrosis factor α and intercellular adhesion molecules [139]. Furthermore, the tetraspanin CD151 negatively regulates the proteolytic activity of matrix metalloproteinase 1 leading to a decrease in degradation of the extracellular matrix [140]. A more recent study was the first to identify an interaction between a tetraspanin, CD81, and a proprotein convertase, subtilisin/kexin type 9, at the cell surface [137].

These observations have important implications for enveloped virus entry that depends on concentrated cell-surface proteases.

Tetraspanin function in viral infections. Several virus infections are facilitated by tetraspanins. These viruses include the myxoviruses influenza A virus (IAV) [141] and canine distemper virus (CDV) [142]; the retroviruses HIV [143, 144], feline immunodeficiency virus (FIV) [145], and human T-lymphocytic virus 1 (HTLV-1) [146]; herpes simplex virus 1 (HSV-1) [147]; the hepatitis C virus [148]; and several human papillomavirus (HPV) subtypes [149]. In these infections, tetraspanins facilitate viral entry (CoVs, IAVs, HCV, HPVs) syncytia formation (CDV, HIV, FIV, HTLV-1), or promote viral exit (IAVs, HSV-1 and HIV). Many of the functions of the tetraspanins described in these studies is to form complexes of cellular proteins that facilitate viral infection.

Perhaps the best studied example of a tetraspanin that facilitates viral entry is CD81. CD81 acts as a co-receptor for the HCV E2 protein [130]. CD81 also links HCV co-receptors scavenger receptor class B I (SR-BI) [148] and claudin-1 [150] into a complex necessary for viral endocytosis (reviewed in [151]). Thus, CD81 acts as both a co-receptor and a scaffolding protein holding multiple HCV entry factors together.

Organism	Phenotype	Source
Mouse aortic smooth muscle cells KO	Increased migration	Scherberich et al, 2002
Mouse monocyte KO	Increased number of nuclei in multinucleated giant cells upon ConA stimulation	Takeda et al, 2003
Mouse axoglial paranodal junction KO	Disrupted junction attachment, abnormal myelin formation	Ishibashi et al, 2004
Mouse KO	Reduced number and size of granulomas in liver following P. acnes infection of liver. Reduction of TNFa, IFNy	Yamane et al, 2005
Mouse Oocyte KO	No fusion, decrease in microvilli formation and size	Runge et al, 2007
Mouse DCs KO	Decreased association of heterologous MHC II molecules	Unternaehrer et al, 2007
Mouse KO	Decreaed expression of EWI proteins on oocyte surface	He et al, 2008
RAW264.7 KO	Decreased motility	Takeda et al, 2008
Raw264.7 KO, BMDC KD	Increased expression of TNFa, matrix metalloproteinase 2 and 9, CD14, TLR4. Decreased IkBa. Enhanced Mphage infiltration	Suzuki et al, 2009
Mouse KO	Decreased exosome secretion from dendritic cells, downregulation of Wnt signilang pathway	Chairoungdua et al, 2010
Mouse KO	Increased metasis of prostate cancer to liver, but not lungs	Copeland et al, 2013
Human small cell lung cancer KD	Downregulation of calretinin, decreased apoptosis	He et al, 2013
Mouse lymphatic endothelial cells	Decreased lymphangiogenesis (migration and proliferation)	Iwasaki et al, 2013
Mouse macrophages KO	Decreased anti-inflammatory effect of statins,	Jin et al, 2013
HeLa Cells KD	Decreased susceptibility to MERS pp transduction	Earnest et al, 2014 (Mike Hantak performed expts)
293T and HeLa Cells KO	Decreased susceptibility to MERS and 229E infection, mislocalization of DPP4 and APN	Unpublished results
C57Bl6 Mouse KD	Decreased susceptibility to MERS infection	Unpublished results (Kun Li)

Table 1. Phenotypes of CD9 deficient organisms. List of experimental knockdown (KD) and knockouts (KO) of the tetraspanin CD9 in cell lines and mice. While CD9 deficiency is not lethal, there are a wide variety of defects in these organisms. These studies suggest that CD9 is important in a wide array of cellular functions including, but not limited to, motility, attachment, signaling, fusion events, and proliferation.

Another example of a tetraspanin facilitating virus entry is the tetraspanin CD151's role in HPV infection. While CD151 acts as an HPV entry factor, it does not directly interact with the virion itself (reviewed in [152]). CD151 and CD63 hold growth factor receptors and integrins together at the cell surface. These proteins are co-receptors for HPV and these complexes are necessary for HPV endocytosis [149].

Two recent screens have shown that the tetraspanin CD81 is an important entry factor for influenza A viruses [153, 154]. In both cases, CD81 was knocked down in target cells before infection with IAV. In both cases, IAV entry into these cells was significantly inhibited. Further studies showed that CD81 was important for both entry and egress of IAV, but the mechanism by which CD81 facilitates these events was unknown [141]. That tetraspanins play a role in the entry process of enveloped viruses expressing type I viral fusion proteins led us to consider if tetraspanins may play a role in CoV S mediated entry.

Purpose of Dissertation.

A review of the literature shows that CoVs depend on multiple host cell factors in order to successfully enter target cells. Of these factors, receptors, transmembrane proteases, and cathepsins have been identified and characterized. However, the mechanisms by which receptors and transmembrane proteases interact on the cell surface remains unknown. Productive, fusion triggering cleavage only occurs when an S protein is bound to a receptor on the cell surface. How this occurs is not clear because the expression and localization of transmembrane proteases is tightly regulated. Our goal was to identify additional cellular factors that might be necessary to facilitate this interaction and promote CoV early entry. Understanding their functions as scaffolding proteins, we hypothesized that tetraspanins are responsible for holding CoV receptors and priming proteases together at the cell surface and this action is required for efficient early entry. Our results are the first to show that CoV early entry is dependent on tetraspanins

and that CD9, specifically, interacts with DPP4 and APN and is necessary for MERS and 229E early entry routes.

CHAPTER II

EXPERIMENTAL METHODS

Cells.

Human embryonic kidney HEK cells 293T and 293β5 and MDCK cells were maintained in Dulbecco's modified Eagle's medium (DMEM) (Thermo Scientific) supplemented with 10% fetal bovine serum (FBS; Atlanta Biologicals), 1X non-essential amino acids, 10 mM HEPES, 1 mM sodium pyruvate, and 100 U/ml penicillin-streptomycin solution (Thermo Scientific). DBT cells were maintained in minimal essential media (MEM) supplemented with 10% tryptose phosphate broth, 5% FBS, 100 U/ml penicillin-streptomycin, and 2 mM L-glutamine. LET-1 cells were obtained from BEI Resources and were maintained in DMEM supplemented with 10% FBS, 100 U/ml penicillin G, and 100 μg/ml streptomycin. Cells were maintained in a humidified environment at 37^{o}C and 5% CO_2.

Plasmids.

Codon-optimized MERS S containing sequences for a C-terminal C9 epitope tag was purchased from Genscript and subsequently cloned into pcDNA3.1+ between the *EcoRI* and *NotI* restriction sites. pcDNA3.1-229E-S-C9 and pcDNA3.1-hAPN plasmids were provided by Dr. Fang Li, University of Minnesota. pcDNA3.1-SARS-S-C9 and pcDNA3.1-ACE2-C9 plasmids were provided by Dr. Michael Farzan, Scripps Research Institute. pcDNA3.1-HA5-QH-trypsin site was provided by Dr. Lijun Rong, University of Illinois-Chicago, and is previously described [155]. The pHEF-VSV-G plasmid was

obtained from BEI Resources. pcDNA3.1-murine carcinoembryonic antigen-related cell adhesion molecule (mCEACAM) was described previously [116]. C-terminal FLAG-tagged human DPP4 plasmid pCMV6-Entry-hDPP4 (NCBI Reference Sequence NM_001935) was purchased from OriGene. pCAGGS-TMPRSS2-FLAG and pCAGGS-TMPRSS2-S441A-FLAG were previously constructed [156]. pCMVSport6-human CD9 was purchased from Open Biosystems. pSpCas9-BB-2A-puro was a gift from Feng Zhang (Addgene plasmid # 52961). CD9 and scramble control shRNA constructs flanked by the U6 promoter and a RNA Polymerase III stop sequence were engineered into the pUC57 vector by Genescript. The pNL4.3-HIVluc plasmid was provided by the NIH AIDS Research and Reference library. p [redacted]Cherry [157] was provided by Dr. Edward Campbell, Loyola University Chicago.

Antibodies.

Monoclonal mouse antibodies against CD9 (clone M-L13), CD63 (clone H5C6), and CD81 (clone JS-81) were obtained from BD Pharmingen. Rabbit anti-FLAG and anti-β-actin-HRP antibodies were obtained from Sigma Aldrich. Mouse anti-rhodopsin (C9) antibodies were obtained from Millipore. Rabbit anti-CD13 (APN) antibodies were obtained from Abcam. Mouse anti-CD26 (clone M-A261) was obtained from BD Biosciences. Rabbit anti-TMPRSS2 (clone EPR3681) was obtained from Abcam. Mouse anti-calnexin antibodies were obtained from Cell Signaling. A mouse monoclonal antibody to IAV H1 HA (clone PY102) was provided by Dr. Balaji Manicassamy, University of Chicago. Secondary antibodies were purchased from Invitrogen and include goat-anti-rabbit-AlexaFluor 488, goat-anti-mouse-AlexaFluor 488, and goat-anti-

mouse-AlexaFluor 568. Donkey-anti-goat, goat-anti-mouse, and goat anti-rabbit HRP conjugated antibodies were purchased from Thermo Scientific.

Viruses.

Influenza A/Puerto Rico/8/1934 H1N1 (PR8) containing a *Gaussia* luciferase (Gluc) reporter gene [158] was provided by Dr. Peter Palese, Mount Sinai School of Medicine. PR8-Gluc stocks were produced using a standard protocol [159]. Briefly, MDCK cells were inoculated with PR8-Gluc, and incubated in DMEM supplemented with 0.2% BSA. 30 hours post infection (hpi), progeny were collected, treated with TPCK-trypsin (Sigma), and used to infect fresh MDCK cells at MOI =1. Supernatants were then collected, clarified by centrifugation, aliquoted and stored at -80^{o}C. Two strains of recombinant mouse hepatitis viruses (MHV), MHV-A59 and MHV-JHM , each containing a firefly luciferase (Fluc) reporter gene, were produced and titered on DBT cells as described previously [160].

Pseudoviruses.

VSV – based pseudovirus particles (pp) were produced by the methods of Whitt, 2010 [161]. Briefly, 293T cells were transfected with plasmids encoding indicated viral glycoproteins. Two days later, cells were inoculated for 2 h with VSVΔG-luciferase [161], rinsed extensively and incubated for one day. Supernatants were collected, centrifuged at 800 x g for 10 min to remove cellular debris, and stored in aliquots at -80^{o}C. HIV – based pp were produced as previously described [157]. Briefly, 293T cells were co-transfected with pNL4.3-HIV-luc and pcDNAs encoding appropriate glycoproteins, and where indicated, p[illegible]-SIGnL-mCherry was also co-transfected.

After two days, supernatants were collected, centrifuged at 10,000 x g at 4ºC for 10 min to remove cell debris, and stored in aliquots at -80ºC.

Infection in the Presence of Tetraspanin Antibodies.

DBT cells or 293β5 cells were transfected with appropriate plasmids encoding viral receptors or proteases, divided into 96-well cluster plates, and incubated for 30 min at 37ºC with indicated antibodies, at 0.12 µg/µl (~10^7 antibodies / cell). Indicated viruses were then added for 2 h at 37ºC, then cells were rinsed, incubated at 37ºC for 6 h (MHV and PR8), 16 h (VSV), or 48 h (HIV). For PR8, cells were not lysed, and media were analyzed for secreted Gluc. For the other viruses, cells were lysed in passive lysis buffer (Promega). Luciferase levels in media or lysates were measured after addition of either Fluc substrate (Promega) or Gluc substrate (New England Biolabs) using a Veritas microplate luminometer (Turner BioSystems).

Flow Cytometry.

To measure antibody binding, 293β5 cells were lifted with Accutase (Millipore), pelleted and resuspended to 10^6 cells/ml in phosphate buffered saline (PBS) supplemented with 2% FBS containing indicated antibodies at 0.12 µg/µl. After 30 min at 37ºC, cells were rinsed thrice by pelleting and resuspension in PBS-2% FBS, then incubated for 30 min at 4ºC with AlexaFluor 488 – conjugated donkey-anti-mouse IgG. After sequential rinsing, cell fluorescence was detected using a BD C6 Accuri flow cytometer. To measure HIV pp binding, 293β5 cells, transfected with empty pCMV6 or with pCMV6-Entry-hDPP4, were suspended in PBS-2% FBS. Cells were divided and aliquots were incubated for 30 min at 37ºC with tetraspanin antibodies at 0.12 µg/µl.

Cells were chilled, then incubated for 1h on ice with HIV-mCherry-MERS S. Cells were rinsed thrice by pelleting and resuspension, and mCherry fluorescence detected using a BD C6 flow cytometer. All flow cytometric data were analyzed using FlowJo software.

Fluorescence Activated Cell Sorting.

DBT cells were transfected with 0.5 μg of pEGFP, and a total of 4 μg of a pCAGGS empty vector or TMPRSS2 plasmid per 10^6 cells. 24 h after transfection, cells were lifted with trypsin, washed 3 times with cold PBS supplemented with 2% FBS, and sorted using a BD Biosciences FACSAria cell sorter. Live, GFP^+ cells were plated and incubated at 37°C overnight before antibody blockade experiments were performed as described above.

Immunofluorescence Microscopy.

293β5 cells were transfected with indicated plasmid DNAs, incubated for two days, and then cooled to room temperature (RT). Antibodies and HIV-mCherry pps were added, cells incubated for 30 min at RT, 10 min at 37°C, then returned to RT. AlexaFluor – conjugated secondary antibodies were applied for 10 min at RT, along with Hoechst 33258 (Molecular Probes). Cells were rinsed with PBS, fixed with 3.7% paraformaldehyde in 100 mM PIPES buffer [pH 6.8], mounted using PermaMount, and imaged with a DeltaVision microscope (Applied Precision) equipped with a digital camera (CoolSNAP HQ; Photometrics), using a 1.4-numerical aperture 60X objective lens. Images were deconvolved with SoftWoRx deconvolution software (Applied Precision). Co-localization was measured and quantified using Imaris version 6.3.1 (Bitplane Scientific Solutions).

Isolation of Tetraspanin-enriched Membranes.

Adherent 293β5 cells (~10^5 / cm^2) were rinsed with ice-cold PBS, incubated for 30 min at 4°C with 1 mg / ml EZ-Link Sulfo-NHS-LC-Biotin (Pierce) in PBS, rinsed, then incubated for 20 min at 4°C with 100 mM glycine in PBS. Cells were rinsed with PBS, then incubated for 20 min at 4°C in MES buffer (25 mM MES [pH 6.0], 125 mM NaCl, 1 mM $CaCl_2$, 1 mM $MgCl_2$) containing 1% 3-[(3-Cholamidopropyl)dimethylammonio]-1-propanesulfonate (CHAPS) detergent (Calbiochem Cat # 220201) or 1% TritonX-100 detergent (Sigma). Cell lysates (10^7 / ml) were removed from plates and emulsified by 20 cycles of extrusion through 27G needles. Nuclei were removed by centrifugation, lysates mixed with equal volumes of 80% w/v sucrose in MES buffer, placed into Beckman SW60 tubes, and overlaid with 3 ml of 30% w/v sucrose, then with 0.5 ml of 5% w/v sucrose, both in MES buffer. Samples were centrifuged with a Beckman SW60 rotor at 370 K x g for 18 h at 4°C. Fractions were collected from air-gradient interfaces. Biotinylated proteins in gradient fractions were bound to streptavidin agarose beads (Pierce). Non-reducing dot- and western-blotting procedures were used to identify the distributions of proteins in gradient fractions, as described previously [162].

Virus Priming Assays.

PR8 or MERS pp were incubated at 37°C for 30 min with equal volumes of low-density (LD) or high-density (HD) sucrose gradient fractions, or with 2.5 U trypsin / reaction (in 50 µl total) (Sigma). Treated PR8 and MERS pp were divided, and proteins in one set of aliquots were precipitated with trichloroacetic acid and analyzed by western

blotting. The other set were used to transduce 293β5 cells. Cells transduced with MERS pp were pre-treated for 1h with or without 10 μM leupeptin (Sigma), inoculated for 2 h, rinsed and incubated without leupeptin for 18 h. Cells were then lysed and luciferase levels were measured. Cells infected with PR8 viruses were infected at an MOI=1, rinsed after 2 h, and incubated for an additional 6 h. Media were collected and Gluc levels were measured.

Production of Knockout Cell Lines.

pSpCas9-BB-2A-puro was digested with Esp3I (Fermentas) for 4h at 37ºC. The digested plasmid was purified and ligated with annealed guide DNAs specific for CD9 or CD81. Tetraspanin-specific pSpCas9-BB-2A-puro plasmids were transfected into 293T cells. After 72h, cells were selected with 4 μg/ml puromycin for 96h. Selected cells were serially-diluted to isolate clonal populations and clones were selected by western blot.

Proximity Ligation Assay.

HeLa cells were transfected with indicated plasmid DNAs and a GFP reporter, incubated for two days, and then lifted from tissue culture plates using 0.05% trypsin. Cells were transferred to microscope coverslips coated with fibronectin. Cells were allowed to adhere for 24h. Cells were then fixed for 30 minute at 37ºC with 3.7% paraformaldehyde in 0.1 M piperazine-N,N′-bis(2-ethanesulfonic acid) buffer (pH 6.8). Coverslips were washed with PBS and PLA was performed using DuoLink® Proximity Ligation Assay (Sigma-Aldrich) using primary antibodies against TMPRSS2 and CD26. Images were captured using a DeltaVision microscope (Applied Precision) equipped with

a digital camera (CoolSNAP HQ; Photometrics), using a 1.4-numerical aperture 60X objective lens. Images were deconvolved with SoftWoRx deconvolution software (Applied Precision). PLA foci were detected and quantified using Imaris version 6.3.1 (Bitplane Scientific Solutions).

Protease Inhibitor Assays.

293T cells were transfected with DPP4 and an empty vector or the complementing tetraspanin. Cells were pre-treated for 1h with 100 μM camostat, 100 μM bafilomycin, or 10 μM E64D before transduction with MERS pps in the presence of the inhibitors. After 2h, cells were washed to remove drugs and unadsorbed virus. Luciferase assays were performed as described above.

Entry Kinetics Assay.

293T cells were transfected with DPP4 and either an empty vector or complementing tetraspanin. 24h after transfection, cells were plated in a 96-well plate. MERS pps were added to cells at 4^{o}C for 1 hour to allow viral binding. Media was removed and replaced with 37^{o}C media and the plates were moved to an incubator. At sequential time points following the shift to 37^{o}C, a protease inhibitor cocktail was added to cells such that the final concentration was 100 μM bafilomycin, 10 μM E64D, and 100 μM camostat. These drugs were left on cells overnight before cells were lysed and luciferase was measured as described above. Luciferase levels were compared to that of cells treated only with DMSO control.

Cholesterol Depletion Assay.

293T cells were transfected with DPP4 and either an empty vector or complementing tetraspanin. After 2 days, cells were plated in serum-free media for 18 h before treatment with the indicated concentration of methyl-beta-cyclodextrin (Sigma) for 4 h. Cells were transduced with HIV-MERS pp for 2 h. Cells were washed to remove virus and cyclodextrin and allowed to incubate for 48h. Cells were lysed and lysates were analyzed for luciferase reporter gene expression as described above.

HR2 Inhibition Assay.

DBT cells were pretreated with the indicated concentration of MERS HR2 peptides (kindly provided by Dr. Matteo Porotto) tagged through maleimide reactions with lipid moieties. After 30 min, cells were infected with rMHV-A59, rMHV-JHM, or 100 pfu MHV-2. 1 hpi, cells were washed to remove virus and peptides. For rMHV-A59 and rMHV-JHM, the cells were incubated for 18 h and lysed. MHV infection was measured by luciferase assay as described above. For MHV-2, cells were covered with 0.5 % agarose in complete media. 48 hpi, cells were fixed with 10 % paraformaldehyde for 10 minutes and stained with a 1% crystal violet solution at RT for 2 h. Agar was removed and cells were washed with water 3 times. Plaques were then counted.

CHAPTER III

RESULTS

SECTION 1: Tetraspanin-rich Membranes as Viral Entry Portals.

Tetraspanin antibodies inhibit infection of coronaviruses and influenza A.

We hypothesized that tetraspanins function as scaffolding proteins holding viral entry factors together. To determine whether entering CoVs utilize tetraspanins, we evaluated the effects of tetraspanin antibodies on MHV strains A59 and JHM infections. Murine DBT cells were incubated for 30 min with mouse monoclonal antibodies against the tetraspanins CD9, CD63, CD81, or with an equimolar mixture of the three (αTspan). A monoclonal antibody against transferrin receptor (TfR) was used as an isotype – matched control for general cell coating by antibodies. Cells were then inoculated with luciferase-expressing recombinant MHV-A59 or –JHM for 2 h, then unadsorbed viruses and antibodies were rinsed away. As measured by luciferase levels at 8 hpi, the two viruses were significantly inhibited by all three tetraspanin antibodies, with the antibody combination (αTspan) inhibiting A59 and JHM strains by ~50% and ~90% , respectively (Figure 6A). The TfR antibodies did not block the viruses. None of the antibodies interfered with transduction by VSV pps bearing VSV G proteins (VSV pp), indicating that tetraspanin antibodies do not generally suppress virus entry or reporter gene expression.

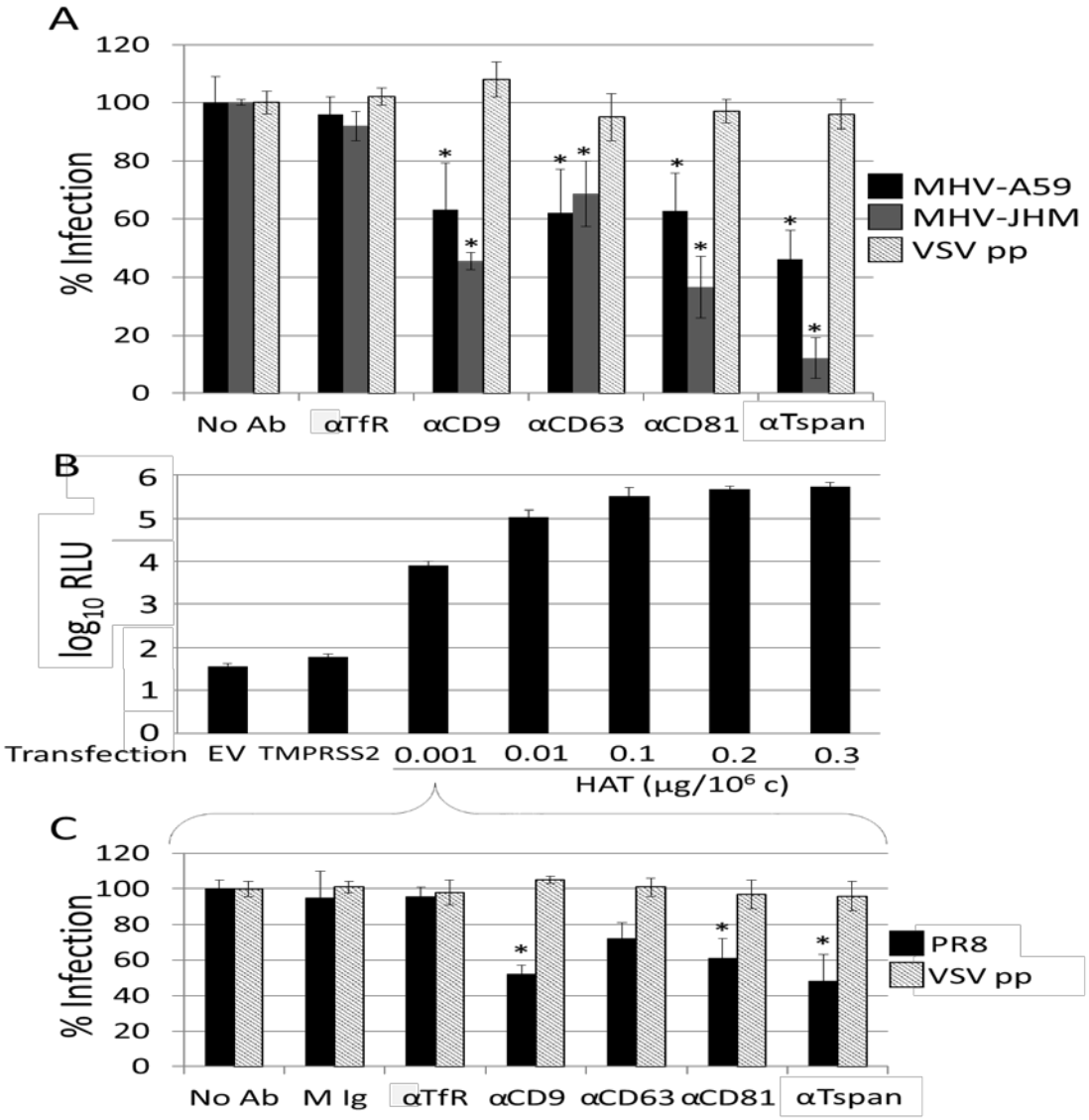

Figure 6. Effect of tetraspanin antibodies on MHV and IAV infection. **(A)** DBT cells were treated with monoclonal antibodies to CD9, CD63, CD81, or an equimolar mixture of the three (αTspan) for 30 min. Cells were then infected with rMHV-A59 or rMHV-JHM viruses containing an Fluc reporter gene. 8 hpi, infection was quantified by measuring Fluc reporter gene products and were normalized to the untreated controls. A control VSV-G pseudotyped reporter virus was also used (VSV pp). A monoclonal antibody against transferrin receptor (TfR) was used as a control for both antibody subtype and irrelevant cell binding. Results are representative of three independent experiments. *$p<0.05$ when compared to "No Ab". **(B)** Cells transfected with an empty vector (EV) or the indicated amounts of HAT were infected with a PR8 influenza virus containing a Gluc reporter gene. 8 hpi, media was sampled from cells and analyzed for secreted Gluc. **(C)** 293β5 cells transfected with 0.001 μg/10^6 cells of HAT were treated with antibodies as described in (A). This experiment also included a non-specific Mouse IgG control antibody (M Ig). Media was sampled and analyzed for secreted Gluc 8 hpi. *$p<0.05$ when compared to "No Ab".

While it is known that CD81 knockdown inhibits IAV entry [141], it is not known whether antibodies to CD81 or other tetraspanins also inhibit IAV infection. We determined whether the tetraspanin antibodies inhibit influenza A/Puerto Rico/8/1934 (H1N1), also known as PR8 IAV. For ease of analysis, we used PR8 containing a *Gaussia* luciferase (Gluc) reporter gene [158]. Many host cells, including the cell lines used in these experiments (Figure 6B), are resistant to PR8 infection, because they do not express proteases that prime viral HA proteins. [163]. Therefore, we transfected 293β5 cells with plasmids encoding HAT, then infected with PR8 one day later. By measuring Gluc accumulations in culture media, we determined that transfecting cells with 0.001 μg/10^6 cells of HAT was sufficient to render cells susceptible to PR8 infection and that increasing HAT transfection generally led to increased infection (Figure 6B). Knowing this, we determined whether tetraspanin antibodies might block PR8 infection into the HAT-expressing cells. Indeed, PR8 infection was significantly inhibited by all three tetraspanin antibodies, with the antibody combination (αTspan) effecting ~ 50% blockade. The tetraspanin antibodies did not inhibit VSV pp transductions (Figure 6C).

Tetraspanin antibodies inhibit entry of several coronaviruses. To limit our analyses to virus-cell entry, we produced VSV-based pps that contained the S proteins of several human CoVs, and determined whether their ability to transduce cells was blocked by tetraspanin antibodies. The virus preparations were designated according to their S proteins (MERS pp, SARS pp, 229E pp). Their transduction into cells was taken to reflect features of the authentic MERS, SARS and 229E CoV entry processes [156, 162].

Transduction-susceptible target cells were established by transfecting 293β5 cells with genes encoding virus receptors; hAPN for HCoV-229E [103], hDPP4 for MERS-CoV [100], and hACE2 for SARS-CoV [102]. These target cells were then inoculated with the pp preparations, in the absence or presence of tetraspanin antibodies, as was done with authentic viruses. After 1 h inoculation periods, unadsorbed pps and antibodies were removed, and transduction levels measured the next day by quantifying Fluc gene expressions.

The tetraspanin antibodies impaired transductions by all three CoV pps, with MERS pp and SARS pp most notably inhibited (Figure 7). The only exception was 229E pp which was not blocked significantly by the antibody against CD81. As seen previously, TfR antibodies did not affect transductions nor did the IgG isotype control.

Tetraspanins inhibit entry following receptor binding. To determine whether the antibodies used for virus blockades bound similarly to target cells, we subjected antibody-coated cells to flow cytometry. The inert TfR antibodies and inhibitory tetraspanin antibodies bound similarly (Figure 8A), indicating that virus blockades do not arise simply from high levels of antibodies on cells. Next, to determine whether antibodies on cells interfere with virus-cell binding, we used fluorescently-labeled, HIV-based MERS pps, which we manufactured according to previously described methods [157]. mCherry MERS pps were adsorbed at 4^{o}C to 293β5 cells overexpressing hDPP4 receptors, either in the absence or presence of tetraspanin antibodies. Subsequent flow cytometric analyses revealed that the fluorescent HIV-based MERS pps bound

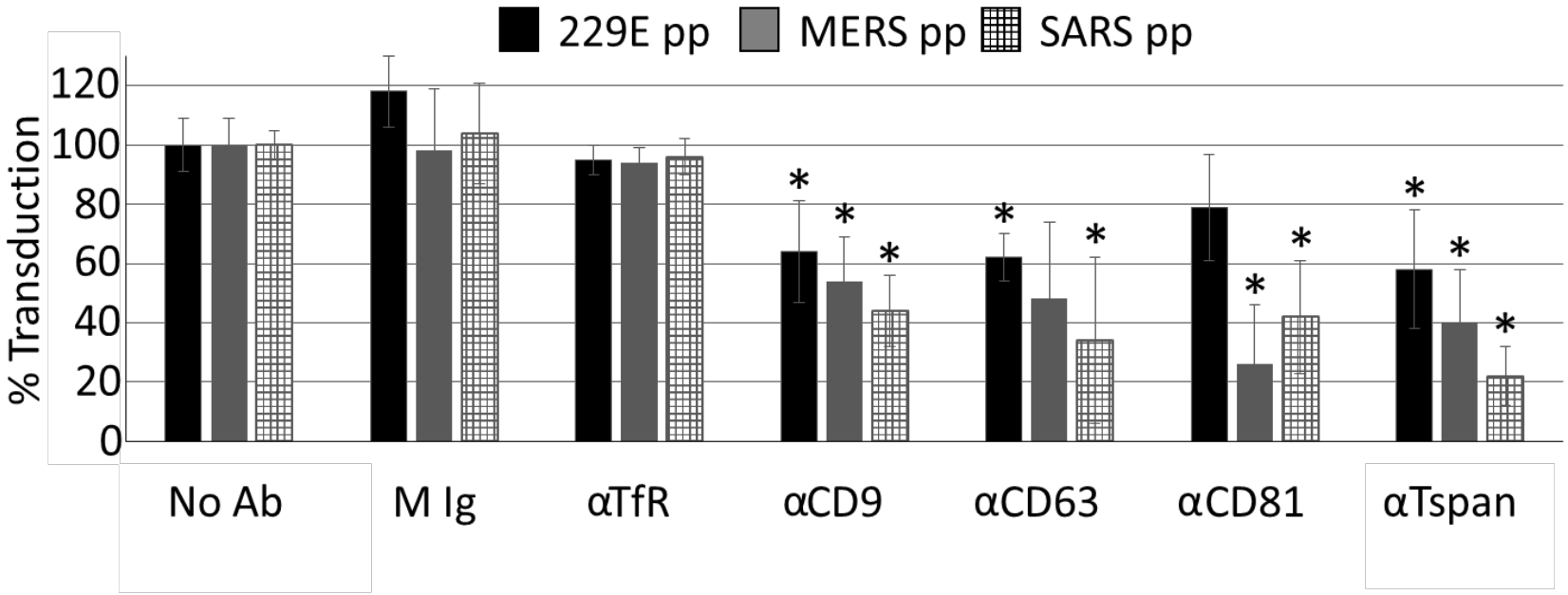

Figure 7. Effect of tetraspanin antibodies on CoV pseudotyped virus cell entry. 293β5 cells overexpressing appropriate receptors (APN for 229E, DPP4 for MERS, ACE2 for SARS) were treated with monoclonal antibodies to CD9, CD63, CD81, or an equimolar mixture of the three (αTspan). After 30 min, cells were transduced with pps pseudotyped with S proteins of 229E (black), MERS (gray), or SARS (hatched). Transduction levels were measured by quantifying Fluc reporter gene products and were normalized to the "No Ab" controls. Mouse IgG (M Ig) and a monoclonal antibody against transferrin receptor (TfR) were used as controls for antibody subtype and irrelevant cell binding, respectively. Results are representative of three independent experiments. *$p<0.05$ when compared to the "No Ab" controls.

abundantly to the ~35% of cells that were overexpressing hDPP4 (Figure 8B, left). The level of MERS pp binding to the ~ 35% of cells was unaffected by tetraspanin antibodies (Figure 8B, right). We concluded from these data that the antibodies do not block virus-cell binding.

These data also indicated that tetraspanin antibodies interfere with virus entry after virus-receptor binding. To explain how the antibodies block viruses, we posited that viruses might associate with TEMs after binding to cells, and that the tetraspanin antibodies disrupt some tetraspanin-associated process that facilitates virus entry. We determined whether the mCherry MERS pps reside in close proximity to tetraspanin proteins during their cell entry. To do this, we incubated chilled 293β5 cells with the fluorescent pps along with anti-CD81 antibodies, then shifted to 37^{o}C for 10 min to permit "patching", i.e., antibody-mediated tetraspanin cross-linking into larger structures [164]. Quantitative confocal microscopy revealed that CD81 colocalized with ~20% of MERS pps, but with only ~10% of VSV pps (Figure 8C, right). Absence of "bald", i.e. viral glycoprotein free, fluorescent pp binding (Figure 8C, left) confirmed viral glycoprotein-dependent interactions with cells. Similar, but less compelling co-patching of IAV pp and CD81 were also observed in these experiments, however IAV pp co-localization was not statistically significantly higher than VSV pp (Figure 8C). These data indicate that, shortly after binding to cells, some MERS and IAV pp are present near tetraspanin proteins.

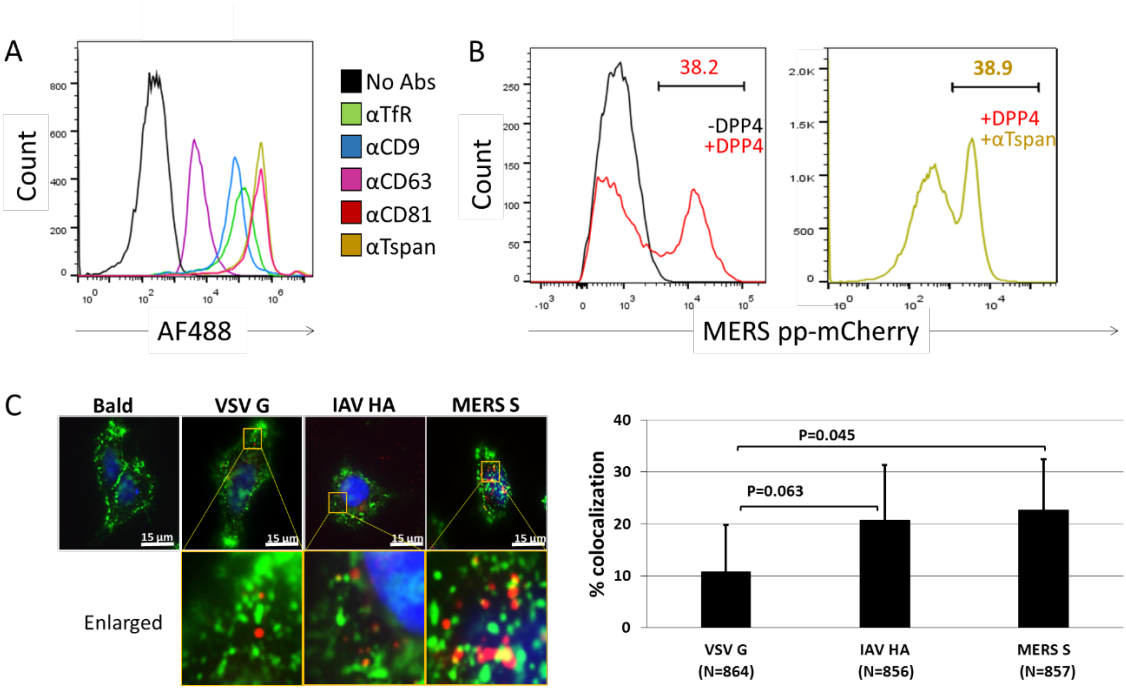

Figure 8. Immunofluorescent analysis of pseudoparticle binding to cells in the presence of tetraspanin antibodies. **(A)** Flow cytometric analysis of the binding efficiencies of the antibodies used in tetraspanin blockade experiments in figures 6 and 7. 293β5 cells were incubated without antibodies (black) or with the indicated antibodies. Following a 30 min incubation, cells were washed and incubated with an anti-mouse AlexaFluor-488 (AF488) secondary antibody. AF488 intensity was measured by flow cytometry. **(B)** 293β5 cells overexpressing DPP4 (+DPP4) or an empty vector (-DPP4) were incubated with MERS-S pseudotyped HIV-mCherry for 1 h at 4ºC. Following incubation, cells were washed of unbound virus and analyzed by flow cytometry to detect mCherry. The percentage of mCherry-positive cells is indicated above the gate (left panel). +DPP4 cells were treated with αTspan antibodies. After 30 min at 37ºC, HIV-mCherry-MERS pseudoviruses were inoculated for 2 h at 4ºC. Following washing of unadsorbed virus and antibody, flow cytometry was performed to detect bound HIV pseudoviruses (right panel). **(C)** HIV-mCherry pseudoviruses without glycoproteins (Bald) or with VSV G, IAV HA, or MERS S, were mixed with anti-CD81 antibodies and inoculated onto +DPP4 cells for 30 min at 4ºC. After a 10 min, 37ºC patching period, cells were fixed and analyzed by confocal microscopy to determine the location of the pseudoviruses (red) and CD81 (green). Co-localization of CD81 and HIV-positive puncta were quantified using Imaris software. Data were plotted as percent of HIV pseudoviruses that were localized to CD81. The experiments in (C) were performed by Dr. Jung-Eun Park.

Using MERS pp, we further determined that tetraspanin antibodies were inhibitory only at the pp entry stage, with no effects on transduction when added 30 min following virus inoculation (Figure 9). These data, considered with the data in Figure 8, led us to the conclusion that tetraspanin antibodies inhibit an early stage of entry, following virus binding.

Tetraspanin antibodies do not block infection when TTSPs are overexpressed. One of the major roles of tetraspanins is regulating transmembrane protease location on the cell surface. To do this, tetraspanins are known to partner with a variety of cell-surface proteases [165], among which may be one or several CoV and IAV -priming proteases [73, 156, 163, 166]. This led us to hypothesize that tetraspanin antibodies interfere with tetraspanin-facilitated proteolytic priming, possibly by preventing tetraspanin-associated proteases from accessing receptor-bound viruses. By this hypothesis, CoVs which can access non-tetraspanin-associated TTSPs should not rely on tetraspanins for entry, and thus should be unaffected by tetraspanin antibodies. To address this suggestion, we overexpressed priming proteases in target cells and performed antibody blockade experiments. One frequently-cited CoV priming protease is TMPRSS2 [73, 83]. We found that DBT cells expressing human TMPRSS2 were hypersensitized to MHV infection, indicating that this protease is utilized by MHV and is limiting in the DBT cell context. Therefore, we supplied DBT cells with graded doses of TMPRSS2 – encoding plasmids, along with small constant amounts of a GFP reporter plasmid. Following expression, FACS was used to isolate the GFP^+ cells, which were then used in antibody blockade experiments, as described above (Figures 6 and 7). The results indicated that tetraspanin antibodies blocked MHV infection into normal DBT

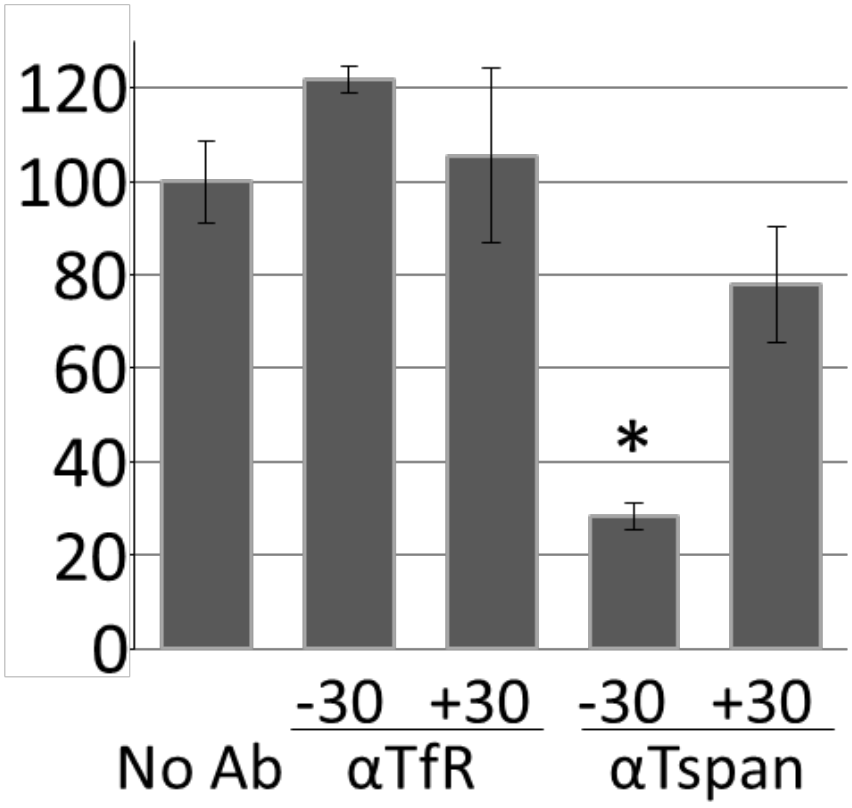

Figure 9. Tetraspanin antibodies block CoV entry at an early stage. 293β5 cells were incubated without antibodies (No Ab), with control anti-transferrin receptor antibodies (αTfR), or with a mixture of anti-tetraspanin antibodies (αTspan) for 30 min periods immediately before (-30) or after (+30) a 60 min MERS pp pseudovirus inoculation period. Transduction levels were measured by quantifying luciferase and were normalized to the "No Ab" control. *$p<0.05$ when compared to "No Ab".

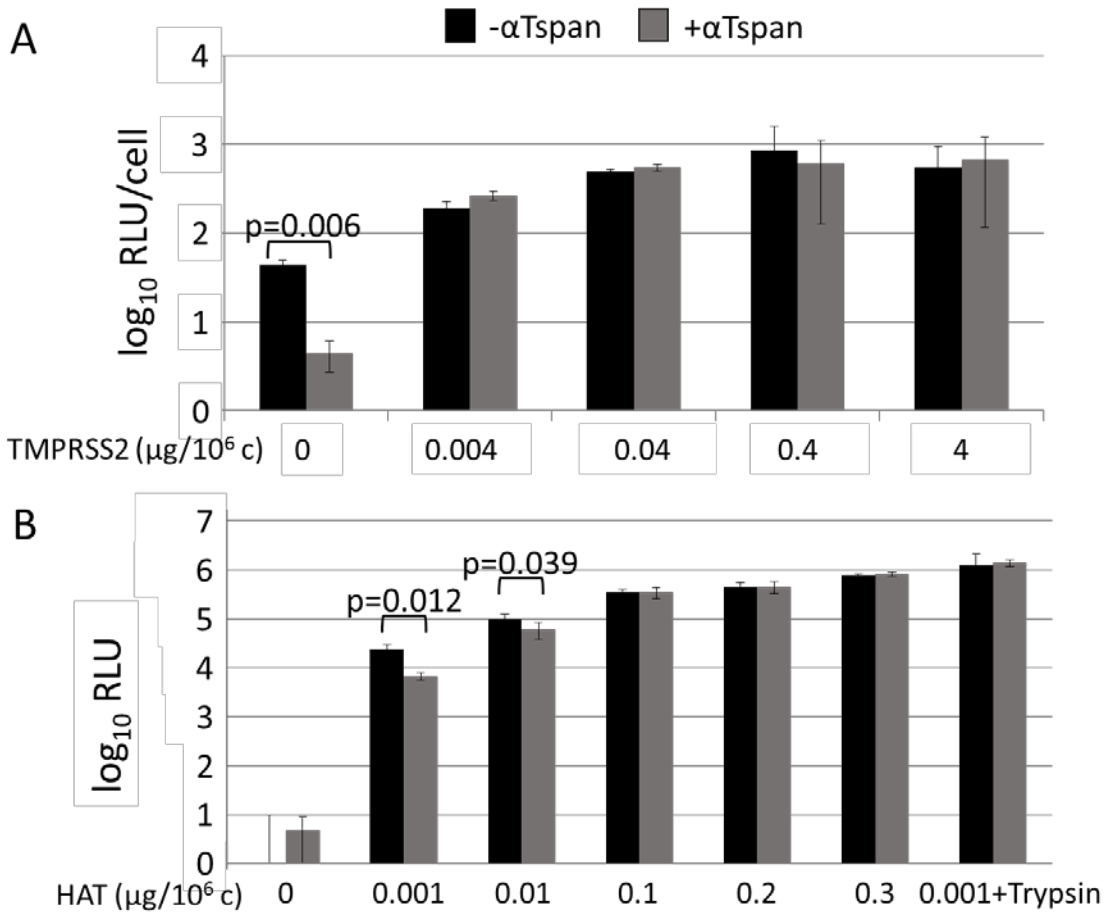

Figure 10. Effect of transmembrane protease expression on tetraspanin blockade of MHV-JHM and PR8. **(A)** DBT cells were transfected with increasing amounts of TMPRSS2 plasmid and a small amount of GFP reporter. Following isolation of transfected cells by FACS, cells were treated with either a mixture of tetraspanin antibodies (+Tspan) or media (-Tspan). After 30 min, cells were infected with rMHV-JHM. 2 hpi, cells were washed to removed unadsorbed virus and antibody. 8 hpi cells were lysed and analyzed for Fluc reporter expression. Luciferase units were normalized to the average number of cells infected under each condition. **(B)** 293β5 cells were transfected with increasing amounts of HAT before being exposed to the same antibody blockade experiment described in (A). Cells were infected with PR8 for 2 h, washed, and secreted Gluc was measured 8 hpi.

cells (Figures 6A and 10A), but not into DBT cells expressing TMPRSS2 (Figure 10A). Of note, 10^6 cells transfected with 0.004 μg of TMPRSS2 plasmid contained TMPRSS2 protein levels that were far below our western blot and immunofluorescent assay (IFA) detection limits, making it clear that even small amounts of priming proteases will bypass the tetraspanin antibodies (Figure 10A). We speculate that overexpressing TMPRSS2 in cell lines overwhelms the ability of tetraspanins to regulate the localization the protease. Data using biochemical isolation and proximity ligation assay (PLA) (Figures 17, 21, and 22) which show large amounts of non-tetraspanin associated TMPRSS2 suggest this may be the case. However, definitive data on this subject remains elusive. Regardless, we conclude from these data that overexpressed TTSPs overcome the dependence of viruses on tetraspanins.In similar experiments, PR8 and its priming protease HAT were evaluated in entry assays. Here, 293β5 cells were transfected with graded doses of HAT-encoding plasmids, and then infected with PR8, either in the absence or presence of tetraspanin antibodies. The results indicated that HAT bypassed the antibody blockades in a dose-dependent manner (Figure 10B). Furthermore, trypsin pre-treated viruses also bypassed the antibody blockades (Figure 10B). Therefore, the hypothesis that proteases mitigate the antiviral activities of tetraspanin antibodies applies to TMPRSS2, HAT and trypsin proteases, and to MHV and PR8 viruses.

Protease treated viruses are not blocked by tetraspanin antibodies. Trypsin is often used as a surrogate for TTSPs and other serine proteases in labs that study enveloped virus entry. Trypsin treatment cleaves the S1/S2 region of MERS pps and destabilizes them to a degree, possibly relieving MERS dependence on tetraspanin-induced concentration of TTSPs for entry. Alternately, trypsin-cleaved MERS may

utilize endosomal proteases much more efficiently than uncleaved MERS for S triggering. Therefore, we hypothesized that upon trypsin treatment, MERS pp is less likely to rely on TTSPs and tetraspanins for entry. To investigate this, we pre-treated MERS pps with 2.5 units of trypsin for 10 minutes. After inactivating the trypsin, we performed the antibody blockade experiments described previously. As expected, uncleaved MERS pp entry into target cells was less efficient in the presence of anti-tetraspanin antibodies. However, when pretreated with trypsin, MERS pp entry into target cells was almost entirely independent of tetraspanin antibody blockade (Figure 11). These results corroborate the similar bypass of antibody blockade observed upon overexpression of TTSPs.

Biochemical analysis of tetraspanin-enriched membranes. Our findings fit with the hypothesis that tetraspanins facilitate the interaction of viral receptor and priming proteases. Antibody binding to tetraspanins interferes with these encounters, reducing infection. To further evaluate the interactions of CoV entry factors and tetraspanins, we used a biochemical approach to determine whether cell receptors and priming proteases are present within TEMs. Surface-biotinylated 293β5 cells were lysed in buffers containing CHAPS, a zwitterionic detergent that emulsifies cell membranes without disrupting primary or secondary TEM interactions [132]. After sucrose density gradient fractionation, CHAPS-soluble proteins remained near the bottom of sucrose gradients, designated as the high-density (HD) regions, while CHAPS-insoluble protein-lipid complexes floated to the top, low-density (LD) ($\rho<1.13$ g/ml) regions. Dot-blotting revealed that ~ 20% of biotinylated (plasma membrane) proteins were in the LD region (Figure 12, upper left). Streptavidin pulldowns of the isolated HD and LD fractions

revealed that within the top 20% were all detectable cell-surface CD9, CD63, and CD81 proteins (Figure 12, lower left), indicating that the LD region includes the TEMs. Notably, cells lysed by Triton X-100 (TX-100), a detergent known to solubilize TEMs, also generated an LD fraction that comprised ~20% of plasma membrane proteins (Figure 12, upper right), but was devoid of any cell-surface tetraspanins (Figure 12, lower right). Thus, we confirmed that CHAPS LD subcellular fractions represent "TEMs" and the TX-100 LD fractions as "lipid rafts".

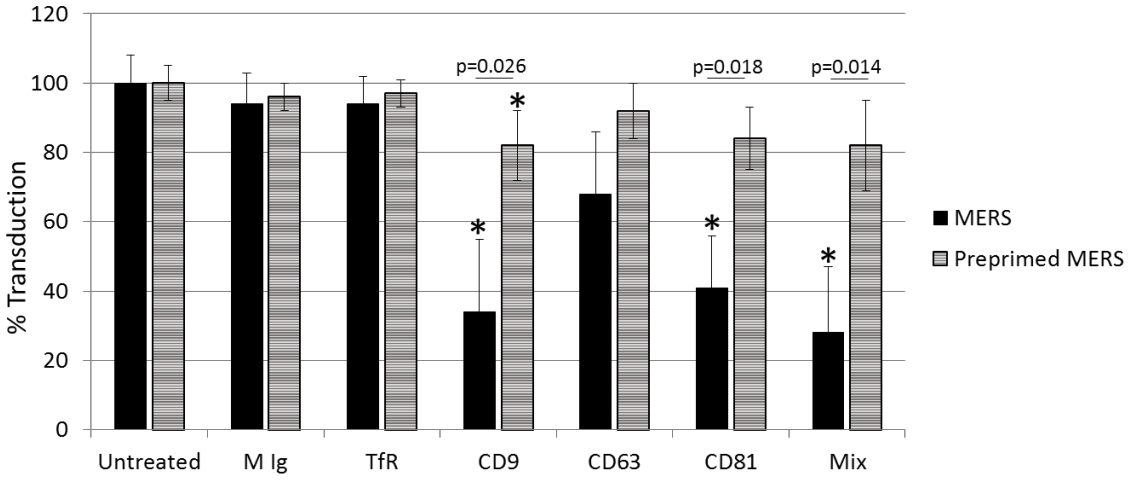

Figure 11. Effect of tetraspanin antibodies on entry of trypsin pre-treated MERS pp. MERS pseudoviruses were either untreated or preprimed with 2.5 units of trypsin for 30 min before being used in a TEM blockade experiment as described previously (Figure 5). Before addition to cells, any trypsin was neutralized using soybean trypsin inhibitor. Transduction efficiency was determined by reporter gene expression. Results are representative of three independent experiments. *$p<0.05$ when compared to "Untreated" control.

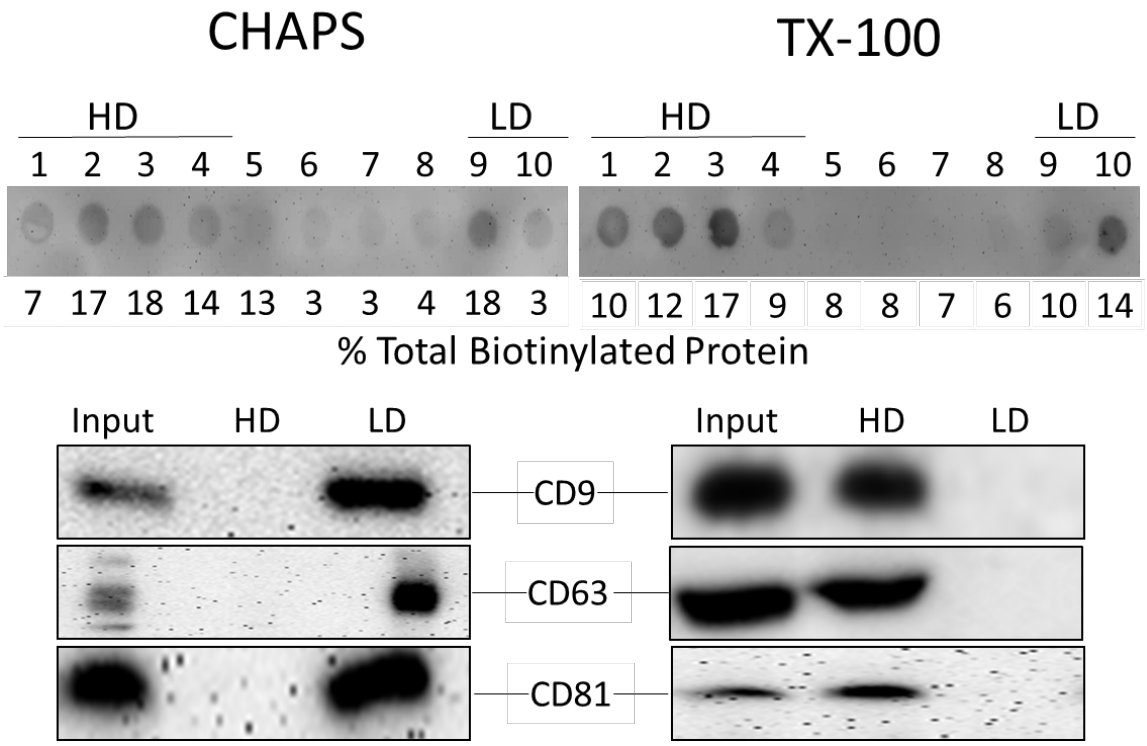

Figure 12. Biochemical isolation of tetraspanin enriched membranes. 293β5 cells were surface-biotinylated before lysis with CHAPS or TX-100 detergent. Following differential centrifugation, 10 fractions were collected from each tube and analyzed by dot blot using a streptavidin HRP for total-cell surface, biotinylated proteins (top). Following collection of HD and LD fraction, streptavidin pulldowns were performed and each fraction was analyzed for cell surface CD9, CD63, and CD81 (bottom).

To determine whether CoV receptors and priming proteases partition into TEMs, it was necessary that 293β5 cells were first transfected to overexpress ACE2, APN, CEACAM, or DPP4. The transfected cells were then lysed in CHAPS, and TEMs isolated by two sequential cycles of floatation on sucrose gradients. Western immunoblotting revealed that ~ 90% of ACE2, APN, and CEACAM and ~ 50% of the DPP4, were partitioned into TEM fractions (Figure 13).

Cells overexpressing the virus-priming proteases TMPRSS2 and HAT were similarly fractionated, and roughly 50% of these proteases were found in the TEM fractions (Figure 13). TMPRSS2 can self-proteolyze, releasing the extracellular domain into the media. Thus, the ability to detect intact, closely complexed TMPRSS2 in cell membranes may be limited. To avoid this issue, we expressed a proteolytically inactive TMPRSS2 mutant ($TMPRSS2_{S441A}$) and found that it more prominently partitioned into the TEM fractions (Figure 13). We concluded from these data that TTSPs concentrate in TEMs. Some β-actin (<10%) partitioned with TEMs, consistent with known TEM – cytoskeleton interactions [167]. Calnexin, a transmembrane protein abundant in the endoplasmic reticulum [168], was excluded from the TEMs, indicating complete cell solubilization by CHAPS detergent. Attempts to isolate non-TEM associated proteins failed, but there is evidence that inclusion in CHAPS-LD fractions is dependent on protein interaction with tetraspanins (Figure 21).

As the TEM fractions contain ~ 20% of the total plasma membrane proteins, these results indicated that the CoV receptors and priming proteases were at least 5- to 50-fold more abundant in TEMs than elsewhere on cell surfaces. TEM localization of one CoV receptor (DPP4) and one priming protease (TMPRSS2) was validated by immunofluorescence microscopy. DPP4 and TMPRSS2 were both found near or within CD81-encriched cell-surface puncta (Figure 14). Similar partitioning of CD81 with a catalytically-inactive mutant $TMPRSS2_{S441A}$ was also observed (Figure 14), indicating that enzymatic activity has no effect on subcellular localization. Thus, there are recognizable proportions of CoV receptors and priming proteases residing within TEMs.

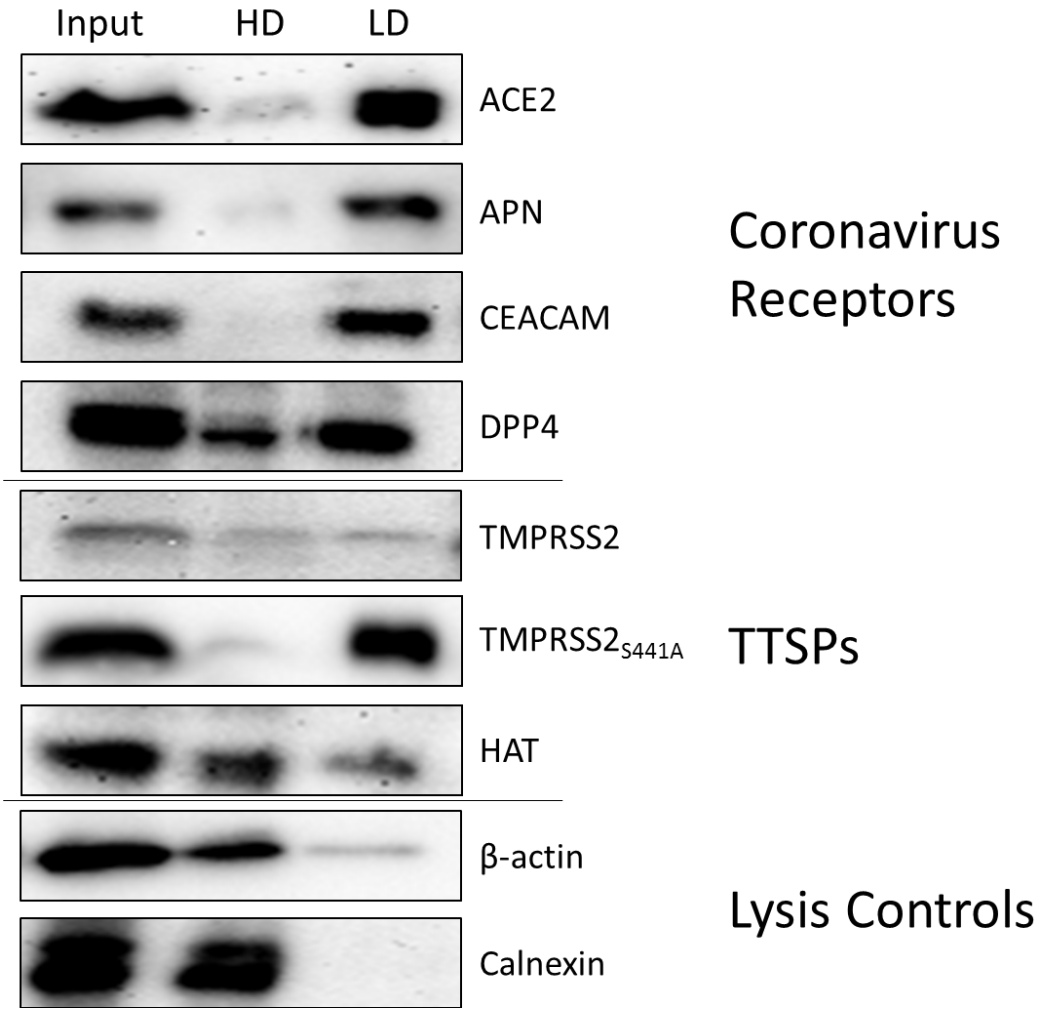

Figure 13. Analysis of CoV entry factors in tetraspanin enriched membranes. 293β5 cells overexpressing epitope-tagged CoV receptors ACE2, APN, CEACAM, and DPP4, or FLAG-tagged TTSPs TMPRSS2, TMPRSS2-S441A or HAT. Transfected cells were subjected to CHAPS lysis and density gradient centrifugation, as described in figure 10. Western blot was used to determine the relative presence of the indicated proteins into HD and LD fractions. β-actin and calnexin were used as controls for complete cell lysis and proteins not present in CHAPS LDs.

Tetraspanin-enriched membranes productively cleave viral glycoproteins.

Because TEMs contain both viral receptors and priming proteases, we determined whether the isolated TEMs have virus-priming activities. Like exogenously cleaved MHV in Figure 11, we expected that pre-cleaved MERS-CoV would become less reliant on cellular TTSPs for entry. We mixed TEMs with MERS pps, inoculated the mixtures onto susceptible target cells and then measured transduction efficiencies. To ensure that the transduction measurements reflected proteolytic priming by the TEMs, and not by endogenous target cell proteases, we suppressed target 293β5-cell priming proteases with leupeptin, a broad-spectrum protease inhibitor. Leupeptin-treated 293β5 cells were profoundly resistant to MERS pp transduction (Figure 15A; top), indicative of requirements for the host proteases. However, MERS pp that were exposed to TEM fractions transduced the leupeptin-treated cells (Figure 15A, top), indicating priming. Of note, the bypass of leupeptin was pronounced when MERS pp were exposed to trypsin, or to TEMs containing overexpressed TMPRSS2, but did not reach the levels observed in the absence of leupeptin. These findings indicated that MERS entry-priming activities were greatly concentrated in the TEMs.

MERS pp that had been exposed to TEMs were also evaluated to assess the extents of S protein cleavage. Western immunoblots indicated that the TEMs effected cleavage of S proteins, generating proteolytic patterns that were largely indistinguishable from those generated by trypsin (Figure 15A; bottom). The apparent molecular weights of the N-linked glycoprotein products were consistent with cleavages at three multibasic sites, one at amino acids 626-629 (RQQR) to create the minor 130 kDa fragment, one at 884-887 (RSAR) S2' site to create the major 70 kDa fragment, and one at 1110-1113

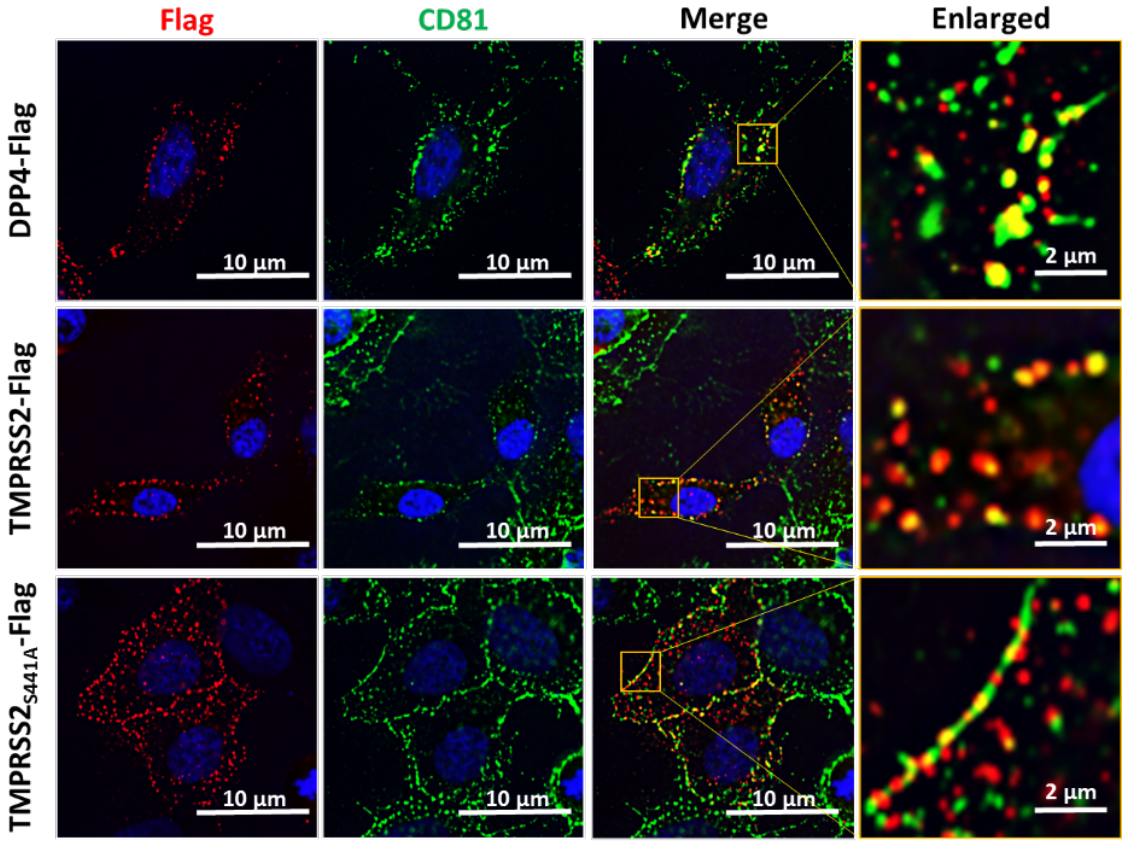

Figure 14. Localization of MERS-CoV entry factors DPP4 and TMPRSS2 in relation to tetraspanin CD81. 293β5 cells were transfected with plasmids encoding the indicated FLAG-tagged proteins. 24 h later, live cells were co-incubated with anti-FLAG and anti-CD81 antibodies, with a 10 min incubation at 37ºC to induce patching. Fluorescent secondary antibodies were applied to mark the positions of FLAG-tagged proteins and CD81, and Hoescht 33258 (blue) mark the positions of cell nuclei. Images show 0.5-micron thick confocal slices through the top section of cells. These experiments were performed by Dr. Jung-Eun Park.

(QSKR) to create the minor 40 kDa fragment. Somewhat surprisingly, cleavage of MERS at S2' prior to encountering the cell did not completely inactivate the virus. This may be due to incomplete cleavage of all the S proteins or because S1 failed to dissociate from S2 under these conditions. Interestingly, TEM-mediated cleavage of S proteins led to less generation of the 40 kDa fragment when compared to trypsin treated S. We speculate that the cleavage that generates this fragments may be inactivating and may be less prevalent when TEM-associated receptors are bound to S proteins simultaneous to cleavage, as seen previously [65].

Analogous experiments were completed with IAV PR8 viruses. In these assays, however, inactivation of host proteases by leupeptin was not required, as PR8 did not respond to endogenous levels of 293β5-cell proteases. The results of these experiments demonstrated that TEM fractions activated PR8 infectivities, nearly as much as TEMs with overexpressed HAT (Figure 15B, top). The fact that the TEMs were isolated from IAV-resistant 293β5 cells, yet were capable of priming IAV for infection, are potentially explained by the significant concentration of cell proteases achieved through TEM isolation.

As with the MERS S on viral pps, PR8-associated HA proteins were analyzed for cleavage status by western immunoblotting. Here, the TEMs effected cleavage of HA0 into HA1, irrespective of whether HAT was overexpressed and equal to that achieved by trypsin (Figure 15B; bottom). Thus, the TEM fractions harvested from 293β5 cells have proteases that cleave and prime both MERS-CoV S and PR8 IAV HA proteins.

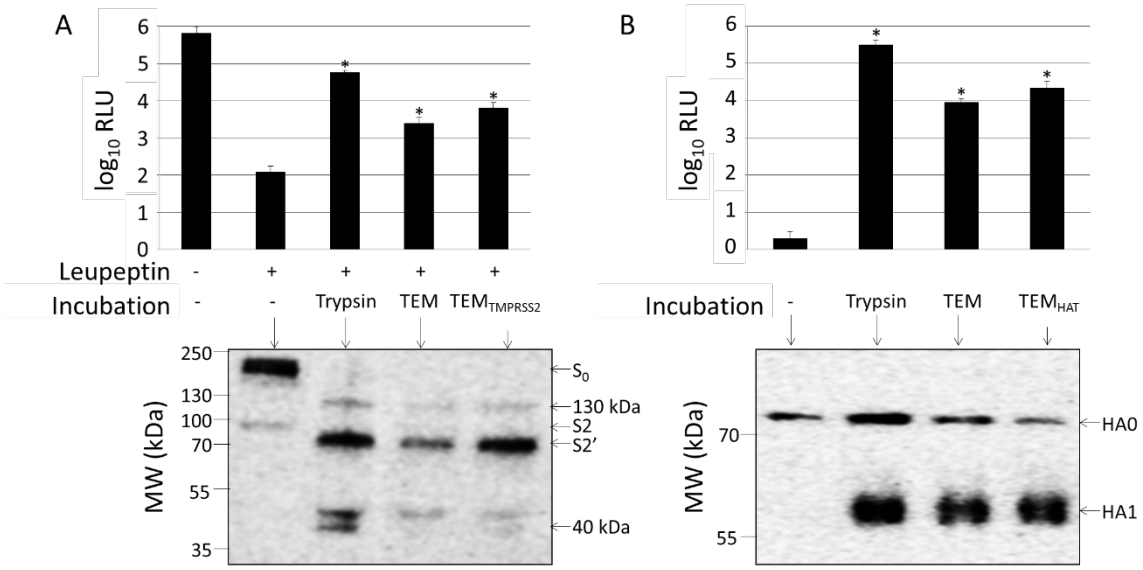

Figure 15. Virus priming activity of TEMs. **(A)** MERS pps were used to transduce 293β5 cells treated with leupeptin or a media control. Prior to transduction, MERS pps were treated with trypsin, TEMs isolated from untransfected cells, or TEMs isolated from TMPRSS2 overexpressing cells. Transduction levels were measured by luciferase reporter gene expression (top). The MERS pps were also concentrated and analyzed by western blot with an antibody to detect a C-terminal C9 tag on the MERS spike (bottom) **(B)** 293β5 cells were infected with PR8 that was treated with trypsin, TEMs isolated from untransfected cells, or TEMs from HAT overexpressing cells. Infection was measured by Gluc expression (top). Viruses were concentrated and analyzed by western blot (bottom). *$p<0.05$ when compared to "–" incubation

SECTION 2: CD9 as an Entry Factor for HCoV-MERS and HCoV-229E.

Our initial discoveries provided insight on how tetraspanin interaction with viral entry factors may affect CoV and IAV entry into target cells. However, the role of individual tetraspanins remained to be investigated. We hypothesized that CoV receptors and priming proteases had individual tetraspanin binding partners that facilitated their interaction with other tetraspanin-associated proteins. We therefore endeavored to

identify the individual tetraspanins that facilitate TTSP-mediated CoV entry and characterize tetraspanin-dependent CoV entry.

There is evidence that CD9 directly interacts with the MERS receptor DPP4. The first indication comes from studies of biochemically isolated of TEMs, similar to described above, in which CD9 was immunoprecipitated (IP). Mass spectrometry identified DPP4, along with many other transmembrane proteins, as a protein that co-IPs with CD9 under these conditions [165]. More recently, a direct interaction between CD9 and DPP4 was identified by co-IP of the proteins under detergent conditions that solubilize TEMs [169]. Therefore, we hypothesized that CD9 may be the specific tetraspanin partner that is responsible for holding DPP4 in close proximity with TTSPs and thus for MERS early entry (Figure 3). Furthermore, we aimed to determine if CD9 was a common entry factor for all CoVs or if it plays a specific role in MERS entry.

In order to investigate these questions, we produced CD9 knockout (KO) cell lines. These cells permitted complementation assays to be performed to determine the role of the tetraspanins CD9 and CD81. We then analyzed the efficiency and nature of CoV entry in the presence and absence of these tetraspanins as well as the localization of CoV entry factors. To analyze these tetraspanins in the context of authentic viral infections of host lungs, we developed novel methods of knocking down or knocking out CD9 in host organisms. A member of our lab, Mike Hantak, along with our colleagues at the University of Iowa, developed an adenovirus 5 (Ad5) transgene expression system that allowed for targeted knockdown of CD9 in virus target cells. With these tools, we identified CD9 as an entry factor for MERS-CoV and 229E-CoV that facilitates rapid,

TTSP-dependent early entry of these viruses. Furthermore, we quantified the entry efficiency of MERS-CoV in lung cells deficient in early entry factors.

Tetraspanin knockout cell lines. Analyzing the potential role of tetraspanins in CoV entry events necessitated the creation of tetraspanin KO cell lines. With these cells, we could analyze viral entry in the presence and absence of a specific tetraspanin. We chose CD9 and CD81 as our tetraspanin target because both were indicated to participate in CoV entry in our antibody experiments (Figures 6 and 7) and both typically reside on the cell surface, unlike CD63.

We used CRISPR/Cas technology [170] to remove selected tetraspanins from cells. 293T and HeLa cells were transfected with Cas9/guide RNAs targeting CD9 or CD81, selected for puromycin resistance, and cloned by endpoint dilution. All KO cell lines grew equivalent to parallel "WT" control clones, and the only observable distinctions were with the CD9KO cells, which were slightly less adherent than WT or CD81KO cells. For the clones used in this study, western blot analyses were performed and the results confirmed the absence of CD9 or CD81, with maintenance of a control tetraspanin CD63 (Figure 16A). Interestingly, CD9 appeared slightly reduced in CD81KO cells. However, IFA of unpermeabilized cells showed similar cell-surface expression and localization of CD9 in WT and CD81KO cells (Figure 16B). IFA also confirmed the absence of the respective tetraspanins in KO cells. CD63 distribution remained unchanged in all cell lines.

CD9 inhibits MERS and 229E entry, but not MHV or SARS. We measured the entry of CoVs into tetraspanin-deficient cells to determine which, if any, CoVs

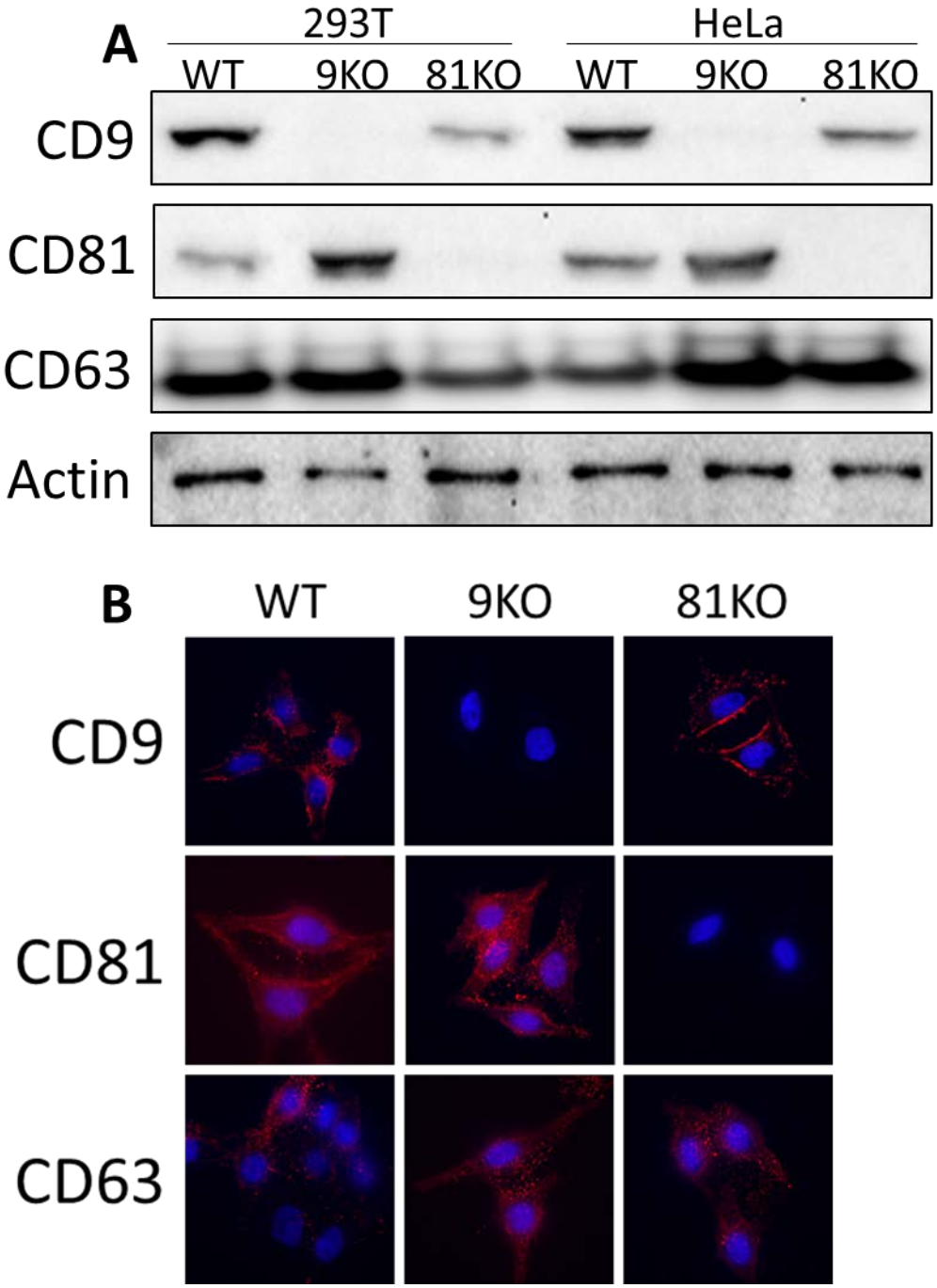

Figure 16. Analysis of tetraspanin KO cells. **(A)** Western blot analysis of 293T and HeLa clonal cell lines knocked out for the indicated tetraspanin. Actin and the tetraspanin CD63 are used as loading controls. **(B)** Immunofluorescent analysis of HeLa clonal cell lines. Unpermeabilized cells were incubated with primary antibodies against CD9, CD81 or CD63 as indicated.

depend on either tetraspanin for entry. To focus on S-mediated entry, we utilized pp transduction. We first sensitized the cells to transduction by overexpressing CoV receptors, then transduced cells with the respective CoV pps. Relative to WT cells, CD9KO cells were 94% less susceptible to MERS pp transduction (Figure 17A), a result that reflects the data. Furthermore, we found CD9KO cells were 80% less susceptible to 229E pp transduction (Figure 17B), indicating that CD9 acts as an entry factor for 229E-CoV as well as MERS-CoV. However, CD9KO cells remained fully susceptible to SARS pp or MHV pp transduction (Figure 17C and D). As expected, CD9 complementation restored susceptibility to MERS pp and 229E pp transductions (Figure 17A and B).

CD81 KO cells were fully susceptible to all four of the CoV pps (Figure 18). The lone exception is a statistically insignificant decreased in SARS pp entry into CD81KO cells. These data along with those in Figure 17 suggest that CD9, but not CD81, acts as a specific tetraspanin partner for MERS-CoV and 229E-CoV entry factors. Furthermore, CD9 does not affect an entry factor common to all CoVs.

Our previous results using tetraspanin antibodies suggested that CoV reliance on tetraspanins correlated with TTSP expression levels in target cells. We found that massive overexpression of these proteases bypasses CoV reliance on tetraspanins (Figure 10) which we believe is likely due to high levels of non-tetraspanin associated TTSP localization (Figures 13 and 21). Therefore, we hypothesized that MERS and 229E entry into the CD9KO cells was less efficient because the viruses were significantly less likely to encounter priming TTSPs at the cell surface. To test this hypothesis, we overexpressed

TMPRSS2 in the CD9KO cells. Like our observations with antibody experiments (Figure 10), overexpression of TMPRSS2 in the CD9KO cells eliminated the effect of CD9 depletion on both MERS and 229E entry (Figure 19). Furthermore, TMPRSS2 overexpression alone significantly increased entry of all CoV pps (compare Figures 17 and 19).

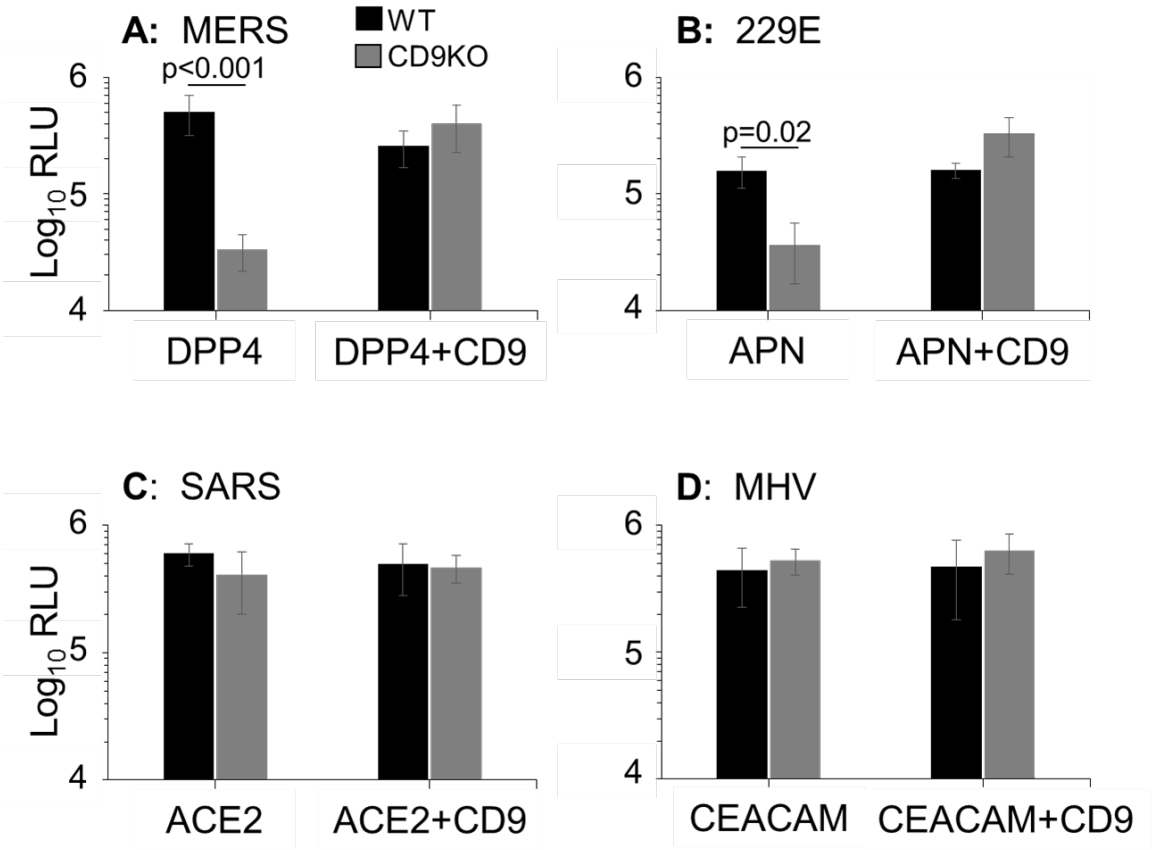

Figure 17. COV-S mediated entry into CD9 knocked out 293 cells. 293T WT or CD9KO cells were transfected with appropriate receptors and either an EV or CD9 where indicated. These cells were transduced with HIV pseudoviruses carrying S proteins of MERS **(A)**, 229E **(B)**, SARS **(C)**, or MHV **(D)**. Pseudovirus transduction was measured using luciferase assay.

CD9 is required to deposit DPP4 and APN into tetraspanin-enriched membranes. The observation that a single tetraspanin family member, CD9, facilitated cell entry for some, but not all CoVs, suggested the existence of specific interactions between CD9 and one or more MERS-CoV and 229E-CoV entry factors. We considered whether CD9 directs DPP4 and APN, the MERS-CoV and 229E-CoV receptors, to TTSP-enriched membrane microdomains. Furthermore, we considered whether CD9 does not direct ACE2 and CEACAM, the receptors for CD9-independent SARS-CoV and MHV. This was first investigated through biochemical isolation and analysis of TEMs for CoV entry factors, as described above (Figures 12 and 13). To this end, CD9 or CD81 KO cells overexpressing CoV receptors or TMPRSS2 were surface-biotinylated, solubilized in CHAPS detergent, and membrane fractions were separated by 2 rounds of differential centrifugation. After streptavidin pulldown, HD and LD fractions were analyzed for CoV entry factors.

Strikingly, the LD fractions from WT control cells contained ~60% of cell-surface DPP4, while LD fractions from CD9KO cells completely lacked DPP4 (Figure 20A, rows 1 and 2). Complementing CD9 back into CD9KO cells restored LD-associated DPP4 (Figure 20A, row 3). The presence or absence of CD81 had no effect on DPP4 distribution between HD and LD fractions (Figure 20A, rows 4 and 5). Similar results were observed with the

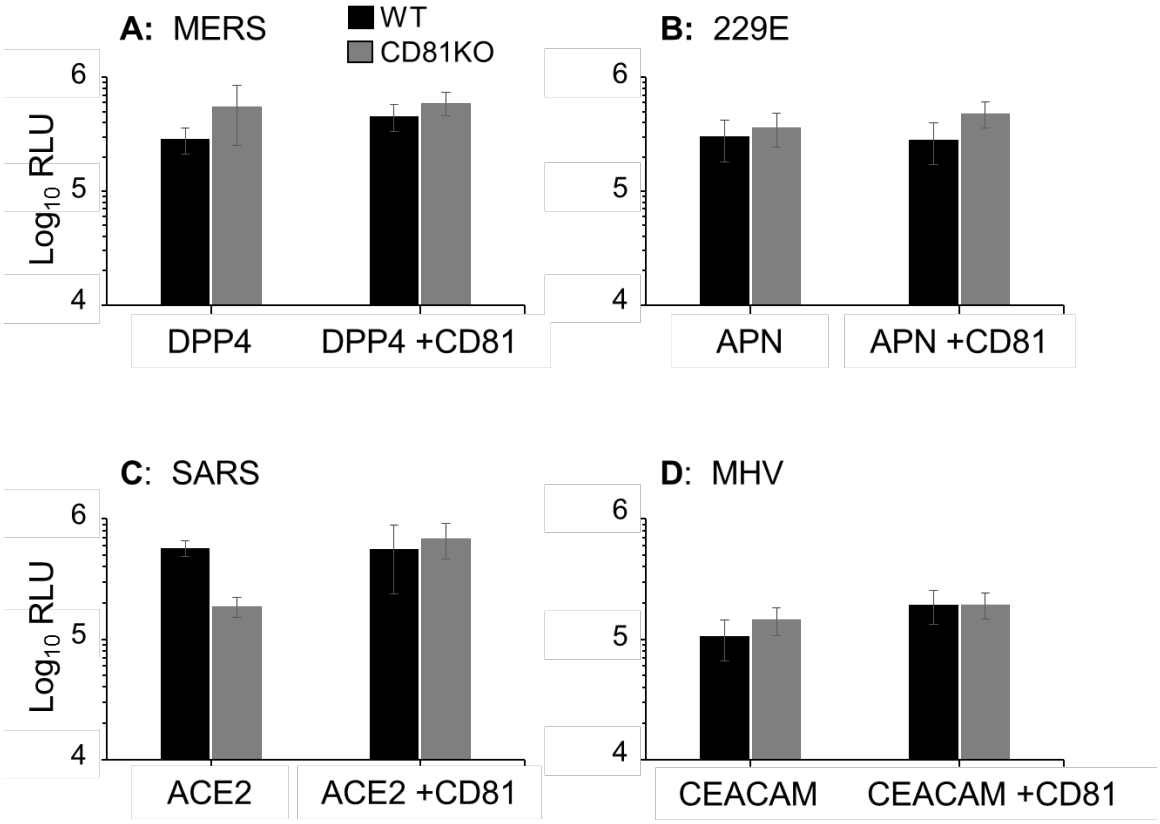

Figure 18. CoV Transduction of CD81KO 293T cells. 293T WT or CD81KO cells were transfected with appropriate receptors and either an EV or CD81 as indicated. These cells were transduced with HIV pseudoviruses carrying the indicated CoV S proteins as in figure 16. Pseudovirus transduction was measured using luciferase assay.

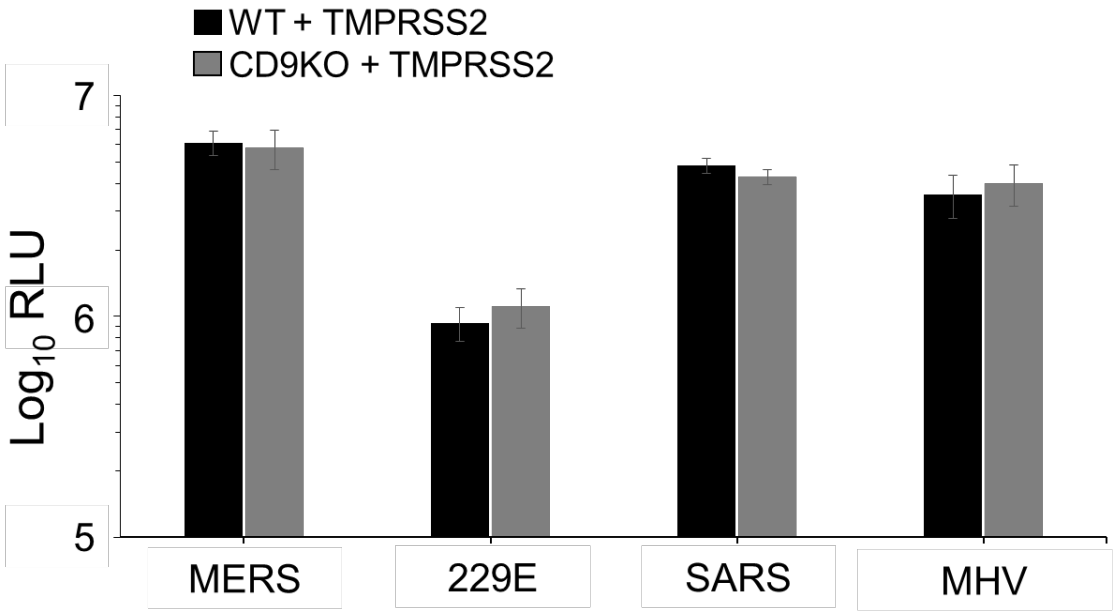

Figure 19. Effect of TMPRSS2 overexpression on transduction of CD9KO cells. 293T WT or CD9KO cells were transfected with TMPRSS2 and the appropriate viral receptor as in figure 16. Cells were transduced with the indicated pseudovirus. Transduction levels were measured by luciferase assay.

229E receptor APN (Figure 20B). By contrast, CD9 and CD81 expression had little effect on the distribution of ACE2, CEACAM, or TMPRSS2, all of which distributed about equally between LD and HD fractions (Figure 20C-E). These data indicate that the positioning of DPP4 and APN into TEMs requires CD9, which suggests that CD9 interacts with these receptors and co-localizes them with other tetraspanin-associated proteins, such as TMPRSS2. The fact that CD9 repositioned DPP4 and APN, but not ACE2 or CEACAM, correlated with the fact that CD9 facilitated DPP4- and APN-utilizing MERS and 229E pps, but not ACE2- or CEACAM-utilizing SARS and MHV pps.

CD9 holds DPP4 and TMPRSS2 in close proximity. As discussed in Chapter I and observed in Figure 12, TEMs can accurately identify tetraspanin partner proteins. However, these collected membrane fractions likely do not accurately reflect interactions in the tetraspanin web in intact cells. Therefore, we endeavored to analyze tetraspanin-mediated interaction of CoV entry factors *in situ*. Specifically, we attempted to determine if CD9 facilitates the close interaction of the MERS entry factors DPP4 and TMPRSS2 in target cells. To this end, we performed proximity ligation assays (PLAs), which can determine whether two or more transmembrane proteins are adjacent [135], in CD9KO cells. As discussed in Chapter I, PLA allows for detection of proteins that are within 40 nm.

HeLa cells were chosen for PLA assays because their relatively flat morphology facilitated quantification of fluorescent foci. CD9KO HeLa cells transfected with

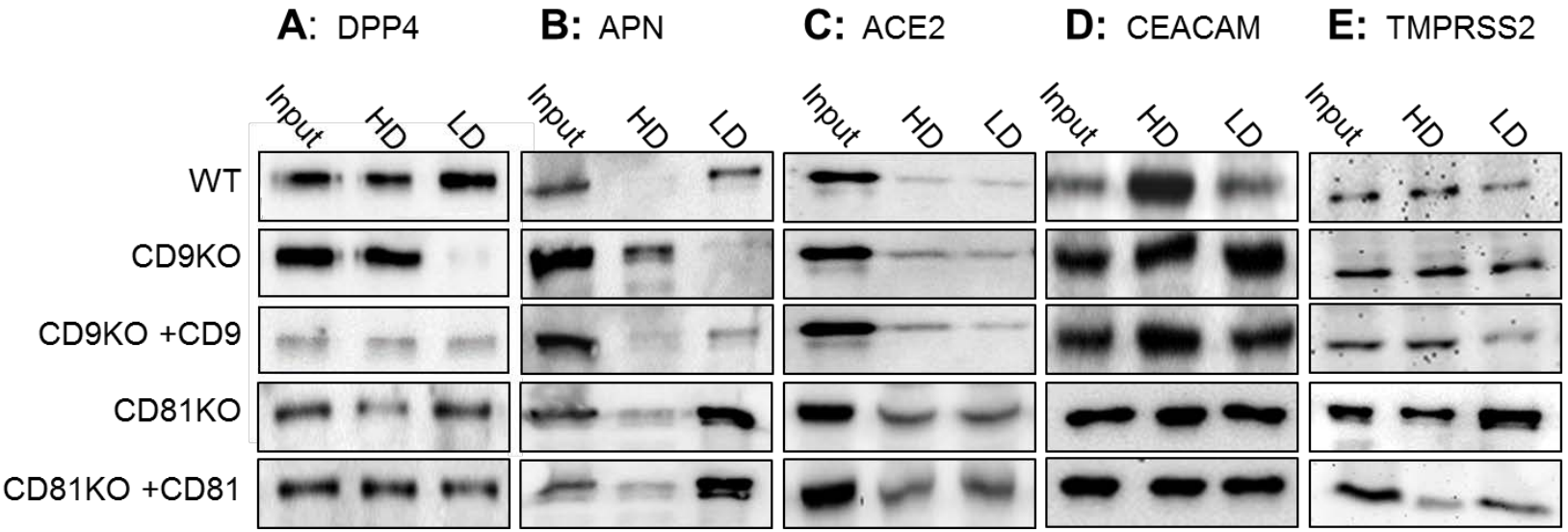

Figure 20. Association of CoV entry factors with CHAPS-resistant membranes in the presence or absence of CD9 or CD81. 293T WT, CD9KO, or CD81KO cells were transfected with the CoV receptors DPP4 **(A)**, APN **(B)**, ACE2 **(C)**, CEACAM **(D)**, or the protease TMPRSS2 **(E)**. KO cells were also complemented with the appropriate tetraspanin as indicated on the left. Cell-surface proteins were biotinylated before cells were lysed in cold CHAPS and cleared lysates were subjected to differential centrifugation. Cell surface proteins were isolated by streptavidin pulldown and analyzed in high density (HD) and low density (LD) fractions by western blot.

combinations of CD9, DPP4, and/or TMPRSS2 proteases, were fixed on fibronectin-coated coverslips and incubated with primary antibodies against these proteins. Following secondary antibody incubation and amplification of ligated oligonucleotide templates, punctate fluorescent DNAs were detected by confocal microscopy and counted using Imaris version 6.3.1 software.

Using hDPP4 and hTMPRSS2 antibodies, fluorescent foci were rarely observed on the HeLa-CD9KO cells (Figure 21A). Foci were ~ 10-fold more abundant after transfection with CD9 alone (Figure 21D), indicating that CD9 alone was responsible for connecting these two entry factors. These results were corroborated under conditions in which hDPP4 and hTMPRSS2 were exogenously overexpressed. With overexpression of both proteins, ~30 foci/cell were observed (Figure 21E), and this increased to ~80 foci/cell in the presence of CD9 (Figure 21F). Transduction experiments indicated that MERS pp entry into cells correlated with the number of foci present, at least at values up to ~30 foci/cell (Figure 21H). We speculate that the ~30 foci/cell observed in DPP4/TMPRSS2 overexpressing CD9- cells is sufficient to maximize susceptibility to MERS pp which explains the similar transduction levels observed in the CD9- and CD+ cells (compare Figure 21G and 21H). Thus, these results indicated that CD9 connects the DPP4 and TMPRSS2 entry factors together, and suggest that cell surface complexes of DPP4, TMPRSS2, and CD9 function as MERS-CoV entry portals.

These data suggest that exogenous overexpression of proteins overwhelms the ability of endogenous tetraspanins to localize/sequester them in tetraspanin-rich regions.

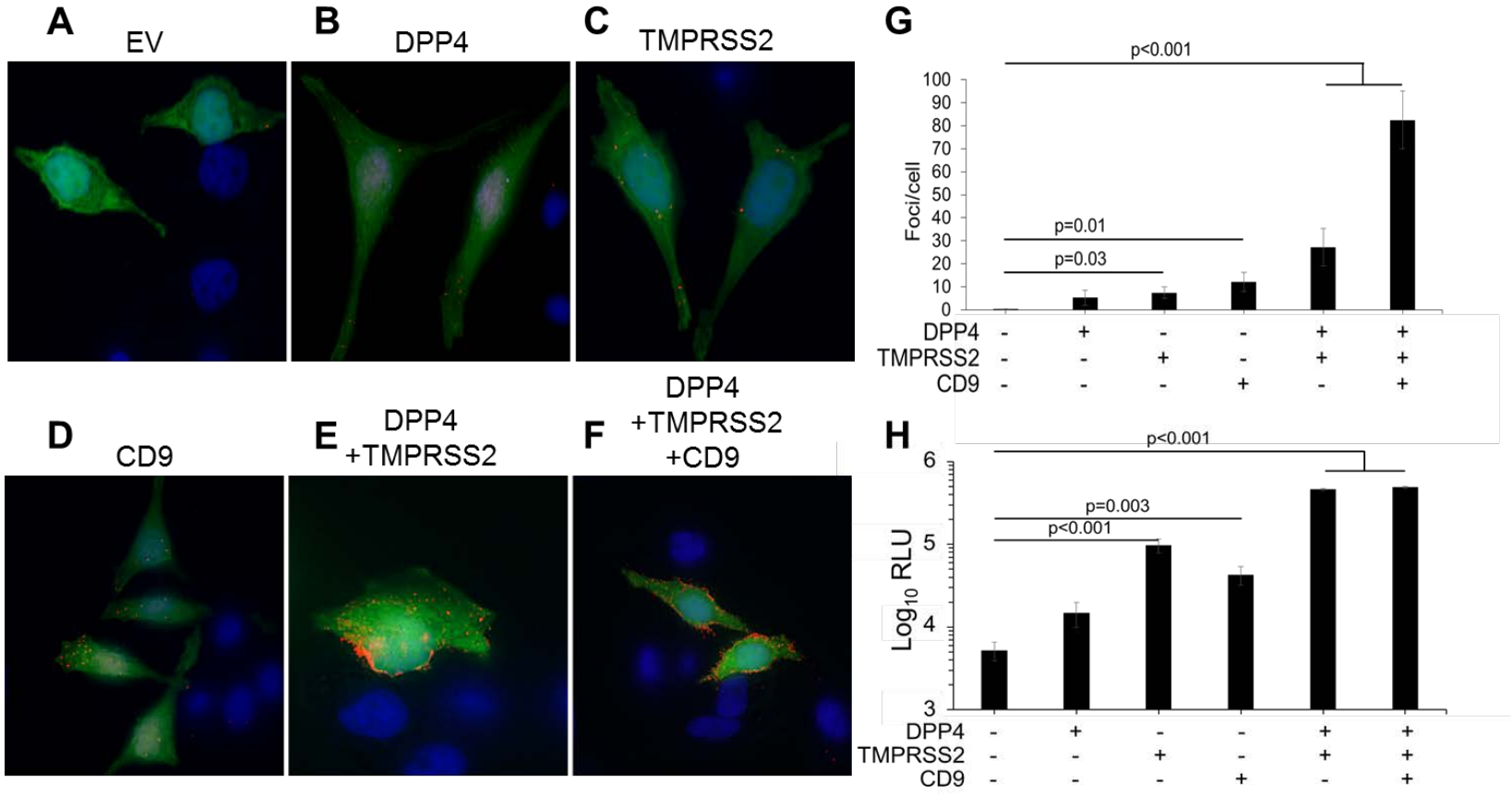

Figure 21. Proximity ligation assay of DPP4 and TMPRSS2 in CD9KO cells. **(A-F)** HeLa CD9KO cells were transfected with the indicated genes and a GFP reporter before being mounted on microscopy slides. Proximity ligation assay was performed using primary antibodies against hDPP4 and hTMPRSS2. Red dots indicate close proximity of the two proteins. **(G)** The average number of foci/cell in GFP+ cells in each group was quantified. **(H)** MERS pp transduction of HeLa cells overexpressing the indicated proteins.

This can potentially explain why TMPRSS2 alleviated inhibition of MERS entry by tetraspanin antibody blockade and CD9KO (Figures 10 and 19), as overexpressed TMPRSS2 was no longer fully sequestered in tetraspanin-rich regions. Regardless, in overexpressing cells, TMPRSS2 and DPP4 proximity was either more common or more stable in cells expressing CD9 (Figure 21H).

MERS entry kinetics in CD9-deficient cells. CoVs can enter cells through early or late entry routes depending on protease availability (see Figure 3). While early entry requires fusion-activating TTSPs at the cell surface, late entry requires fusion-activating endosomal cathepsins [65, 66]. Because CD9 brought DPP4 in proximity with one of the TTSPs, we hypothesized that CD9 facilitates rapid, early cell entry. To test this, we performed entry kinetics assays. In these assays, MERS pps are bound to cells at 4^{o}C to synchronize viral-cell binding, then shifted to 37^{o}C to allow entry for timed intervals. MERS entry was halted by adding a nontoxic protease inhibitor cocktail and quantified relative to entry into untreated control cells (experiment was adapted from[79]). Since CoVs cannot complete fusion in the presence of these inhibitors, the transduction readouts indicate the extent of virus entry taking place within the inhibitor-free time periods.

MERS pp entry rates were slowed in the absence of CD9 (Figure 22A). Compared to WT cells, the initiation of entry into CD9KO cells was delayed by 10 minutes and remained significantly delayed until 1 hour after temperature shift, when all measured viral fusion had occurred (Figure 22A). Complementation of CD9 into the CD9KO cells

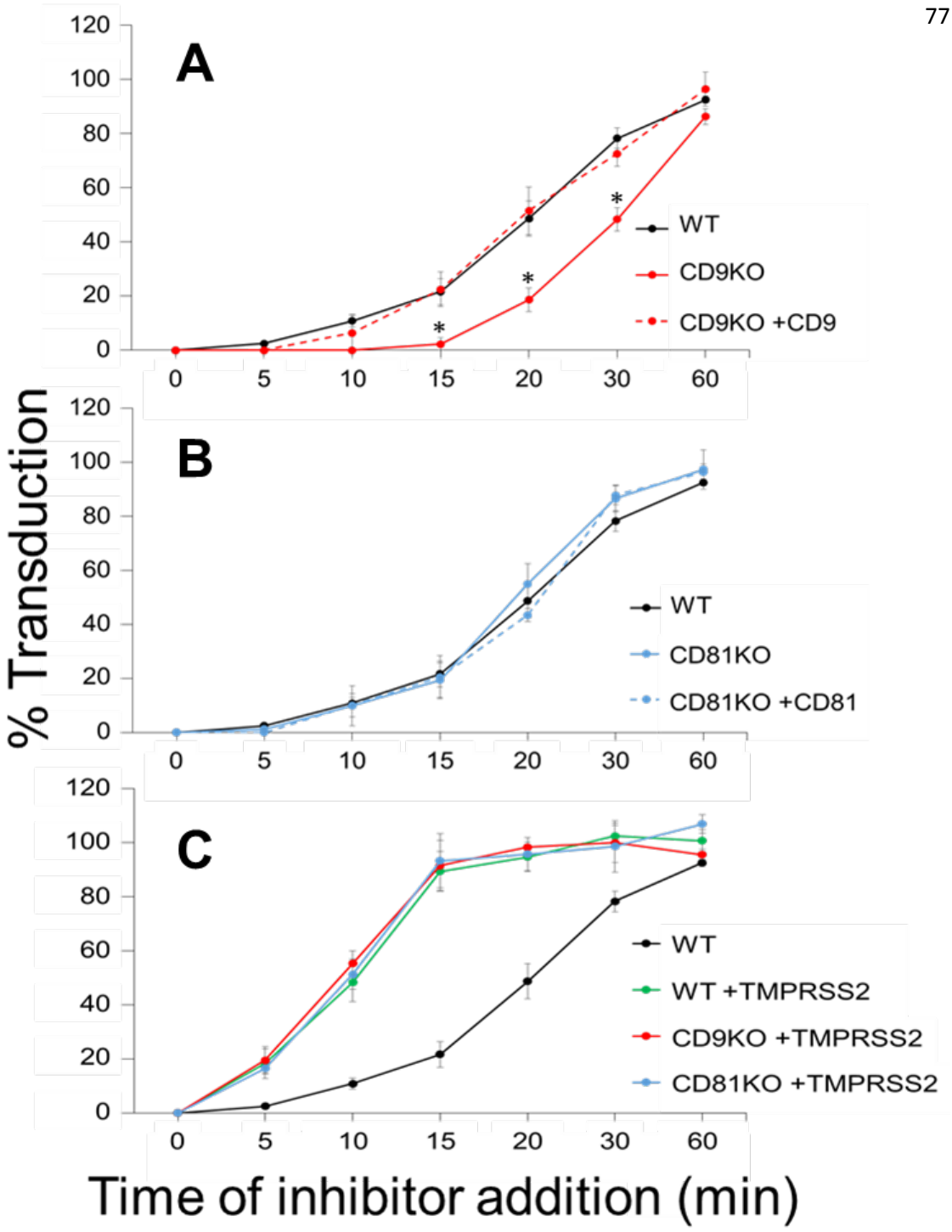

Figure 22. Entry kinetics of MERS pp in tetraspanin KO cells. The entry kinetics of MERS pps were measured in 293T WT, CD9KO **(A)**, and CD81KO **(B)** cells. Cells were bound with MERS pps and incubated with entry inhibiting protease cocktail at the indicated time point. Luciferase levels were measured and plotted relative to untreated control cells. **(C)** Entry kinetics into KO cells complemented with cells overexpressing TMPRSS2. *$p<0.01$ compared to WT cells.

restored MERS pp entry kinetics to those observed with WT cells (Figure 22A). MERS pp entry into CD81KO cells was nearly identical to the WT cells (Figure 22B). Thus, we concluded that CD9 facilitates rapid MERS entry into target cells. From these data, we also speculated that late entering viruses begin to fuse between 15-20 min after cell binding and that late entry can take up to 60 min.

We have observed that TMPRSS2 overexpression can alleviate CoV dependence on tetraspanins for entry. Specifically, forced overexpression of TMPRSS2 made MHV resistant to tetraspanin antibody blockade (Figure 10), obviating the need for CD9 in MERS pp entry (Figure 19), and led to a large number of DPP4/TMPRSS2 foci in PLA (Figure 21). Therefore, we posited that MERS entry into TMPRSS2-overexpressing cells would be both rapid and CD9 independent. As expected, WT and KO cells that overexpressed TMPRSS2 were similarly susceptible to a very rapid MERS virus entry, with 50% of maximal entry by 10 min, regardless of CD9 or CD81 expression (Figure 22C).

MERS protease utilization in CD9-deficient cells. As discussed in Chapter I (see Figure 3), CoV early entry depends on TTSPs, which are inactivated by the serine protease inhibitor camostat [73]. Since our data suggest that MERS early entry is CD9-dependent, we expected that MERS pp entry in CD9KO cells would not rely on these camostat-sensitive proteases. To test this, we transduced DPP4 overexpressing 293T WT, CD9KO, and CD81KO cells. Camostat suppressed MERS pp transduction into WT cells by ~50% compared to untreated cells, but did not affect transduction into CD9KO cells (Figure 23A). CD9 complementation modestly restored

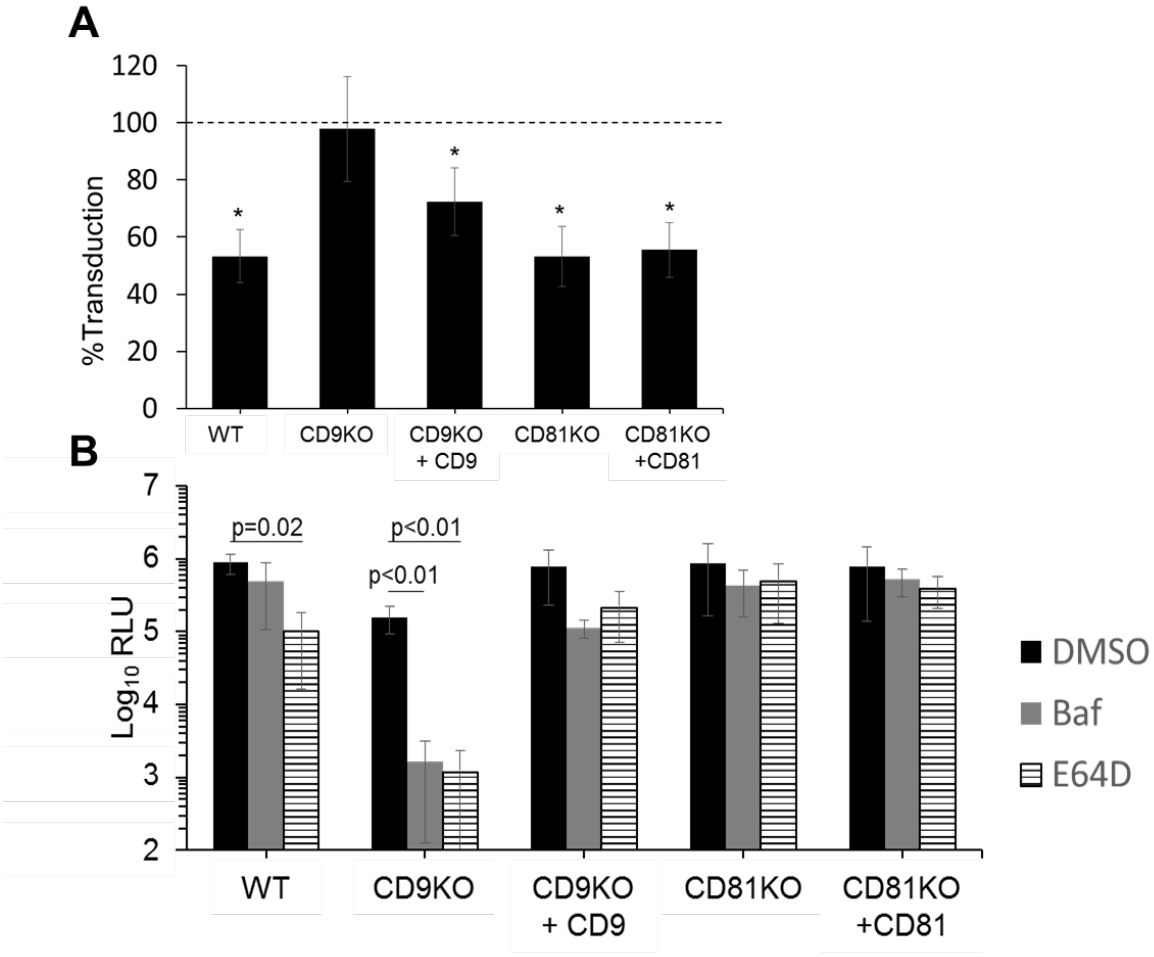

Figure 23. Protease utilization of MERS pp entry in tetraspanin KO cells. **(A)** WT or KO cells were transfected with DPP4 and either an empty vector or the complementing tetraspanin as indicated. The cells were pretreated with camostat before transduction with MERS pps. MERS entry was measured by luciferase assay and the percent transduction levels of viruses into camostat treated cells is plotted relative to untreated cells (dotted line). **(B)** WT or KO cell lines were transfected with DPP4 and either an empty or the complimenting tetraspanin as indicated. The cells were pretreated with bafilomycin or E64D before transduction with MERS pp. MERS entry was measured by luciferase assay.

MERS pp sensitivity to camostat to around 70% of transduction of untreated cells. Furthermore, CD81 had no effect, as MERS pp entry into CD81KO and CD81-positive cells were equally suppressed by camostat and indistinguishable from WT cells (Figure 23A). These data suggest that camostat-sensitive early entry requires CD9.

Previous studies in our lab have characterized a MERS S mutation that prevent participation in early entry. This mutation changes the amino acids in the S1/S2 cleavage site from the furin target RSVR (see Figure 2) to a serine-protease resistant YSAS. MERS pps produced with the S1/S2 mutant enter cells in a manner independent of TTSP activity and completely dependent on cathepsins. We hypothesized that CD9 depletion would have no effect on a virus that cannot participate in early entry. As expected, YSAS pp transduction of target cells was inefficient compared to WT and was completely independent of CD9 expression (Figure 24). From this, we concluded that CD9 plays no role in MERS late entry.

Without CD9, the MERS pp entry may be forced to late, endosomal routes in which cathepsins provide fusion-activating triggers (see Figure 3). To test this, we blocked late entry in WT and CD9KO cells by introducing two inhibitors of endosomal cathepsins. Cells were pretreated with 100 μM bafilomycin A (Baf) or 10 μM of the cysteine protease inhibitor E64D before transduction with MERS pp. In WT cells, Baf did not significantly decrease entry, while E64D decreased entry ~4-fold (Figure 23B). However, in CD9KO cells, these inhibitors were far more antiviral, decreasing entry 20- and 100-fold, respectively. Complementing CD9 back into the CD9KO cells restored the WT condition in which the inhibitors were only weakly antiviral (Figure 23B). CD81

expression had no effect on cathepsin-dependence (Figure 23B). From these results, and from the entry kinetics assays (Figure 22), we inferred that CD9 is necessary for early, cell-surface cell entry by MERS-CoV.

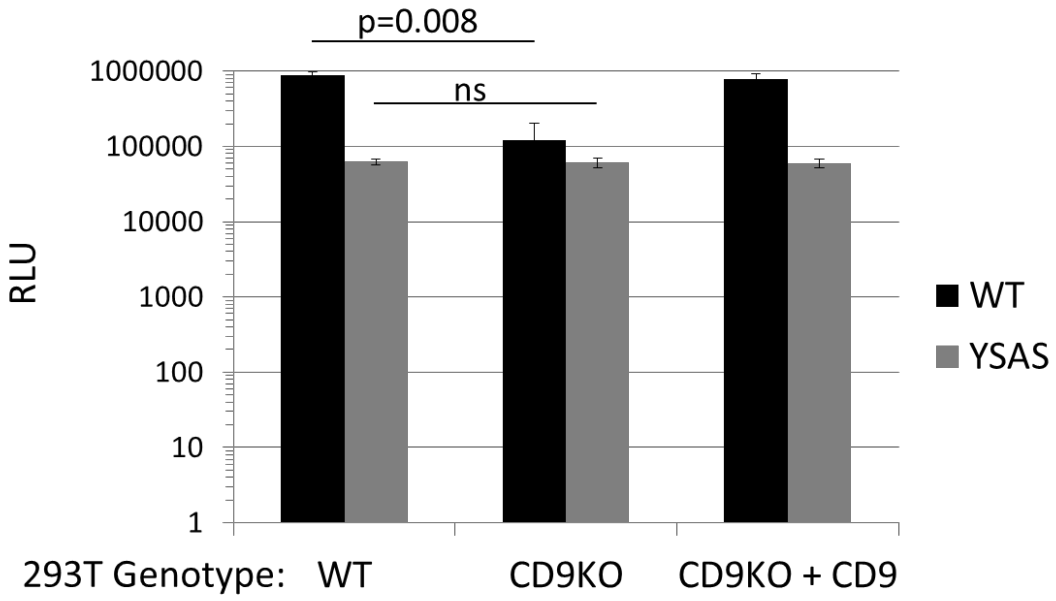

Figure 24. Effect of CD9 expression on MERS S1/S2 mutant. 293T WT and CD9KO cells were transfected with DPP4 and either an EV or CD9. Cells were transduced with MERS pp produced with an S containing a WT RSVR (black) or YSAS (gray) S1/S2 cleavage site. The YSAS mutant has been shown to enter cells through late entry. Transduction of cells was measured using luciferase assay.

Cholesterol depletion inhibits infection in CD9-deficient cells. Recent structural studies of the tetraspanin CD81 revealed that the transmembrane domains associate with a single molecule of cholesterol [118]. Furthermore, the presence or absence of cholesterol was shown to affect the ability of CD81 to associate with partner proteins. As discussed in Chapter I, cholesterol has commonly been identified as an entry co-factor for a variety of CoVs, including MERS [171] and MHV [116] but the mechanism for this is unclear. We hypothesized that cholesterol mediates the interaction of tetraspanins and CoV entry factors. Thus, cholesterol depletion of target cells would interfere with tetraspanin-mediated early entry of MERS-CoV. If this were the case, MERS entry into CD9KO cells would be cholesterol independent. To test this hypothesis, we serum starved 293T CD9KO cells, transfected with DPP4 or CEACAM, before treating the cells with methyl-beta-cyclodextrin (MβCD), a cholesterol chelating agent. We transduced these cells with CD9-independent MHV pp or MERS pp. Cholesterol starvation rendered WT and CD9KO about 30% and 40% resistant to MERS and MHV transduction, respectively at 10 mM cyclodextrin (Figure 25). There was no significant difference observed between the susceptibility of WT and CD9KO cells to either pp. Higher doses of cyclodextrin were likely lethal to target cells. While these results did not support our hypothesis, further studies using tetraspanin mutants incapable of binding cholesterol may obviate the need for drug treatment and allow us to draw conclusions on cholesterol's effects on early entry.

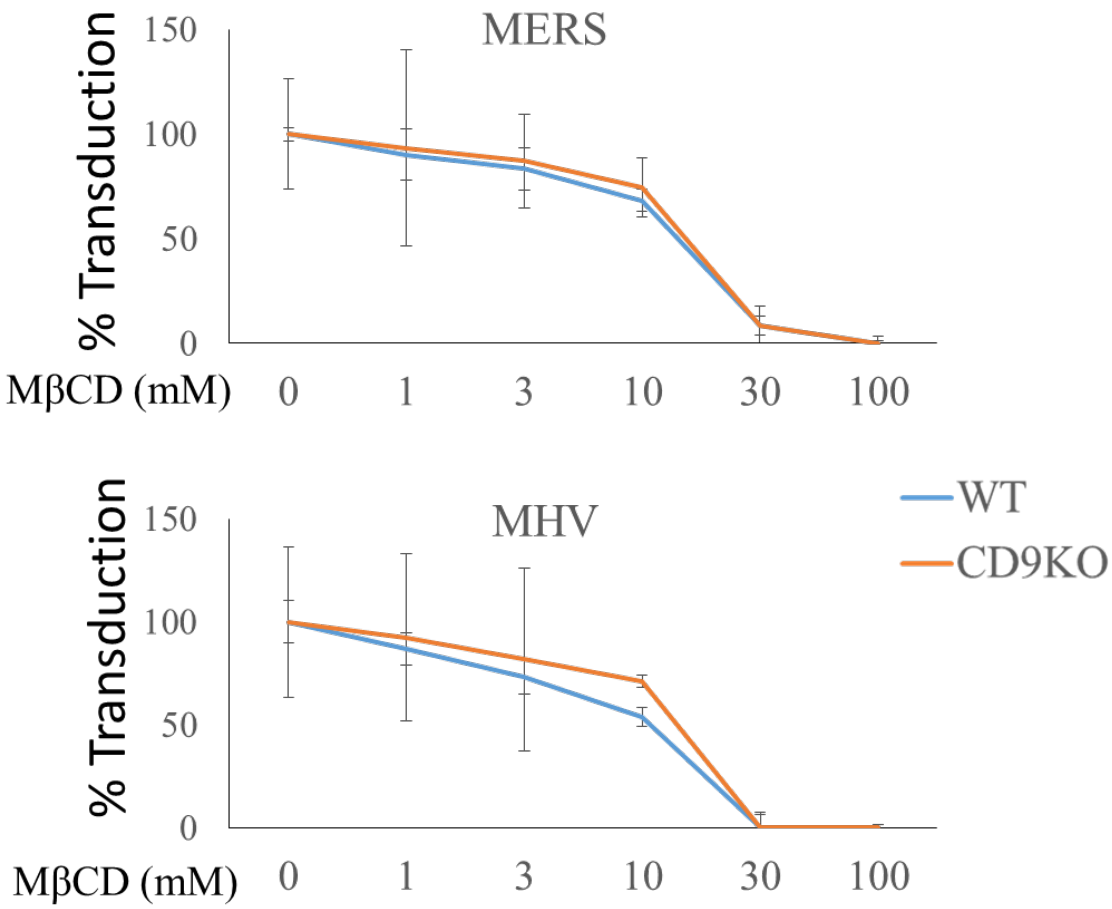

Figure 25. Effect of cholesterol depletion on CoV entry into CD9KO cells. 293T WT or 293T CD9KO were transfected with DPP4 (for MERS pp) or CEACAM (for MHV pp). Cells were serum-starved and treated with the indicated concentration of MβCD for 4 h before transduction with MERS pp or MHV-A59 pp. Cells were washed after 2 h and pseudovirus entry was measured by luciferase assay.

SECTION 3: Importance of Early MERS-CoV Entry in Mice.

No study to date has determined the relative importance of CD9 or TMPRSS2-mediated early entry in MERS-CoV infection in the lung environment. Indeed, there are

34 human tetraspanins and at least 17 members of the TTSP protease family [106] as well as several soluble extracellular proteases, such as elastases [73], in the lung parenchyma, making it unclear whether CD9 or TMPRSS2 stand out *in vivo* as the single necessary proviral members of their respective protein families. Therefore, we attempted to determine whether and to what extent MERS-CoV utilizes CD9 and TMPRSS2 during *in vivo* infection. To this end, we established a mouse model in which virus-resistant mice are rendered susceptible to MERS-CoV infection by expression of human *DPP4* (h*DPP4*). The system utilizes an adenovirus type 5 (Ad5) to transduce the h*DPP4* gene, thereby sensitizing only the Ad5-transduced lung cells to subsequent MERS-CoV infection [172]. The Ad5-h*DPP4* vectors were engineered to include additional genes encoding human TMPRSS2 or potential virus-restricting factors, in the form of shRNAs targeting murine *Tmprss2* and *Cd9*. We considered the Ad5-h*DPP4* system to be especially valuable, as MERS-CoV infection can only occur in cells expressing hDPP4 and, thus, only in cells simultaneously expressing the putative virus-promoting or virus-restricting factors. Therefore, the dual-expressing Ad5 vectors might be excellent tools to rapidly obtain clean results that identify *in vivo* pro- and anti-viral host factors.

Adenovirus vectored knockdown of CD9 and TMPRSS2 in target cells. Our mechanistic insights of CD9-mediated MERS early entry encouraged us to determine the importance of CD9 and early entry *in vivo*. However, we first determined whether the rAd5 constructs could manipulate protein expression in mouse cells *in vitro*. We tested the following rAd5 vectors: rAd5-hDPP4-hTMPRSS2, the shRNA-encoding rAd5-hDPP4-shTmprss2 and rAd5-hDPP4-shCd9, and the control viruses rAd5-hDPP4-empty and rAd5-GFP. We chose to test these constructs in the Lung Epithelial Type 1 (LET1)

cell line which was derived through immortalization of alveolar type 1 cells from C57/Bl6 mice [110]. LET1 cells were transduced with the rAd5 vectors at MOI 10. Following a 3 d incubation, the cells were lysed and analyzed for the presence of DPP4, TMPRSS2, and CD9 by western blot (Figure 26A). Cells transduced with the control rAd5-GFP had detectable levels of CD9, but barely detectable levels of DPP4 and TMPRSS2. The respective experimental Ad5 vectors produced abundant, recognizable DPP4 and TMPRSS2, and those Ad5 vectors expressing shRNAs reduced the levels of endogenous CD9 proteins (Figure 26A). These results indicate that the rAd5 vectors, transduced into cells derived from mouse alveolar epithelia, consistently and equally express hDPP4 while simultaneously increasing or decreasing TMPRSS2 or CD9. Experiments examining rAd5-hDPP4-shTmprss2 knockdown of an endogenously expressed, detectable level of TMPRSS2 are ongoing.

Knockdown of CD9 and TMPRSS2 inhibit MERS-CoV infection. We determined whether the rAd5-transduced LET1 cells were susceptible to MERS-CoV S protein-directed virus entry. To this end, the cells were inoculated with the rAd5s for 3 d before being transduced with MERS pp. As expected, cells transduced with Ad5-GFP were resistant to MERS pp entry due to lack of hDPP4 receptors. Cells transduced with any of the Ad5-hDPP4 vectors were permissive (Figure 26B). TMPRSS2 expression from the Ad5 vectors increased permissivity to MERS pps by ~ 4-fold, while shTmprss2 and shCd9 both restricted MERS pps by ~3 fold (Figure 26B). These results indicated that CD9 and TMPRSS2 act as entry factors in mouse lung-derived LET1 cells, and suggested that the dual-expressing Ad5 vectors might be effective tools for identifying viral entry factors in the mouse lung.

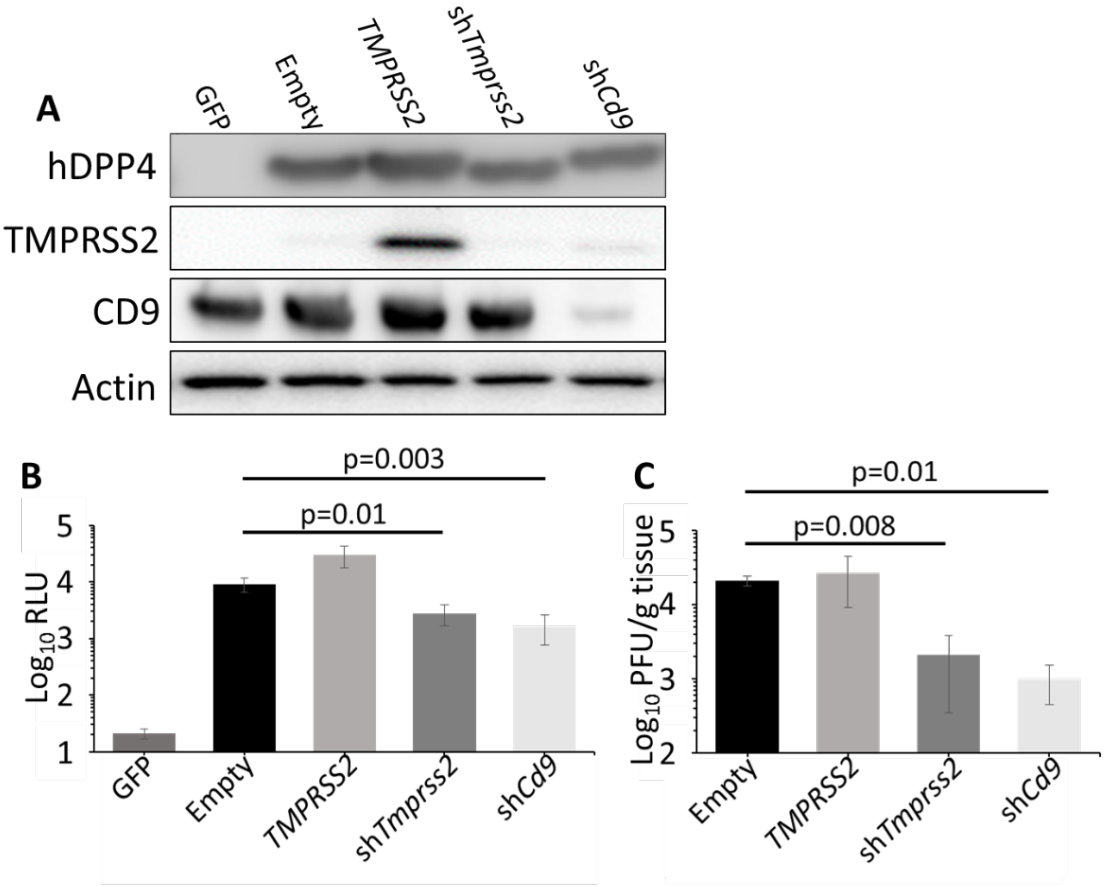

Figure 26. Analysis of Adenovirus mediated knockdown of CD9. **(A)** LET-1 cells were transduced with an adenovirus carrying a GFP gene or an adenovirus carrying hDPP4 and either an empty vector, the TMPRSS2 gene, or a U6-driven shRNA against TMPRSS2 or CD9. After 3 days, cells were lysed and analyzed by western blot for the indicated proteins. **(B)** LET1 cells were transduced with the indicated Ad5 vector before transducing with MERS pp. Transduction was measured by luciferase assay. **(C)** The indicated Ad5 vector were installed intranasaly in C57/Bl6 mice. 3 days later, mice were infected with MERS-CoV. 2 dpi lungs were isolated and viral titers were measured by plaque assay. The experiments in (C) were performed by Dr. Kun Li at the University of Iowa.

To identify the role of CD9 and TMPRSS2 *in vivo*, the Ad5 vectors were intranasally installed into mice, allowed to express transgenes for 5 d, and then challenged with MERS-CoV (strain HCoV-EMC/2012). Lungs were harvested 2 days post-infection (d.p.i.) and MERS-CoV titers were measured as plaque forming units (PFU)/gram of tissue. Relative to MERS-CoV titers in rAd5-hDPP4 transduced animals, the MERS-CoV titers in rAd5-hDPP4-shCd9 transduced animals were ~20-fold lower (Figure 26C). Furthermore, the MERS-CoV titers in rAd5-hDPP4-shTmprss2 transduced mice were reduced by ~10-fold. Interestingly, overexpression of TMPRSS2 by the rAd5-hDPP4-TMPRSS2 vector had no effect on MERS-CoV titers in the lungs, presumably because the lung environment has sufficient endogenous TMPRSS2 to facilitate efficient MERS-CoV infection. These data indicate that CD9 and TMPRSS2 act as MERS-CoV susceptibility factors in the lung parenchyma and that their role in entry is more pronounced *in vivo* than in *in vitro* LET1 mouse alveolar cell cultures. Indeed, these data show that CD9 and TMPRSS2 are responsible for ~90% of MERS-CoV titers *in vivo*.

SECTION 4: Membrane-targeted Antiviral Small Molecules.

One of the advantages of identifying the subcellular location of CoV fusion reactions is being able to target these areas with antiviral drugs. HR2 peptides, as discussed in Chapter I, can be effective in blocking enveloped virus entry. However, to do so, the peptides must encounter viral glycoproteins in the meta-stable extended intermediate state (see Figure 1). This conformation is likely short-lived in CoVs which limits the effectiveness of HR2 peptides as antiviral therapies for CoVs.

Previous studies have shown that tagging HR2 peptides with lipid moieties can increase their effectiveness in blocking enveloped virus fusion [173]. We hypothesized that CoV HR2 peptides targeted to the specific subcellular location of viral entry would show similar efficacy. Surprisingly, Dr. Jung-Eun Park found HR2 peptides derived from MERS can potently inhibit MHV infection, despite little amino acid conservation in the HR1 regions of the two viruses. We took advantage of this by analyzing lipid-tagged HR2 blockade of early and late entering MHV strains. MHV-A59 and MHV-JHM utilize early entry as evidenced by their reliance on tetraspanins (Figure 6) and utilization of TMPRSS2 (Figure 10A). Conversely, MHV strain 2 (MHV-2) uses the late entry route almost exclusively, due to the lack of an ideal serine protease cleavage site at S1/S2 [63]. Therefore, we hypothesized the HR2 peptides tagged with cholesterol and palmitic acid, which likely accumulate at the cell surface and possibly near tetraspanin-rich regions [131, 174], would effectively block MHV-A59 and -JHM but not MHV-2. However, HR2 peptides tagged with tocopherol, which would likely accumulate in the endosome [175], would preferentially block a late entering virus like MHV-2.

Lipid-conjugated HR2 peptides potently inhibit MHV infection. To test the efficacy of lipid-tagged HR2 peptides, we infected DBT cells with rMHV-A59 and -JHM in the presence of the peptides. We obtained, from our collaborator Dr. Matteo Porotto, HR2 peptides tagged with maleimide chemistry to cholesterol, palmitic acid, or tocopherol through a polyethylene glycol (PEG) linker. As controls, we used untagged HR2 peptides and HR2 peptides only tagged with the PEG linker. When pretreated with the cholesterol- and tocopherol- tagged HR2 peptides, DBT cells became significantly more resistant to infection by MHV-A59 and -JHM (Figure 27). In both cases, the

palmitic acid nearly eliminated infection when used as a 1 μM dose. Untagged and PEG tagged had little effect on MHV-A59 infection and no effect on MHV-JHM infection. Interestingly, the tocopherol-tagged HR2 peptides showed only limited efficacy against these two viruses and only at the highest dose. These results were consistent with our hypothesis that cholesterol and palmitic acid-tagged, but not tocopherol-tagged, HR2 peptides can be targeted to early entry events.

Tocopherol-tagged HR2 peptides only inhibit late-entering MHV-2 strain.

To further investigate the role of the lipid tags in increasing HR2 peptide efficacy, we determined if a late entering MHV-2 virus would be more effectively inhibited by a tocopherol-tagged HR2 than the early entering MHVs. We performed a MHV-2 plaque reduction assay using the untagged, cholesterol tagged, and tocopherol tagged HR2 peptides. Interestingly, we found that tocopherol tagged HR2 peptides had a lower ED50 than the cholesterol tagged HR2 (Figure 28, solid lines). These data support our hypothesis that lipid tags target the HR2 to specific subcellular locations. To further investigate this, we manipulated the MHV-2 entry route by pre-treating the virus with trypsin. While trypsin destabilized the MHV-2 viruses and decreased their specific infectivity, it also likely allowed the virus to participate in early entry and expose extended intermediate conformations at the cell surface. Following trypsin treatment, the efficacy of the cholesterol-tagged HR2 peptide increased dramatically (Figure 28, dashed lines). However, the efficacy of the tocopherol tagged HR2 decreased by a similar degree. These data strongly suggest that the lipid tags increase HR2 efficacy by targeting the peptides to the specific membranes at which CoVs participate in fusion.

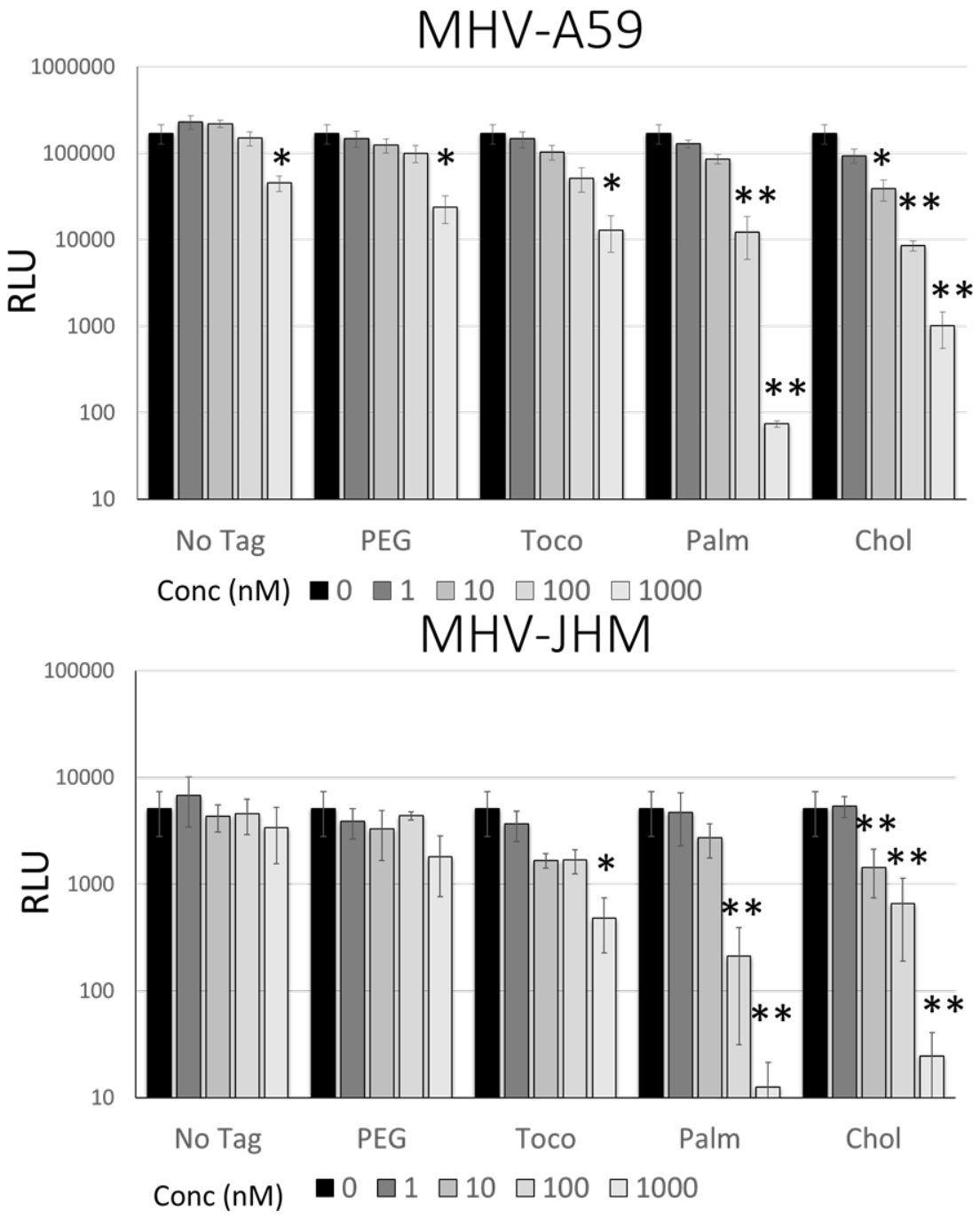

Figure 27. Inhibition of MHV infection by lipid-tagged HR2 molecules. DBT cells were incubated for 30 min with the indicated concentrations of HR2 peptides with no modification (No Tag), a polyethylene glycol linker (PEG), or the PEG linker attached to tocopherol (Toco), palmitic acid (Palm), or cholesterol (Chol). Cells were infected with rMHV strain A59 or JHM as indicated. 8 hpi, cells were lysed and infection was measured by luciferase assay. *$p<0.01$, **$p<0.001$ compared to untreated cells.

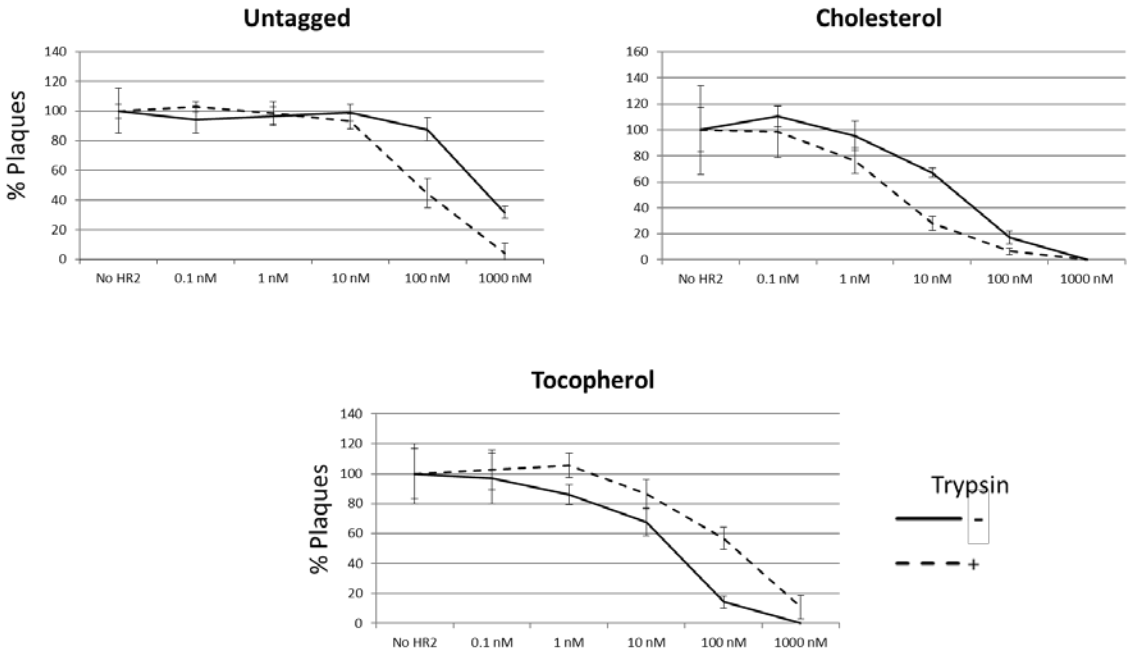

Figure 28. Inhibition of MHV-2 infection by lipid-tagged HR2 peptides. DBT cells were incubated for 30 min with the indicated HR2 molecule. Concurrently, 100 pfu of MHV-2, pretreated for 10 minutes with media (-trypsin) or 2.5 units trypsin (+trypsin), was mixed with soybean trypsin inhibitor and inoculated onto the cells. 1 hpi, cells were washed of unbound virus and HR2 and immobilized in agar. 2 dpi, cells were fixed, stained and plaques were counted. Plaque reduction is plotted as % plaques compared to the "No HR2" control.

CHAPTER IV

DISCUSSION

Summary and Significance.

We endeavored to identify and characterize CoV entry routes and the cellular factors that contribute to early entry. We found that expression of receptors and transmembrane proteases is not sufficient for CoV early entry. Our results are the first to demonstrate this phenomenon and are also the first to identify tetraspanins as CoV entry factors. Furthermore, our results expand on what was previously known about tetraspanin-facilitated enveloped virus entry, especially the role of tetraspanins in IAV infections. Our studies found that all tested CoVs, as well several influenza A subtypes, depend on tetraspanins for efficient entry into target cells. Furthermore, we identified CD9 as a MERS and 229E-CoV entry factor and defined its role in holding viral receptors and the protease TMPRSS2 in close proximity at the cell surface. Our results indicate that enveloped viruses that require multiple entry factors likely evolve to utilize complexes that form from natural cellular processes and are not induced by viral binding or infection. Our membrane scaffolding model may be generalizable to other enveloped viruses which participate in cell-surface fusion events.

While previous studies have suggested that early entry is important *in vivo*, our studies are the first to quantify the effect removing early entry factors from mouse lungs

has on MERS-CoV infections. Our collaborators and we did this with recombinant adenoviruses (rAd5), which sensitize experimental animals to CoV infection [172]. By incorporating RNA silencing genes into rAd5 viruses carrying hDPP4, we were able to analyze the role of CD9 and TMPRSS2 as relevant proviral factors. This approach involving dual-expressing adenovirus vectors can potentially be utilized to identify any MERS-CoV or other zoonotic virus host factor. The system does not require time-consuming and costly establishment of transgenic mice, like those used in studies of SARS [176] and MERS [177], to perform *in vivo* analyses of novel human CoV entry factors. Importantly, the Ad5 dual-expression system has additional advantages over transgenic animals, since the modulation of pro- and anti-viral factors is always restricted to the virus-susceptible cells, making for robust readouts of any change in virus susceptibility. Using this system, we determined that >90% of MERS-CoV titers in mouse lungs depends on CD9 and TMPRSS2.

In addition to characterizing *in vivo* MERS infections, we used our observations of tetraspanin-mediated early entry to design antiviral therapies. We observed that lipid-tagging HR2 peptides could increase their antiviral efficacy by almost 1000-fold. Using our knowledge of the subcellular location of different entry routes, we were able to predict which lipid tags would be most effective at blocking early vs. late entering strains of MHVs. Further analysis of CoV entry factors will allow for the development of an expanded repertoire of rAd5 and HR2 antiviral therapies.

Early and Late CoV Entry.

Most enveloped viruses exhibit little variation in the subcellular location of membrane fusion, but CoVs exhibit a great flexibility in this regard. As discussed in Chapter I, there are two broad categories of subcellular location at which enveloped viruses fuse and deliver their genetic materials; i) direct fusion at cell surface (e.g., HIV, paramyxovirus) and ii) fusion out of the endosome (e.g., influenza, flavivirus)[178]. Cell-surface early entry occurs in less time than late entry (Figure 25). A variety of host factors are necessary to facilitate CoV early entry in target cells. These factors are present to facilitate the interaction of viral receptors and priming proteases at or near the surface of the cell. We determined that these factors are held together by tetraspanins at the cell surface (Figure 22). In the absence of early entry factors, CoV entry is dependent on cathepsins (Figure 23).

While we have defined the cellular factors required for each entry route, we are just beginning to measure which entry pathway is more relevant *in vivo*. Data from our collaborators strongly suggest that MERS infection of mouse lungs is acutely sensitive to knockdown of cellular early entry factors (Figure 26). These data agree with observations that late-entering MERS-CoVs inefficiently infect lung-derived Calu3 and human epithelial cell cultures [65] and clinical isolates of HCoV-229E preferentially utilize cell surface proteases [79]. Furthermore, the role of early entry *in vivo* has also been inferred in a study that determined that serine protease inhibitors render mice resistant to SARS-CoV infection to a significantly greater degree than cathepsin inhibitors [74]. These results taken together suggest that CoVs evolve S proteins that can utilize cell surface TTSPs for early entry.

These hypotheses may have significant relevance in regards to isolation and characterization of future pandemic CoVs. SARS and MERS were both identified following growth of the virus in cell culture, a common tactic for identifying novel pathogens. While the prototype SARS virus was identified following only one passage in Vero cells [179], the prototype MERS strain HCoV-EMC/2012 was passaged 6 times in Vero cells before characterization [180] and likely acquired several cell culture adaptation mutations. Importantly, the experiments described above suggest that cell culture adaptation can occur quickly and that the mutations that arise in cell culture can severely attenuate viruses in vivo. Thus, we suggest that accurate analysis of pandemic CoV entry factors require direct sequencing of patient samples.

Our conclusion that early entry is more efficient *in vivo* does not explain why CoVs retain the ability to participate in late entry. One possibility is that the integrity of tetraspanin clusters is interrupted by increases in temperature, as seen in lipid rafts [181], upon onset of fevers. This may lead to late entry being preferred during late stages of CoV infection. Another possibility is that the unstable structures of CoV S needed for early entry decrease the ability of CoVs to spread between hosts. This has been observed with pandemic influenza A viruses, which acquire more pH stable HA glycoproteins over time. This increase in stability correlates with increased transmission among in humans and ferrets, especially via the airborne route [182]. It is possible that the ability to undergo late entry is a byproduct of CoV S stability. Furthermore, the ability to utilize both entry routes may allow CoVs to infect various cell types that have disparate expression of CoV entry factors, such as tetraspanins, TTSPs, and cathepsins. This ability may increase CoV host range. Thus, we propose that late the mechanisms that

lead to late entry in CoVs may provide an evolutionary advantage to these viruses, especially in their ability to spread between hosts.

Benefits of Early Entry.

Early entry allows for rapid infection of target cells. Furthermore, S proteins that are suited for early entry are also more likely to lead to cell-cell fusion of infected cells and may facilitate easier cell-cell spread of infectious virions. The early entry route also bypasses certain, potent innate immune effectors such as interferon induced transmembrane proteins [77, 171, 183] and the humoral immune response [70].

Perhaps the most important benefit of early entry is that it bypasses the requirement of late entry in the endosomal compartments. This late entry route requires furin proprotein convertases [59, 92] and / or cathepsin L [57, 61, 77], cathepsin B [63], cathepsin K [73] cleavage of S proteins in the late endosome. However, the late endosomal environment can be very rich in proteases and other hydrolases [87], which probably generate inactivating cleavages of CoV proteins. There are several observations of S protein fragments, 40 kDa and smaller (Figure 15, for example), that are consistent with permanent inactivation [65, 184]. Therefore, there may be a short time span between a cathepsin-activated fusogenic state and a permanently inactivated, excessively proteolyzed state during virus entry. This may account for inefficient late entry. Inefficient late entry may also be explained by differences in lysosomal and plasma membranes, which have unique lipid profiles [185] and therefore may be differentially susceptible to S -catalyzed fusion.

Model of Tetraspanin-mediated CoV Early Entry.

Our results indicate that tetraspanins are necessary for efficient entry of CoVs into target cells. Furthermore, we characterized tetraspanin-mediated entry events as TTSP-dependent early entry. We propose a model for CoV early entry that is dependent on tetraspanin scaffolding of multiple viral early entry factors into close proximity (Figure 3). Recent studies have provided insights into the nature of tetraspanin "web" interactions. These results allow us to speculate the nature of clustering of CoV early entry factors.

We concluded that CD9-mediated clustering of receptors and TTSPs promoted MERS-CoV and 229E-CoV early entry at the cell surface. Receptor/protease clustering is necessary because CoV S proteins requiring simultaneous receptor engagement and proteolysis at S2' for fusion activation [65]. While the exact nature of TMPRSS2 interactions with these cleavage sites is unclear, due to lack of TMPRSS2 structural data, the effective distance between TMPRSS2 and the DPP4/S complexes must be constrained by the "reach" of the TMPRSS2 itself. Interestingly, TMPRSS2 is one of the smallest characterized TTSPs which suggests a short range of proteolytic activity [106]. Thus the early virus entry process requires very closely-spaced DPP4 and TMPRSS2 proteins. Furthermore, it is likely that the successful activation of several adjacent S proteins is needed for successful membrane fusion, as has been observed with influenza HA [2] and HIV env [186, 187]. The tetraspanin-facilitated complexes of DPP4 and TMPRSS2 likely permit rapid and simultaneous cleavage of multiple adjacent S proteins that accounts for early entry.

That an as-yet unidentified tetraspanin is a partner for one or more relevant TTSPs is evidenced by the fact that CD9KO does not affect entry of MHV or SARS-CoVs. Both of these CoVs can utilize TMPRSS2 for early entry. Based on our model, if CD9 is necessary for TMPRSS2-rich clusters at the cell surface then CD9KO would affect the entry of all of the tested CoVs. As it stands, the tetraspanin partners for CEACAM, ACE2, and TMPRSS2 remain unidentified.

Our observations align with previous studies that describe tetraspanins holding complexes of viral entry factors together at the cell surface (reviewed in[134]). To determine which CoV entry factors interact with tetraspanins, our first experiments involved the isolation and analysis of CHAPS detergent-resistant membranes. These isolated membrane fractions contained a large diversity of tetraspanins and tetraspanin partner proteins. Thus, these experiments assume a model of tetraspanin scaffolding dependent on the existence of complex tetraspanin interactions that form tetraspanin-enriched microdomains. These TEMs were thought to be large complexes of diverse tetraspanins and tetraspanin-partner proteins forming stable structures at the cell surface. These structures were thought to be formed largely due to favorable membrane conditions, much like lipid rafts [188]. While this model of TEMs is based on the bulk of the tetraspanin literature, we have come to appreciate that it is likely inaccurate because it is based on an artefact of the solubilization of cellular membranes that leads to condensation of tetraspanin clusters. A less heterogeneous model of tetraspanin interactions has recently been described and may provide insight into how CoV entry factors are held in close proximity.

Recent studies using single-molecule resolution microscopy techniques refute the old model that suggests TEMs are stable structures that contain a wide array of different tetraspanins and transmembrane proteins [189, 190]. These data suggest individual tetraspanins and their partner proteins exist as units at the cell surface and exhibit Brownian diffusion through the plasma membrane. This complex roams the membrane freely until it encounters other homotypic tetraspanins. The interaction with other homotypic tetraspanins decreases both the diffusion rate and distance of the individual tetraspanin unit and couples movement with the other homotypic tetraspanin(s). These semi-stable interactions lead to the formation of clusters of homotypic tetraspanins and their partner proteins that consist of 3-6 tetraspanin molecules (Figure 29).

Tetraspanin "web" interactions consist of these homotypic tetraspanin complexes residing in close proximity with other homotypic tetraspanin complexes. This model suggests that tetraspanins can not only promote close proximity of partner proteins, but can also sequester partner proteins from each other. For example, the tetraspanin CD82 clusters major histocompatibility complex (MHC) proteins on antigen presenting cells, which is necessary for efficient antigen presentation to T cells. However, the tetraspanin CD37 can sequester MHC in these cells and prevent its interaction with CD82 [191]. The earlier models for TEMs suggested that tetraspanins facilitate partner protein interactions based largely on clustering of tetraspanins in membrane raft domains. However, the new model suggests that the interaction of partner proteins is less dependent on the membrane composition and more dependent on tetraspanin-tetraspanin interactions.

While CHAPS detergent-resistant membranes are not representative of native tetraspanin clusters at the cell surface, our results confirm that they remain a valuable tool to analyze tetraspanin-partner protein interactions. CHAPS DRMs clearly purify membranes that contain tetraspanins (Figure 12) and we have shown that this analysis can be used to identify specific tetraspanin-partner protein interactions. For example, DPP4 and APN are absent from CHAPS DRMs in CD9 depleted cells, but present in CD9 replete cells (Figure 21). However, the proximity of different tetraspanin partner proteins (such as DPP4 and TMPRSS2) at the cell surface cannot be determined with certainty by these methods. Therefore, we conclude that analysis of protein complexes in intact cells, by means such as PLA (Figure 22), is necessary to draw conclusions about the clustering of these partner proteins at the cell surface.

Tetraspanins can form interactions with partner proteins in the endoplasmic reticulum (ER) or at the cell surface. In the cases where tetraspanin-partner proteins interactions are formed in the ER, tetraspanin expression can affect trafficking of the partner protein to the cell surface. This is the case for CD81 and CD19 in B cells. When CD81 was knocked out, CD19 accumulated in the ER but not at the cell surface [192]. Similar experiments determined that the tetraspanin UPIA forms interactions with uroplakin proteins in the ER and is necessary for trafficking the uroplakins to the Golgi and ultimately the cell surface [193]. We propose that the tetraspanin CD9 forms an interaction with DPP4 at the cell surface, because we observed similar amounts of surface DPP4 in the presence or absence of CD9 (Figures 8 and 20). Identifying the subcellular location where DPP4 meets CD9 may facilitate the development of antiviral therapies that may prevent this interaction.

Potential Role for Cholesterol in CoV Early Entry.

Recent structural studies indicate that cholesterol is a determinant of tetraspanin interactions with partner proteins [118]. The presence or absence of a single cholesterol molecule in the TM domains of CD81 (Figure 4) determines both the tertiary structure of the LEL and the ability to interact with a specific partner protein. Interestingly, cholesterol is a known entry factor for MHV [116], SARS [113], 229E [114], and MERS [171]. These studies emphasize the importance of cholesterol-rich lipid raft regions on the cell surface for CoV endocytosis and/or fusion events. We propose that cholesterol acts as a structural determinant of tetraspanin proteins and the absence of cholesterol ablates tetraspanin interactions with CoV entry factors. While our initial experiments failed to observe this phenomenon, we propose experiments in which CD9KO cells are complemented with CD9 mutants incapable of binding to cholesterol. The mutations needed to produce this mutant have already been characterized by Zimmerman et al. Our hypothesis is that MERS early entry would not be restored in CD9KO cells overexpressing the CD9 mutant. This result would provide a mechanistic understanding of the role of cholesterol in CoV entry.

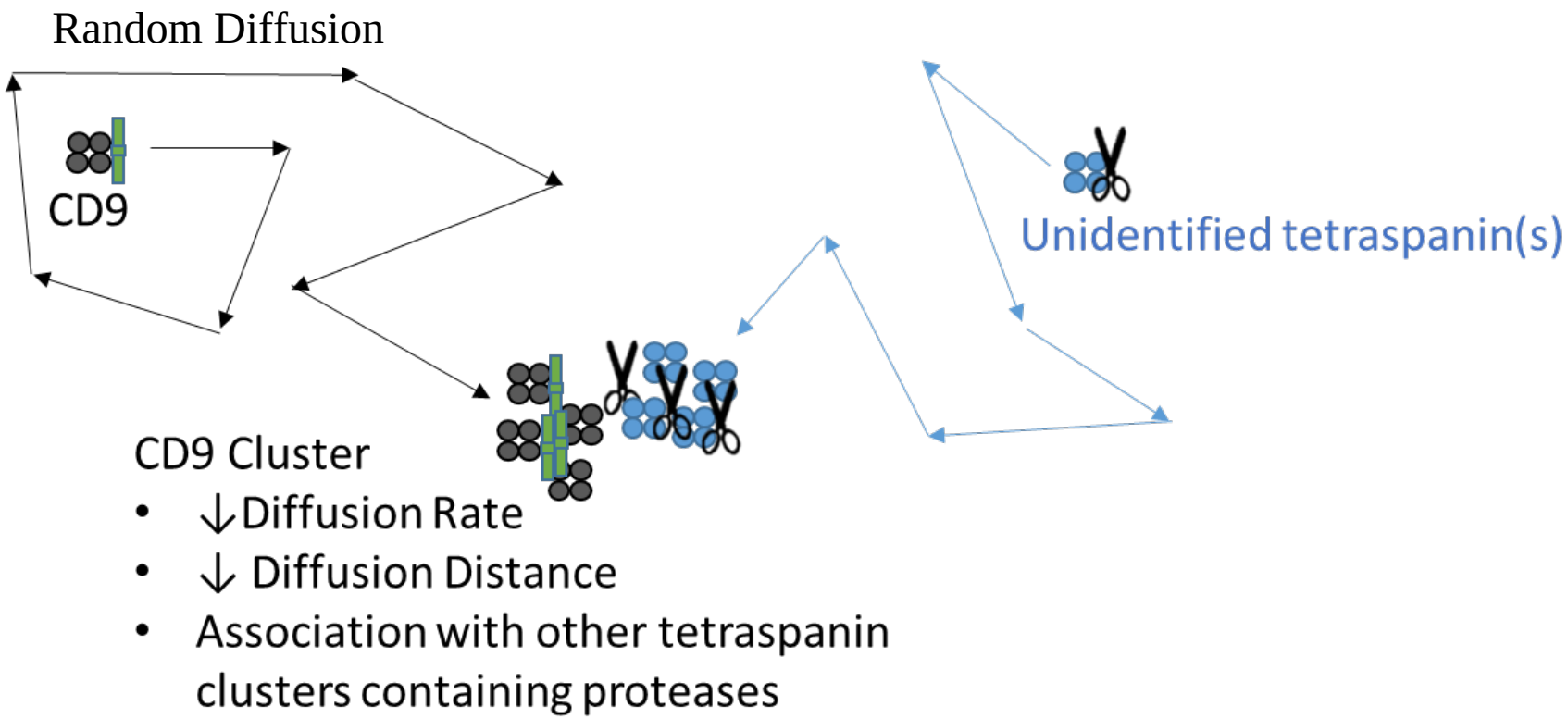

Figure 29. Proposed model of tetraspanin-mediated clustering of MERS entry factors. The movement and clustering of tetraspanins and partner proteins is depicted from a top down view. DPP4 (green) interacts with an individual CD9 tetraspanin protein (4 gray TM domains shown) and exhibits Brownian diffusion through the membrane. Upon encountering one or several other CD9 molecules, the rate and distance of diffusion of the CD9-DPP4 complex decreases significantly. Clustered, interacting CD9-DPP4 complexes exist in close proximity with complexes of an as-yet unidentified tetraspanin (blue) that clusters TMPRSS2 (scissors). Thus, MERS entry factors are concentrated in complexes formed of homotypic tetraspanin interactions and are held in close proximity to other homotypic tetraspanin complexes.

CoV Evolution to Utilize Tetraspanin-associated Entry Factors.

The human CoVs use the transmembrane ectopeptidases ACE2 [102], APN [103], and DPP4 [100] as host cell receptors. These receptors do not share any obvious structural similarities, and while they do share ectopeptidase activities, these enzymatic functions are dispensable for virus entry [100, 102, 103]. Localization in TEMs, therefore, may be a shared feature that is relevant to the selection of these ectopeptidases as CoV receptors.

We therefore find it likely that the CoVs evolved to use tetraspanin-associated receptors so that, once bound to cells, the viruses are poised for cleavage by adjacent proteases. It is possible, however, that the viruses adapted to use tetraspanin-associated receptors for unknown reasons and then further evolved to utilize the abundant nearby proteases for cleavage and priming. Regardless, the proteolytic environment created by tetraspanin interactions is the preferred location for receptor-induced conformational changes of S proteins, rapid proteolytic cleavage of the intermediate S conformations, and possibly the subsequent refolding to postfusion forms, in spatial and temporal patterns that foster efficient virus entry.

To determine if CoVs utilize different entry routes in cell culture and in mice, our colleagues, Drs. Park and Li, have isolated and characterized a mouse adapted MERS-CoV. A cell culture adapted HCoV-MERS was passaged 30 times in a permissive mouse model and mutations were analyzed. Mutations occurred in the S1/S2 cleavage site, in the S1 domain, and in the HR1 region of S2. These mutations increased the virulence of the cell adapted strains and led to lethal infection. The majority of mutations observed at

the S1/S2 region involved replacing serine residues with arginine. This would likely make the S1/S2 a more efficient cleavage target for TTSPs and facilitate early entry. The other mutations observed might lead to destabilized S trimers which facilitate cell-surface entry in a similar manner as our trypsin destabilizations (Figure 11). We propose that these mutations would increase the mouse adapted MERS-CoV reliance on CD9-mediated early entry. Thus, utilization of CD9 entry routes may correlate with increased MERS virulence.

Targeting Antiviral Peptides to Membranes.

Identifying and characterizing the entry factors and subcellular locations of CoV early entry has provided us a unique opportunity to design antiviral therapies that specifically target this route. As described in Chapter 1, HR2 peptides can block the fusion reaction of type I viral fusion glycoproteins by binding to the HR1 region of the extended intermediate and preventing complete zippering of the fusion domain (Figure 1). The efficacy of these peptides is limited by the relatively short duration of these extended intermediate structures. Thus, soluble HR2 peptides need to be used in very high concentrations to provide modest inhibition of infection (Figure 27) [194].

Our goal was to use our knowledge of the subcellular location of fusion to increase the efficacy of antiviral HR2 peptides. Previous studies have shown that lipid tagging HR2 peptides increases their efficacy, ostensibly by binding the HR2 to the target-cell membrane [173, 195]. We know that tetraspanins are concentrated in membrane regions that are rich in saturated fatty acids and cholesterol [196]. Interestingly, we observed that HR2 peptides tagged with these lipids were drastically

more effective at blocking infection by early entering MHV-A59 and -JHM. We concluded that palmitic acid and cholesterol tagged HR2s interact with the membranes near tetraspanin complexes. These results also suggest that extended intermediate structures form at or near tetraspanin complexes.

We also demonstrated the ability to predict which lipid tag would be effective against a given CoV based on the likelihood of that virus entering early or late. Unlike the MHV-A59 and -JHM strains, MHV-2 enters cells through an almost exclusively late entry route. This MHV-2 virus was blocked by a tocopherol-tagged HR2 peptide that was unable to efficiently block infection by the two early-entering MHVs. Because tocopherol concentrates in the membranes of endosomes [175], these results confirm our hypothesis that late entry occurs in the endosome. These results confirm that lipid-tagged HR2 peptides can be effective tools for both blocking CoV infections and characterizing which entry route a given CoV utilizes.

REFERENCE LIST

1. Harrison, S.C., *Viral membrane fusion.* Virology, 2015. **479–480**: p. 498-507.

2. Ivanovic, T., et al., *Influenza-virus membrane fusion by cooperative fold-back of stochastically induced hemagglutinin intermediates.* eLife, 2013. **2**: p. e00333.

3. Plemper, R.K., M.A. Brindley, and R.M. Iorio, *Structural and mechanistic studies of measles virus illuminate paramyxovirus entry.* PLoS Pathog, 2011. **7**(6): p. e1002058.

4. Kuzmin, P.I., et al., *A quantitative model for membrane fusion based on low-energy intermediates.* Proceedings of the National Academy of Sciences, 2001. **98**(13): p. 7235-7240.

5. Chakraborty, H., P.K. Tarafdar, and B.R. Lentz, *A novel assay for detecting fusion pore formation: implications for the fusion mechanism.* Biochemistry, 2013. **52**(47): p. 8510-7.

6. Bullough, P.A., et al., *Structure of influenza haemagglutinin at the pH of membrane fusion.* Nature, 1994. **371**(6492): p. 37-43.

7. Bottcher-Friebertshauser, E., et al., *Cleavage of influenza virus hemagglutinin by airway proteases TMPRSS2 and HAT differs in subcellular localization and susceptibility to protease inhibitors.* J Virol, 2010. **84**(11): p. 5605-14.

8. Netter, R.C., et al., *Heptad Repeat 2-Based Peptides Inhibit Avian Sarcoma and Leukosis Virus Subgroup A Infection and Identify a Fusion Intermediate.* Journal of Virology, 2004. **78**(24): p. 13430-13439.

9. Melikyan, G.B., et al., *Low pH Is Required for Avian Sarcoma and Leukosis Virus Env-Induced Hemifusion and Fusion Pore Formation but Not for Pore Growth.* Journal of Virology, 2004. **78**(7): p. 3753-3762.

10. Wilson, I.A., J.J. Skehel, and D.C. Wiley, *Structure of the haemagglutinin membrane glycoprotein of influenza virus at 3 [angst] resolution.* Nature, 1981. **289**(5796): p. 366-373.

11. Yang, L. and H.W. Huang, *Observation of a membrane fusion intermediate structure.* Science, 2002. **297**(5588): p. 1877-9.

12. Lee, K.K., *Architecture of a nascent viral fusion pore.* Embo j, 2010. **29**(7): p. 1299-311.

13. Floyd, D.L., et al., *Single-particle kinetics of influenza virus membrane fusion.* Proc Natl Acad Sci U S A, 2008. **105**(40): p. 15382-7.

14. Schalk, A. and M. Hawn, *An apparently new respiratory disease of baby chicks.* J. Am. Vet. Med. Assoc, 1931. **78**(19): p. 413-422.

15. Doyle, L. and L. Hutchings, *A transmissible gastroenteritis in pigs.* Journal of the American Veterinary Medical Association, 1946. **108**: p. 257-259.

16. Cheever, F.S., et al., *A MURINE VIRUS (JHM) CAUSING DISSEMINATED ENCEPHALOMYELITIS WITH EXTENSIVE DESTRUCTION OF MYELIN : I. ISOLATION AND BIOLOGICAL PROPERTIES OF THE VIRUS.* The Journal of Experimental Medicine, 1949. **90**(3): p. 181-194.

17. Almeida, J.D. and D.A.J. Tyrrell, *The Morphology of Three Previously Uncharacterized Human Respiratory Viruses that Grow in Organ Culture.* Journal of General Virology, 1967. **1**(2): p. 175-178.

18. Bradburne, A.F., M.L. Bynoe, and D.A. Tyrrell, *Effects of a "new" human respiratory virus in volunteers.* Br Med J, 1967. **3**(5568): p. 767-9.

19. McIntosh, K., et al., *Seroepidemiologic studies of coronavirus infection in adults and children.* Am J Epidemiol, 1970. **91**(6): p. 585-92.

20. Lipsitch, M., et al., *Transmission Dynamics and Control of Severe Acute Respiratory Syndrome.* Science, 2003. **300**(5627): p. 1966-1970.

21. Zaki , A.M., et al., *Isolation of a Novel Coronavirus from a Man with Pneumonia in Saudi Arabia.* New England Journal of Medicine, 2012. **367**(19): p. 1814-1820.

22. Drosten, C., et al., *Clinical features and virological analysis of a case of Middle East respiratory syndrome coronavirus infection.* Lancet Infect Dis, 2013. **13**(9): p. 745-51.

23. Eckerle, I., et al., *In-vitro renal epithelial cell infection reveals a viral kidney tropism as a potential mechanism for acute renal failure during Middle East Respiratory Syndrome (MERS) Coronavirus infection.* Virology Journal, 2013. **10**(1): p. 359.

24. Kocherhans, R., et al., *Completion of the porcine epidemic diarrhoea coronavirus (PEDV) genome sequence.* Virus Genes, 2001. **23**(2): p. 137-44.

25. Vijgen, L., et al., *Complete genomic sequence of human coronavirus OC43: molecular clock analysis suggests a relatively recent zoonotic coronavirus transmission event.* J Virol, 2005. **79**(3): p. 1595-604.

26. Demogines, A., M. Farzan, and S.L. Sawyer, *Evidence for ACE2-utilizing coronaviruses (CoVs) related to severe acute respiratory syndrome CoV in bats.* J Virol, 2012. **86**(11): p. 6350-3.

27. Wang, Q., et al., *Bat origins of MERS-CoV supported by bat coronavirus HKU4 usage of human receptor CD26.* Cell Host Microbe, 2014. **16**(3): p. 328-37.

28. Yang, Y., et al., *Receptor usage and cell entry of bat coronavirus HKU4 provide insight into bat-to-human transmission of MERS coronavirus.* Proc Natl Acad Sci U S A, 2014. **111**(34): p. 12516-21.

29. Alexander, D.J., *A review of avian influenza in different bird species.* Veterinary microbiology, 2000. **74**(1): p. 3-13.

30. Leroy, E.M., et al., *Fruit bats as reservoirs of Ebola virus.* Nature, 2005. **438**(7068): p. 575-576.

31. Dick, G.W.A., S.F. Kitchen, and A.J. Haddow, *Zika Virus (I). Isolations and serological specificity.* Transactions of The Royal Society of Tropical Medicine and Hygiene, 1952. **46**(5): p. 509-520.

32. Go, Y.Y., U.B.R. Balasuriya, and C.-k. Lee, *Zoonotic encephalitides caused by arboviruses: transmission and epidemiology of alphaviruses and flaviviruses.* Clinical and Experimental Vaccine Research, 2014. **3**(1): p. 58-77.

33. Ge, X.-Y., et al., *Isolation and characterization of a bat SARS-like coronavirus that uses the ACE2 receptor.* Nature, 2013. **503**(7477): p. 535-538.

34. Li, W., et al., *Bats are natural reservoirs of SARS-like coronaviruses.* Science, 2005. **310**(5748): p. 676-9.

35. Azhar , E.I., et al., *Evidence for Camel-to-Human Transmission of MERS Coronavirus.* New England Journal of Medicine, 2014. **370**(26): p. 2499-2505.

36. Ziad, A.M., et al., *Middle East Respiratory Syndrome Coronavirus in Bats, Saudi Arabia.* Emerging Infectious Disease journal, 2013. **19**(11): p. 1819.

37. Marcel, A.M., et al., *MERS Coronavirus Neutralizing Antibodies in Camels, Eastern Africa, 1983–1997.* Emerging Infectious Disease journal, 2014. **20**(12): p. 2093.

38. Cui, J., et al., *Adaptive evolution of bat dipeptidyl peptidase 4 (dpp4): implications for the origin and emergence of Middle East respiratory syndrome coronavirus.* Virology Journal, 2013. **10**: p. 304-304.

39. Bosch, B.J., et al., *The Coronavirus Spike Protein Is a Class I Virus Fusion Protein: Structural and Functional Characterization of the Fusion Core Complex.* Journal of Virology, 2003. **77**(16): p. 8801-8811.

40. White, J.M., et al., *Structures and Mechanisms of Viral Membrane Fusion Proteins: Multiple Variations on a Common Theme.* Critical reviews in biochemistry and molecular biology, 2008. **43**(3): p. 189-219.

41. Wild, C., T. Greenwell, and T. Matthews, *A synthetic peptide from HIV-1 gp41 is a potent inhibitor of virus-mediated cell-cell fusion.* AIDS Res Hum Retroviruses, 1993. **9**(11): p. 1051-3.

42. Wang, X.J., et al., *Structure and function study of paramyxovirus fusion protein heptad repeat peptides.* Arch Biochem Biophys, 2005. **436**(2): p. 316-22.

43. Gao, J., et al., *Structure of the fusion core and inhibition of fusion by a heptad repeat peptide derived from the S protein of Middle East respiratory syndrome coronavirus.* Journal of virology, 2013. **87**(24): p. 13134-13140.

44. Weissenhorn, W., et al., *Atomic structure of the ectodomain from HIV-1 gp41*. Nature, 1997. **387**(6631): p. 426-30.

45. Blacklow, S.C., M. Lu, and P.S. Kim, *Trimeric subdomain of the simian immunodeficiency virus envelope glycoprotein.* Biochemistry, 1995. **34**(46): p. 14955-14962.

46. Li, F., *Evidence for a common evolutionary origin of coronavirus spike protein receptor-binding subunits.* J Virol, 2012. **86**(5): p. 2856-8.

47. Krempl, C., et al., *Point mutations in the S protein connect the sialic acid binding activity with the enteropathogenicity of transmissible gastroenteritis coronavirus.* J Virol, 1997. **71**(4): p. 3285-7.

48. Peng, G., et al., *Crystal Structure of Bovine Coronavirus Spike Protein Lectin Domain.* The Journal of Biological Chemistry, 2012. **287**(50): p. 41931-41938.

49. Promkuntod, N., et al., *Mapping of the receptor-binding domain and amino acids critical for attachment in the spike protein of avian coronavirus infectious bronchitis virus.* Virology, 2014. **448**: p. 26-32.

50. Liu, C., et al., *Receptor usage and cell entry of porcine epidemic diarrhea coronavirus.* Journal of Virology, 2015.

51. Breslin, J.J., et al., *Human Coronavirus 229E: Receptor Binding Domain and Neutralization by Soluble Receptor at 37°C.* Journal of Virology, 2003. **77**(7): p. 4435-4438.

52. Babcock, G.J., et al., *Amino acids 270 to 510 of the severe acute respiratory syndrome coronavirus spike protein are required for interaction with receptor.* J Virol, 2004. **78**(9): p. 4552-60.

53. Wang, N., et al., *Structure of MERS-CoV spike receptor-binding domain complexed with human receptor DPP4.* Cell Res, 2013. **23**(8): p. 986-93.

54. Peng, G., et al., *Crystal structure of mouse coronavirus receptor-binding domain complexed with its murine receptor.* Proceedings of the National Academy of Sciences, 2011. **108**(26): p. 10696-10701.

55. Walls, A.C., et al., *Cryo-electron microscopy structure of a coronavirus spike glycoprotein trimer.* Nature, 2016. **531**(7592): p. 114-117.

56. Kirchdoerfer, R.N., et al., *Pre-fusion structure of a human coronavirus spike protein.* Nature, 2016. **531**(7592): p. 118-121.

57. Belouzard, S., V.C. Chu, and G.R. Whittaker, *Activation of the SARS coronavirus spike protein via sequential proteolytic cleavage at two distinct sites.* Proceedings of the National Academy of Sciences, 2009. **106**(14): p. 5871-5876.

58. Li, W., et al., *A Single Point Mutation Creating a Furin Cleavage Site in the Spike Protein Renders Porcine Epidemic Diarrhea Coronavirus Trypsin Independent for Cell Entry and Fusion.* Journal of virology, 2015. **89**(15): p. 8077-8081.

59. Millet, J.K. and G.R. Whittaker, *Host cell entry of Middle East respiratory syndrome coronavirus after two-step, furin-mediated activation of the spike protein.* Proc Natl Acad Sci U S A, 2014. **111**(42): p. 15214-9.

60. Wicht, O., et al., *Identification and Characterization of a Proteolytically Primed Form of the Murine Coronavirus Spike Proteins after Fusion with the Target Cell.* J Virol, 2014.

61. Bosch, B.J., W. Bartelink, and P.J. Rottier, *Cathepsin L functionally cleaves the severe acute respiratory syndrome coronavirus class I fusion protein upstream of rather than adjacent to the fusion peptide.* J Virol, 2008. **82**(17): p. 8887-90.

62. Huang, I.-C., et al., *SARS Coronavirus, but Not Human Coronavirus NL63, Utilizes Cathepsin L to Infect ACE2-expressing Cells.* Journal of Biological Chemistry, 2006. **281**(6): p. 3198-3203.

63. Qiu, Z., et al., *Endosomal Proteolysis by Cathepsins Is Necessary for Murine Coronavirus Mouse Hepatitis Virus Type 2 Spike-Mediated Entry.* Journal of Virology, 2006. **80**(12): p. 5768-5776.

64. Matsuyama, S., et al., *Protease-mediated enhancement of severe acute respiratory syndrome coronavirus infection.* Proceedings of the National Academy of Sciences of the United States of America, 2005. **102**(35): p. 12543-12547.

65. Park, J.-E., et al., *Proteolytic processing of Middle East respiratory syndrome coronavirus spikes expands virus tropism.* Proceedings of the National Academy of Sciences, 2016.

66. Matsuyama, S. and F. Taguchi, *Two-step conformational changes in a coronavirus envelope glycoprotein mediated by receptor binding and proteolysis.* J Virol, 2009. **83**(21): p. 11133-41.

67. Xu, Y., et al., *Structural basis for coronavirus-mediated membrane fusion. Crystal structure of mouse hepatitis virus spike protein fusion core.* J Biol Chem, 2004. **279**(29): p. 30514-22.

68. Xu, Y., et al., *Crystal structure of severe acute respiratory syndrome coronavirus spike protein fusion core.* J Biol Chem, 2004. **279**(47): p. 49414-9.

69. Coughlin, M.M., J. Babcook, and B.S. Prabhakar, *Human monoclonal antibodies to SARS-coronavirus inhibit infection by different mechanisms.* Virology, 2009. **394**(1): p. 39-46.

70. Glowacka, I., et al., *Evidence that TMPRSS2 activates the severe acute respiratory syndrome coronavirus spike protein for membrane fusion and reduces viral control by the humoral immune response.* J Virol, 2011. **85**(9): p. 4122-34.

71. Kawase, M., et al., *Protease-Mediated Entry via the Endosome of Human Coronavirus 229E.* Journal of Virology, 2009. **83**(2): p. 712-721.

72. Kawase, M., et al., *Simultaneous treatment of human bronchial epithelial cells with serine and cysteine protease inhibitors prevents severe acute respiratory syndrome coronavirus entry.* J Virol, 2012. **86**(12): p. 6537-45.

73. Shirato, K., M. Kawase, and S. Matsuyama, *Middle East Respiratory Syndrome Coronavirus Infection Mediated by the Transmembrane Serine Protease TMPRSS2.* Journal of Virology, 2013. **87**(23): p. 12552-12561.

74. Zhou, Y., et al., *Protease inhibitors targeting coronavirus and filovirus entry.* Antiviral Res, 2015. **116**: p. 76-84.

75. Lu, L., et al., *Structure-based discovery of Middle East respiratory syndrome coronavirus fusion inhibitor.* Nature Communications, 2014. **5**: p. 3067.

76. Bosch, B.J., et al., *Coronavirus Escape from Heptad Repeat 2 (HR2)-Derived Peptide Entry Inhibition as a Result of Mutations in the HR1 Domain of the Spike Fusion Protein.* Journal of Virology, 2008. **82**(5): p. 2580-2585.

77. Bertram, S., et al., *TMPRSS2 Activates the Human Coronavirus 229E for Cathepsin-Independent Host Cell Entry and Is Expressed in Viral Target Cells in the Respiratory Epithelium.* Journal of Virology, 2013. **87**(11): p. 6150-6160.

78. Nash, T.C. and M.J. Buchmeier, *Entry of mouse hepatitis virus into cells by endosomal and nonendosomal pathways.* Virology, 1997. **233**(1): p. 1-8.

79. Shirato, K., et al., *Clinical Isolates of Human Coronavirus 229E Bypass the Endosome for Cell Entry.* Journal of Virology, 2016.

80. Burkard, C., et al., *Coronavirus Cell Entry Occurs through the Endo-/Lysosomal Pathway in a Proteolysis-Dependent Manner.* PLOS Pathogens, 2014. **10**(11): p. e1004502.

81. Simmons, G., et al., *Inhibitors of cathepsin L prevent severe acute respiratory syndrome coronavirus entry.* Proceedings of the National Academy of Sciences of the United States of America, 2005. **102**(33): p. 11876-11881.

82. Gierer, S., et al., *The spike protein of the emerging betacoronavirus EMC uses a novel coronavirus receptor for entry, can be activated by TMPRSS2, and is targeted by neutralizing antibodies.* J Virol, 2013. **87**(10): p. 5502-11.

83. Matsuyama, S., et al., *Efficient activation of the severe acute respiratory syndrome coronavirus spike protein by the transmembrane protease TMPRSS2.* J Virol, 2010. **84**(24): p. 12658-64.

84. Watanabe, R., et al., *Entry from the cell surface of severe acute respiratory syndrome coronavirus with cleaved S protein as revealed by pseudotype virus bearing cleaved S protein.* J Virol, 2008. **82**(23): p. 11985-91.

85. Mingo, R.M., et al., *Ebola virus and severe acute respiratory syndrome coronavirus display late cell entry kinetics: evidence that transport to NPC1+ endolysosomes is a rate-defining step.* Journal of virology, 2015. **89**(5): p. 2931-2943.

86. Regan, A.D., et al., *Differential role for low pH and cathepsin-mediated cleavage of the viral spike protein during entry of serotype II feline coronaviruses.* Veterinary microbiology, 2008. **132**(3): p. 235-248.

87. Bohley, P. and P.O. Seglen, *Proteases and proteolysis in the lysosome.* Experientia, 1992. **48**(2): p. 151-7.

88. Yamada, Y. and D.X. Liu, *Proteolytic activation of the spike protein at a novel RRRR/S motif is implicated in furin-dependent entry, syncytium formation, and infectivity of coronavirus infectious bronchitis virus in cultured cells.* Journal of virology, 2009. **83**(17): p. 8744-8758.

89. Bertram, S., et al., *Cleavage and Activation of the Severe Acute Respiratory Syndrome Coronavirus Spike Protein by Human Airway Trypsin-Like Protease.* Journal of Virology, 2011. **85**(24): p. 13363-13372.

90. de Haan, C.A., et al., *Cleavage inhibition of the murine coronavirus spike protein by a furin-like enzyme affects cell-cell but not virus-cell fusion.* Journal of virology, 2004. **78**(11): p. 6048-6054.

91. Yamada, Y., et al., *Requirement of Proteolytic Cleavage of the Murine Coronavirus MHV-2 Spike Protein for Fusion Activity*, in *Coronaviruses and Arteriviruses*, L. Enjuanes, S. Siddell, and W. Spaan, Editors. 1998, Springer US. p. 89-93.

92. Gierer, S., et al., *Inhibition of Proprotein Convertases Abrogates Processing of the Middle Eastern Respiratory Syndrome Coronavirus Spike Protein in Infected Cells but Does Not Reduce Viral Infectivity.* Journal of Infectious Diseases, 2014.

93. Bühling, F., et al., *Pivotal Role of Cathepsin K in Lung Fibrosis.* The American Journal of Pathology, 2004. **164**(6): p. 2203-2216.

94. Zelus, B.D., et al., *Conformational Changes in the Spike Glycoprotein of Murine Coronavirus Are Induced at 37°C either by Soluble Murine CEACAM1 Receptors or by pH 8.* Journal of Virology, 2003. **77**(2): p. 830-840.

95. Matsuyama, S. and F. Taguchi, *Receptor-induced conformational changes of murine coronavirus spike protein.* Journal of virology, 2002. **76**(23): p. 11819-11826.

96. Earnest, J.T., et al., *Coronavirus and influenza virus proteolytic priming takes place in tetraspanin-enriched membrane microdomains.* J Virol, 2015. **89**(11): p. 6093-104.

97. Krempl, C., B. Schultze, and G. Herrler, *Analysis of Cellular Receptors for Human Coronavirus OC43*, in *Corona- and Related Viruses: Current Concepts in Molecular Biology and Pathogenesis*, P.J. Talbot and G.A. Levy, Editors. 1995, Springer US: Boston, MA. p. 371-374.

98. Winter, C., et al., *Sialic acid is a receptor determinant for infection of cells by avian Infectious bronchitis virus.* Journal of general virology, 2006. **87**(5): p. 1209-1216.

99. Li, W., et al., *Angiotensin-converting enzyme 2 is a functional receptor for the SARS coronavirus.* Nature, 2003. **426**(6965): p. 450-4.

100. Raj, V.S., et al., *Dipeptidyl peptidase 4 is a functional receptor for the emerging human coronavirus-EMC.* Nature, 2013. **495**(7440): p. 251-4.

101. Hofmann, H., et al., *Human coronavirus NL63 employs the severe acute respiratory syndrome coronavirus receptor for cellular entry.* Proceedings of the National Academy of Sciences, 2005. **102**(22): p. 7988-7993.

102. Li, W., et al., *The S proteins of human coronavirus NL63 and severe acute respiratory syndrome coronavirus bind overlapping regions of ACE2.* Virology, 2007. **367**(2): p. 367-74.

103. Yeager, C.L., et al., *Human aminopeptidase N is a receptor for human coronavirus 229E.* Nature, 1992. **357**(6377): p. 420-2.

104. Tellier, E., et al., *The shedding activity of ADAM17 is sequestered in lipid rafts.* Experimental Cell Research, 2006. **312**(20): p. 3969-3980.

105. Lucas, J.M., et al., *The androgen-regulated type II serine protease TMPRSS2 is differentially expressed and mislocalized in prostate adenocarcinoma.* J Pathol, 2008. **215**(2): p. 118-25.

106. Bugge, T.H., T.M. Antalis, and Q. Wu, *Type II Transmembrane Serine Proteases.* Journal of Biological Chemistry, 2009. **284**(35): p. 23177-23181.

107. Bertram, S., et al., *Influenza and SARS-coronavirus activating proteases TMPRSS2 and HAT are expressed at multiple sites in human respiratory and gastrointestinal tracts.* PLoS One, 2012. **7**(4): p. e35876.

108. Chen, Y.W., et al., *TMPRSS2, a serine protease expressed in the prostate on the apical surface of luminal epithelial cells and released into semen in prostasomes, is misregulated in prostate cancer cells.* Am J Pathol, 2010. **176**(6): p. 2986-96.

109. Tomlins, S.A., et al., *Recurrent Fusion of TMPRSS2 and ETS Transcription Factor Genes in Prostate Cancer.* Science, 2005. **310**(5748): p. 644-648.

110. Rosenberger, C.M., et al., *Characterization of innate responses to influenza virus infection in a novel lung type I epithelial cell model.* J Gen Virol, 2014. **95**(Pt 2): p. 350-62.

111. Phillips, J.M., T. Gallagher, and S.R. Weiss, *Neurovirulent murine coronavirus JHM.SD uses cellular zinc metalloproteases for virus entry and cell-cell fusion.* J Virol, 2017.

112. Choi, K.S., H. Aizaki, and M.M.C. Lai, *Murine Coronavirus Requires Lipid Rafts for Virus Entry and Cell-Cell Fusion but Not for Virus Release.* Journal of Virology, 2005. **79**(15): p. 9862-9871.

113. Glende, J., et al., *Importance of cholesterol-rich membrane microdomains in the interaction of the S protein of SARS-coronavirus with the cellular receptor angiotensin-converting enzyme 2.* Virology, 2008. **381**(2): p. 215-221.

114. Nomura, R., et al., *Human Coronavirus 229E Binds to CD13 in Rafts and Enters the Cell through Caveolae.* Journal of Virology, 2004. **78**(16): p. 8701-8708.

115. Takano, T., et al., *Differential effect of cholesterol on type I and II feline coronavirus infection.* Arch Virol, 2016. **161**(1): p. 125-33.

116. Thorp, E.B. and T.M. Gallagher, *Requirements for CEACAMs and Cholesterol during Murine Coronavirus Cell Entry.* Journal of Virology, 2004. **78**(6): p. 2682-2692.

117. Huang, S., et al., *The phylogenetic analysis of tetraspanins projects the evolution of cell–cell interactions from unicellular to multicellular organisms.* Genomics, 2005. **86**(6): p. 674-684.

118. Zimmerman, B., et al., *Crystal Structure of a Full-Length Human Tetraspanin Reveals a Cholesterol-Binding Pocket.* Cell, 2016. **167**(4): p. 1041-1051.e11.

119. Hemler, M.E., *Tetraspanin functions and associated microdomains.* Nat Rev Mol Cell Biol, 2005. **6**(10): p. 801-11.

120. Berditchevski, F., et al., *Analysis of the CD151-alpha3beta1 integrin and CD151-tetraspanin interactions by mutagenesis.* J Biol Chem, 2001. **276**(44): p. 41165-74.

121. Bienstock, R.J. and J.C. Barrett, *KAI1, a prostate metastasis suppressor: prediction of solvated structure and interactions with binding partners; integrins, cadherins, and cell-surface receptor proteins.* Mol Carcinog, 2001. **32**(3): p. 139-53.

122. Kovalenko, O.V., et al., *Structural organization and interactions of transmembrane domains in tetraspanin proteins.* BMC Struct Biol, 2005. **5**: p. 11.

123. Charrin, S., et al., *Differential stability of tetraspanin/tetraspanin interactions: role of palmitoylation.* FEBS Lett, 2002. **516**(1-3): p. 139-44.

124. Yang, X., et al., *Palmitoylation of Tetraspanin Proteins: Modulation of CD151 Lateral Interactions, Subcellular Distribution, and Integrin-dependent Cell Morphology.* Molecular Biology of the Cell, 2002. **13**(3): p. 767-781.

125. Berditchevski, F., et al., *Expression of the Palmitoylation-deficient CD151 Weakens the Association of α3β1 Integrin with the Tetraspanin-enriched Microdomains and Affects Integrin-dependent Signaling.* Journal of Biological Chemistry, 2002. **277**(40): p. 36991-37000.

126. Kovalenko, O.V., et al., *Evidence for specific tetraspanin homodimers: inhibition of palmitoylation makes cysteine residues available for cross-linking.* Biochem J, 2004. **377**(Pt 2): p. 407-17.

127. Kitadokoro, K., et al., *CD81 extracellular domain 3D structure: insight into the tetraspanin superfamily structural motifs.* The EMBO Journal, 2001. **20**(1-2): p. 12-18.

128. Kazarov, A.R., et al., *An extracellular site on tetraspanin CD151 determines alpha 3 and alpha 6 integrin-dependent cellular morphology.* J Cell Biol, 2002. **158**(7): p. 1299-309.

129. Higginbottom, A., et al., *Structural requirements for the inhibitory action of the CD9 large extracellular domain in sperm/oocyte binding and fusion.* Biochem Biophys Res Commun, 2003. **311**(1): p. 208-14.

130. Pileri, P., et al., *Binding of hepatitis C virus to CD81.* Science, 1998. **282**(5390): p. 938-41.

131. Silvie, O., et al., *Cholesterol contributes to the organization of tetraspanin-enriched microdomains and to CD81-dependent infection by malaria sporozoites.* Journal of Cell Science, 2006. **119**(10): p. 1992-2002.

132. Claas, C., C.S. Stipp, and M.E. Hemler, *Evaluation of prototype transmembrane 4 superfamily protein complexes and their relation to lipid rafts.* J Biol Chem, 2001. **276**(11): p. 7974-84.

133. Garner, A.E., D.A. Smith, and N.M. Hooper, *Visualization of detergent solubilization of membranes: implications for the isolation of rafts.* Biophys J, 2008. **94**(4): p. 1326-40.

134. Charrin, S., et al., *Lateral organization of membrane proteins: tetraspanins spin their web.* Biochem J, 2009. **420**(2): p. 133-54.

135. Soderberg, O., et al., *Direct observation of individual endogenous protein complexes in situ by proximity ligation.* Nat Meth, 2006. **3**(12): p. 995-1000.

136. Zhou, H., et al., *Two-color, rolling-circle amplification on antibody microarrays for sensitive, multiplexed serum-protein measurements.* Genome Biology, 2004. **5**(4): p. R28.

137. Le, Q.-T., et al., *Plasma Membrane Tetraspanin CD81 Complexes with Proprotein Convertase Subtilisin/Kexin Type 9 (PCSK9) and Low Density Lipoprotein Receptor (LDLR), and Its Levels Are Reduced by PCSK9.* The Journal of Biological Chemistry, 2015. **290**(38): p. 23385-23400.

138. Grigorov, B., et al., *Hepatitis C virus infection propagates through interactions between Syndecan-1 and CD81 and impacts the hepatocyte glycocalyx.* Cellular Microbiology, 2016: p. e12711-n/a.

139. Gutierrez-Lopez, M.D., et al., *The sheddase activity of ADAM17/TACE is regulated by the tetraspanin CD9.* Cell Mol Life Sci, 2011. **68**(19): p. 3275-92.

140. Yañez-Mó, M., et al., *MT1-MMP collagenolytic activity is regulated through association with tetraspanin CD151 in primary endothelial cells.* Blood, 2008. **112**(8): p. 3217-3226.

141. He, J., et al., *Dual function of CD81 in influenza virus uncoating and budding.* PLoS Pathog, 2013. **9**(10): p. e1003701.

142. Loffler, S., et al., *CD9, a tetraspan transmembrane protein, renders cells susceptible to canine distemper virus.* J Virol, 1997. **71**(1): p. 42-9.

143. Krementsov, D.N., et al., *HIV-1 Assembly Differentially Alters Dynamics and Partitioning of Tetraspanins and Raft Components.* Traffic, 2010. **11**(11): p. 1401-1414.

144. Weng, J., et al., *Formation of syncytia is repressed by tetraspanins in human immunodeficiency virus type 1-producing cells.* J Virol, 2009. **83**(15): p. 7467-74.

145. Willett, B., et al., *Inhibition of feline immunodeficiency virus infection by CD9 antibody operates after virus entry and is independent of virus tropism.* J Gen Virol, 1997. **78 (Pt 3)**: p. 611-8.

146. Pique, C., et al., *Interaction of CD82 tetraspanin proteins with HTLV-1 envelope glycoproteins inhibits cell-to-cell fusion and virus transmission.* Virology, 2000. **276**(2): p. 455-65.

147. Wang, L., et al., *Egress of HSV-1 capsid requires the interaction of VP26 and a cellular tetraspanin membrane protein.* Virol J, 2010. **7**: p. 156.

148. Bartosch, B., et al., *Cell Entry of Hepatitis C Virus Requires a Set of Co-receptors That Include the CD81 Tetraspanin and the SR-B1 Scavenger Receptor.* Journal of Biological Chemistry, 2003. **278**(43): p. 41624-41630.

149. Scheffer, K.D., et al., *Tetraspanin CD151 mediates papillomavirus type 16 endocytosis.* J Virol, 2013. **87**(6): p. 3435-46.

150. Krieger, S.E., et al., *Inhibition of hepatitis C virus infection by anti-claudin-1 antibodies is mediated by neutralization of E2-CD81-claudin-1 associations.* Hepatology, 2010. **51**(4): p. 1144-57.

151. Fénéant, L., S. Levy, and L. Cocquerel, *CD81 and Hepatitis C Virus (HCV) Infection.* Viruses, 2014. **6**(2): p. 535-572.

152. Scheffer, K., F. Berditchevski, and L. Florin, *The Tetraspanin CD151 in Papillomavirus Infection.* Viruses, 2014. **6**(2): p. 893.

153. Karlas, A., et al., *Genome-wide RNAi screen identifies human host factors crucial for influenza virus replication.* Nature, 2010. **463**(7282): p. 818-22.

154. Konig, R., et al., *Human host factors required for influenza virus replication.* Nature, 2010. **463**(7282): p. 813-7.

155. Rumschlag-Booms, E., et al., *Comparative analysis between a low pathogenic and a high pathogenic influenza H5 hemagglutinin in cell entry.* Virol J, 2009. **6**: p. 76.

156. Shulla, A., et al., *A transmembrane serine protease is linked to the severe acute respiratory syndrome coronavirus receptor and activates virus entry.* J Virol, 2011. **85**(2): p. 873-82.

157. Campbell, E.M., et al., *Labeling HIV-1 virions with two fluorescent proteins allows identification of virions that have productively entered the target cell.* Virology, 2007. **360**(2): p. 286-293.

158. Heaton, N.S.L.-G., V. H.; Tan, G. S.; Eggink, D.; Hai, R.; Palese, P., *In vivo bioluminescent imaging of influena A virus infection and characterization of novel cross-protective monoclonal antibodies.* J Virol, 2013. **87**(15): p. 8272.

159. Szretter, K.J., A.L. Balish, and J.M. Katz, *Influenza: propagation, quantification, and storage.* Curr Protoc Microbiol, 2006. **Chapter 15**: p. Unit 15G 1.

160. Shulla, A. and T. Gallagher, *Role of Spike Protein Endodomains in Regulating Coronavirus Entry.* Journal of Biological Chemistry, 2009. **284**(47): p. 32725-32734.

161. Whitt, M.A., *Generation of VSV pseudotypes using recombinant DeltaG-VSV for studies on virus entry, identification of entry inhibitors, and immune responses to vaccines.* J Virol Methods, 2010. **169**(2): p. 365-74.

162. Barlan, A., et al., *Receptor variation and susceptibility to Middle East respiratory syndrome coronavirus infection.* J Virol, 2014. **88**(9): p. 4953-61.

163. Bottcher, E., et al., *Proteolytic activation of influenza viruses by serine proteases TMPRSS2 and HAT from human airway epithelium.* J Virol, 2006. **80**(19): p. 9896-8.

164. Ziyyat, A., et al., *CD9 controls the formation of clusters that contain tetraspanins and the integrin alpha 6 beta 1, which are involved in human and mouse gamete fusion.* J Cell Sci, 2006. **119**(Pt 3): p. 416-24.

165. Andre, M., et al., *Proteomic analysis of the tetraspanin web using LC-ESI-MS/MS and MALDI-FTICR-MS.* Proteomics, 2006. **6**(5): p. 1437-49.

166. Hatesuer, B., et al., *Tmprss2 is essential for influenza H1N1 virus pathogenesis in mice.* PLoS Pathog, 2013. **9**(12): p. e1003774.

167. Sala-Valdes, M., et al., *EWI-2 and EWI-F link the tetraspanin web to the actin cytoskeleton through their direct association with ezrin-radixin-moesin proteins.* J Biol Chem, 2006. **281**(28): p. 19665-75.

168. Wada, I., et al., *SSR alpha and associated calnexin are major calcium binding proteins of the endoplasmic reticulum membrane.* J Biol Chem, 1991. **266**(29): p. 19599-610.

169. Okamoto, T., et al., *CD9 negatively regulates CD26 expression and inhibits CD26-mediated enhancement of invasive potential of malignant mesothelioma cells.* PLoS One, 2014. **9**(1): p. e86671.

170. Ran, F.A., et al., *Genome engineering using the CRISPR-Cas9 system.* Nat. Protocols, 2013. **8**(11): p. 2281-2308.

171. Wrensch, F., M. Winkler, and S. Pohlmann, *IFITM proteins inhibit entry driven by the MERS-coronavirus spike protein: evidence for cholesterol-independent mechanisms.* Viruses, 2014. **6**(9): p. 3683-98.

172. Zhao, J., et al., *Rapid generation of a mouse model for Middle East respiratory syndrome.* Proceedings of the National Academy of Sciences, 2014. **111**(13): p. 4970-4975.

173. Pessi, A., et al., *A general strategy to endow natural fusion-protein-derived peptides with potent antiviral activity.* PLoS One, 2012. **7**(5): p. e36833.

174. Yang, X.H., et al., *Contrasting effects of EWI proteins, integrins, and protein palmitoylation on cell surface CD9 organization.* J Biol Chem, 2006. **281**(18): p. 12976-85.

175. Wang, X. and P.J. Quinn, *Vitamin E and its function in membranes.* Prog Lipid Res, 1999. **38**(4): p. 309-36.

176. Tseng, C.-T.K., et al., *Severe Acute Respiratory Syndrome Coronavirus Infection of Mice Transgenic for the Human Angiotensin-Converting Enzyme 2 Virus Receptor.* Journal of Virology, 2007. **81**(3): p. 1162-1173.

177. Agrawal, A.S., et al., *Generation of a transgenic mouse model of Middle East respiratory syndrome coronavirus infection and disease.* J Virol, 2015. **89**(7): p. 3659-70.

178. Dimitrov, D.S., *Virus entry: molecular mechanisms and biomedical applications.* Nature Reviews Microbiology, 2004. **2**(2): p. 109-122.

179. Drosten , C., et al., *Identification of a Novel Coronavirus in Patients with Severe Acute Respiratory Syndrome.* New England Journal of Medicine, 2003. **348**(20): p. 1967-1976.

180. van Boheemen, S., et al., *Genomic Characterization of a Newly Discovered Coronavirus Associated with Acute Respiratory Distress Syndrome in Humans.* mBio, 2012. **3**(6).

181. Dietrich, C., et al., *Lipid Rafts Reconstituted in Model Membranes.* Biophysical Journal, 2001. **80**(3): p. 1417-1428.

182. Russier, M., et al., *Molecular requirements for a pandemic influenza virus: An acid-stable hemagglutinin protein.* Proceedings of the National Academy of Sciences, 2016. **113**(6): p. 1636-1641.

183. Huang, I.C., et al., *Distinct patterns of IFITM-mediated restriction of filoviruses, SARS coronavirus, and influenza A virus.* PLoS Pathog, 2011. **7**(1): p. e1001258.

184. Gierer, S., et al., *The Spike Protein of the Emerging Betacoronavirus EMC Uses a Novel Coronavirus Receptor for Entry, Can Be Activated by TMPRSS2, and Is Targeted by Neutralizing Antibodies.* Journal of Virology, 2013. **87**(10): p. 5502-5511.

185. van Meer, G., D.R. Voelker, and G.W. Feigenson, *Membrane lipids: where they are and how they behave.* Nat Rev Mol Cell Biol, 2008. **9**(2): p. 112-124.

186. Magnus, C., et al., *Estimating the Stoichiometry of Human Immunodeficiency Virus Entry.* Journal of Virology, 2009. **83**(3): p. 1523-1531.

187. Klasse, P.J., *Modeling how many envelope glycoprotein trimers per virion participate in human immunodeficiency virus infectivity and its neutralization by antibody.* Virology, 2007. **369**(2): p. 245-62.

188. Le Naour, F., et al., *Membrane microdomains and proteomics: lessons from tetraspanin microdomains and comparison with lipid rafts.* Proteomics, 2006. **6**(24): p. 6447-54.

189. Espenel, C., et al., *Single-molecule analysis of CD9 dynamics and partitioning reveals multiple modes of interaction in the tetraspanin web.* The Journal of Cell Biology, 2008. **182**(4): p. 765-776.

190. Zuidscherwoude, M., et al., *The tetraspanin web revisited by super-resolution microscopy.* Sci Rep, 2015. **5**: p. 12201.

191. Jones, E.L., et al., *Dendritic Cell Migration and Antigen Presentation Are Coordinated by the Opposing Functions of the Tetraspanins CD82 and CD37.* J Immunol, 2016. **196**(3): p. 978-87.

192. Shoham, T., et al., *The tetraspanin CD81 regulates the expression of CD19 during B cell development in a postendoplasmic reticulum compartment.* J Immunol, 2003. **171**(8): p. 4062-72.

193. Tu, L., T.-T. Sun, and G. Kreibich, *Specific Heterodimer Formation Is a Prerequisite for Uroplakins to Exit from the Endoplasmic Reticulum.* Molecular Biology of the Cell, 2002. **13**(12): p. 4221-4230.

194. Bosch, B.J., et al., *Severe acute respiratory syndrome coronavirus (SARS-CoV) infection inhibition using spike protein heptad repeat-derived peptides.* Proceedings of the National Academy of Sciences of the United States of America, 2004. **101**(22): p. 8455-8460.

195. Lee, K.K., et al., *Capturing a fusion intermediate of influenza hemagglutinin with a cholesterol-conjugated peptide, a new antiviral strategy for influenza virus.* J Biol Chem, 2011. **286**(49): p. 42141-9.

196. Charrin, S., et al., *A physical and functional link between cholesterol and tetraspanins.* European Journal of Immunology, 2003. **33**(9): p. 2479-2489.

VITA

The author, James Thomas Earnest was born in Athens, GA on August 17, 1987 to David and Margaret Earnest. In May, 2009 James received a B.S. in Biology from Wake Forest University. During his undergraduate studies, James received his first laboratory experience working with Dr. Tim Peters, MD in the department of Pediatrics. James also performed epidemiologic research of Chagas disease in Ecuador in June of 2008 under the direction of Mario Grijalva, PhD at the Ohio University Tropical Disease Institute.

James continued to get a M.S. in Veterinary and Biomedical Sciences in the department of Population Health at the University of Georgia. Under the mentorship of Egbert Mundt DVM, PhD and with the help of researchers at the CDC and Emory University, James developed a virus-like particle based vaccine against avian influenza A viruses. This strategy allowed for aerosolized vaccination of chicken flocks against pathogenic influenza A.

In August 2011, James entered the Interdisciplinary Program in Biomedical Sciences at Loyola University Chicago, and transitioned into the Microbiology and Immunology Ph.D. program shortly after. He completed his doctoral work in the laboratory of Tom Gallagher Ph.D., where he focused on cellular factors that promote coronavirus entry. James will continue his postdoctoral research in the laboratory of Dr. Michael Diamond at Washington University in St. Louis. There James will study the pathogenesis of alphaviruses.